# BIOMASS L1c Stack Product ATBD

**Ref**: BIO-BPS-L1-STACK-ATBD-ARE-010166
**Issue**: 1.4.0
**Date**: 02/04/2026

# Document Information

| | |
|---|---|
| **Title** | **BPS L1c Stack ATBD - Algorithms Theoretical Baseline Document** |
| **Internal Ref.** | |
| **External Ref.** | BIO-BPS-L1-STACK-ATBD-ARE-010166 |
| **Date** | 02/04/2026 |
| **Issue** | 1.4.0 |
| **Pages** | 87 |

| **Recipients** | |
|---|---|
| Nuno Miranda | ESA – ESRIN |
| Michele Caccia | ESA – ESRIN |
| Muriel Pinheiro | ESA - ESRIN |
| | |

| **Prepared by** | |
|---|---|
| Riccardo Piantanida | |
| Simone Mancon | |
| Davide D’Aria | |
| Paolo Mazzucchelli | |
| Francesco Banda | |
| Federico Boniardi | |
| Giovanni Amoroso | |
| | |
| | |

| **Checked by** | |
|---|---|
| Davide D’Aria | |

| **Approved by** | |
|---|---|
| Davide D’Aria | |

# Change Log

| Date | Issue | Change | Author |
|---|---|---|---|
| 15/11/2021 | 1.0 | First issue of the document | Riccardo Piantanida |
| 18/03/2022 | 1.1 | CDR1 issue of the document<br>• PDR1-3-57, PDR1-3-80, PDR1-3-99: Added optional SKP phase removal.<br>• PDR1-3-58: Corrected the time span of TOM stack.<br>• PDR1-3-59: Selection of reference image updated.<br>• PDR1-3-60: Removed master and slave terminology.<br>• PDR1-3-61, PDR1-3-62: Back-geocoding sections moved to the SAR ATBD.<br>• PDR1-3-63: Added missing description of: coregistration shifts computation, geometric phase computation, vertical wavenumbers, and image interpolation.<br>• PDR1-3-65: Updated formula in “Model-based inversion of residual shifts”.<br>• PDR1-3-66: Corrected the reference to the equation.<br>• PDR1-3-67: Added the XYZ product as input.<br>• PDR1-3-68, PDR1-3-72: Removed the RFI quality measure for TOM stack.<br>• PDR1-3-70: Removed references to DEM processor.<br>• PDR1-3-72: Moved the “Data quality measure according to RFI pattern” into the Stacking section.<br>• PDR1-3-73: Updated the “Azimuth spectral filtering” section.<br>• PDR1-3-74: Added in the I/O sections if one or multiple polarization will used.<br>• PDR1-3-75: Clarified in “Slow changing ionosphere estimation” which pre-processing will be applied.<br>• PDR1-3-76, PDR1-3-77, PDR1-3-83: Removed the “Multi-baseline/coherence optimization”<br>• PDR1-3-77, PDR1-3-84: Added geometric phase removal to in the “Range spectral filtering” and in the “Slow changing ionosphere estimation”.<br>• PDR1-3-78: Updated the “Range spectral filtering” section.<br>• PDR1-3-79: Updated the Stack processor workflow figure.<br>• PDR1-3-81: Updated the inputs of the “Reference image selection”.<br>• PDR1-3-82: corrected the correlation formula.<br>• PDR1-3-85: Added missing steps description in “Slow changing ionosphere estimation”.<br>• PDR1-3-86: Added Weighted Least Square inversion in the Multi-Baseline using the weights computed in the single baseline steps.<br>• PDR1-3-87: Removed the autofocus inputs | Simone Mancon |

| Date | Issue | Change | Author |
|---|---|---|---|
| | | • PDR1-3-87, PDR1-3-89: added the formulation of the shifts correction in the “Residual coregistration from data” and in the “Baseline error estimation”<br>• PDR1-3-87: The sub-looks computation applied before the coregistration in the “Slow changing ionosphere estimation”.<br>• PDR1-3-87: “Residual coregistration from data” added to the calibration block diagram.<br>• PDR1-3-90: Added the update of the coregistration shifts annotated in the product in the “Residual coregistration from data” and in the “Baseline error estimation”.<br>• PDR1-3-91: Rephrased the sentence.<br>• PDR1-3-92: Removed the duplicated computation of the MS InSAR phase<br>• PDR1-3-92: Provide reference to the computation of the bandwidth of the azimuth sub-looks in the “Residual ionospheric scintillation estimation”.<br>• PDR1-3-94: Updated the I/O section and flow-chart of the “Phase calibration by SKP”<br>• PDR1-3-96: Removed the “Residual ionospheric scintillation estimation” algorithm using SVD.<br>• PDR1-3-97: Added the scintillation DC component removal in the “Residual ionospheric scintillation estimation”<br>• PDR1-3-98: Updated “Stacking” section according to the implementation. | |
| 23/05/2022 | 1.1.1 | • CDR1-224, CDR1-223: New algorithm to compute the RFI impact to the InSAR coherence.<br>• CDR1-152, CDR1-153, CDR1-221: Updated Fig.3 and Section 2.3 with proper naming conventions and last algorithmic updates.<br>• CDR1-251: Split-band parameters (central frequency and bandwidth of sub-looks) stated as configurable.<br>• CDR1-252: The processing chain of the slow ionosphere removal has been restored to PDR1 version (Split-spectrum applied to the coregistered data).<br>• CDR1-231: the “Residual range shift estimation” has been removed.<br>• CDR1-232: Synthetic phase removal moved before the range spectral filtering.<br>• CDR1-233: Corrected the formulation of the central frequency in the “Range spectral filtering”.<br>• CDR1-234: Removed from the ”Azimuth spectral filtering” the dependence from the desired resolution.<br>• CDR1-235: Specified the type of low pass-filtering used in the “Slow ionosphere estimation”.<br>• CDR1-219: Added placemarks for two missing steps: Cross-pol merging and LUT interpolation. | Simone Mancon |

| Date | Issue | Change | Author |
|---|---|---|---|
| | | • CDR1-226: Added list of geometric parameters generated by the back-geocoding.<br>• CDR1-236, CDR1-237: Clarified the dimensions of the matrixes in the single-baseline and multi-baseline of the slow ionosphere.<br>• CDR1-238: Added the formulation of the quality indicator of the multi-baseline results.<br>• CDR1-239: Removed the redundant synthetic phase correction in the “Baseline error estimation”.<br>• CDR1-240: Added the coregistration shift among the output of the “Baseline error correction”.<br>• CDR1-244: Azimuth filtering removed from the configurable parameters of “Fast ionosphere estimation”.<br>• CDR1-246: Clarified the single-baseline “Fast ionosphere estimation” is performed block-wise in range and the block in the same for ionospheric height and ionospheric phase estimation.<br>• CDR1-247: Clarified that “Fast ionosphere estimation” need look angle in input if the ionospheric height is passed as external parameter.<br>• CDR1-248: Stack calibrated by SKP phases defined as optional output.<br>• CDR1-229: Clarified in the formulation that speckle tracking is performed on the intensity of the images.<br>• CDR1-230: Modified the terminology: from scintillation to fast ionosphere. | |
| 08/02/2023 | 1.1.2 draft | Pre-FAT1 issue of the document<br>• Updated the methodology to select the reference image for the coregistration by geometry.<br>• BPS-42: PDR1-2 - Updated the algorithm of the single-baseline estimation of the residual fast-varying ionosphere.<br>• Clarified that the SKP ground phase is composed by both the synthetic phase from geometry plus the residual phase computed by SKP.<br>• BPS-58: PDR1-21 – Added the SKP ground phase quality and the related threshold. | Simone Mancon |
| 24/03/2023 | 1.1.2 | • Explained the method to perform the cross-pol merging.<br>• Updated the methodology to select the reference image for the coregistration using the temporal baseline.<br>• Explained the method to perform the oversampling of geometrical quantity.<br>• Explained the method to perform the shift and interpolation of the LUTs<br>• Add input/output tables to the calibration chapter and other minor refactoring to that chapter.<br>• Add the IOS description of the approach used for the ionosphere height estimation. | Simone Mancon<br><br>Federico Boniardi<br><br>Giovanni Amoroso |

| Date | Issue | Change | Author |
|---|---|---|---|
| | | • Added the revert of the ionospheric phase screen estimated by L1 processor in the slow varying ionosphere estimation.<br>• Added the correction of bias in the slow varying ionosphere estimation due to the combined coregistration mode.<br>• Added the formulation of the estimated accuracy for baseline error estimation and the quality of the step has been modified accordingly.<br>• Removed the direct geocoding step and added the exploitation of the geometric LUT for coregistration and calibration.<br>• The Stack is now split in three sub-processor (according to the code structure of the code): Pre-processing, Stacking and Calibration. | |
| 09/01/2023 | 1.1.3 | Delta-FAT2 issue of the document<br>• Major refactoring of the sections related to calibration:<br>○ Restructured th AZF sections with major corrections.<br>○ Rewritten IOB section.<br>○ Refactored BAE section.<br>○ Updated IOS section.<br>○ Changed $=$ with $\approx$ in equation of SKP phase screen.<br>• Added tables in the stacking section.<br>• Added description of *Automatic* coregistration modality. | Federico Boniardi |
| 17/05/2024 | 1.1.4 | Post-Delta-FAT2 issue of the document<br>• Fixed typos in calibration tables (IOB, IOS, BAE).<br>• Added note on possibility to disable weights in MB estimation of IOS.<br>• Updated fitting quality metric for coregistration.<br>• Removed “scintillation” in favor of “fast-varying ionosphere”.<br>• Added sections that describe how contingency cases are handled:<br>○ Stacking: Section 4.4<br>○ IOB: Section 5.2.5<br>○ BAE: Section 5.3.5<br>○ IOS: Section 5.4.6<br>○ SKP: Section 5.5.3<br>• Refactored Section 4.1, including references to DEM.<br>• Finalized incomplete cross-pol merging (formula) and input table<br>• Added input/output table in Section 3.4.2.<br>• Update quality for BAE’s Single-baseline estimation.<br>• Revised references and formulas (new numbering)<br>• Revised table of acronyms, including removal of unused entries<br>• Major refactoring of the LUT shifting section.<br>○ Include note on the output resolution of LUTs. | Federico Boniardi |
| 06/09/2024 | 1.1.5 | FAT3 issue of the document<br>• Fixed section numbering for AZF.<br>• Updated I/O tables in Sections 5.2.1, Section 5.3.1, and Section 5.4.1.<br>• Addressed BPSCDR1-25 (multi-look size in azimuth and range direction) | Federico Boniardi |

| Date | Issue | Change | Author |
|---|---|---|---|
| | | • Addressed CDR1-245 (how to establish that there's no peak in the ionosphere profiles)<br>• Substitute "Sequestrating" with "suppressing" | |
| 13/12/2024 | 1.1.6 | Post-FAT3 issue of the document | Federico Boniardi |
| 07/03/2025 | 1.2.0 | Post-FAT3 issue of the document<br>• Fixed contingency handling of Multi-baseline method (IOB, BAE, and IOS). Now a check on factor-graph connectivity is used instead of the previous laxer (and wrong) approach.<br>• IOB includes now recommendations from [RD25] (BIO-TOMEX). This includes updated I/O tables consistent with those.<br>• Updated I/O table for BAE with new parameter associated to MB<br>• Added reference to median filtering in SKP and updated I/O table<br>• Fixed notations for *coregistrationShiftsQuality*<br>• Fixed numbering of equations and associated references<br>• Rewritten Section 3.3.3 (same content, better wording) and added missing contingency case in Section 3.3.4<br>• Fixed typos and sentences here and there | Federico Boniardi |
| 30/04/2025 | 1.2.1 | Post-FAT3 issue of the document<br>• Added more details on selection of interferometric pairs in Section 5.2.3 and Section 5.3.3. | Federico Boniardi |
| 23/07/2025 | 1.3.0 | Post-launch issue of the document (associated to BPS V4.0.0)<br>• Add notes to explain a few details about the calculation of the vertical wavenumbers<br>• Deprecate BAE (former Section 5.3)<br>• Deprecate IOS (former Section 5.4)<br>• Substitute former Section 5.3 with newly added BIC, consistently with [RD25] (from BIO-TOMEX) | Federico Boniardi |
| 30/07/2025 | 1.3.1 | Fixes to the post-launch issue of the document<br>• Fix stale *skpPhaseCorrectionFlag*<br>• Fix stale "Phase**s**Screen"<br>• Add *excludeMPMBPolarizationCrossCovarianceFlag* | Federico Boniardi |
| 28/11/2025 | 1.3.2 | Fixes associated to BPS V4.2.0<br>• Deprecated BIC<br>• Added Phase Plane Removal (PPR) module<br>• Updated coregistration outputs (coreg from orbit LUTs)<br>• Added possibility to disable model-based fitting of coreg shifts<br>• Added warning to user to avoid using median-filter in SKP<br>• Updated figures and diagrams | Federico Boniardi |
| 02/04/2026 | 1.4.0 | Post-launch issue of the document (associated to BPS V4.4.1)<br>• Deprecate the range spectral filtering in coregistration<br>• Deprecate the PPR<br>• Added MSC | Federico Boniardi |

| Date | Issue | Change | Author |
|---|---|---|---|
| | | • Added boxcar and Goldstein filter to SKP<br>• Removed warning on filtering the SKP phase with median filter | |

# Table of Contents

# 1. Introduction

## 1.1. Context

BIOMASS is ESA's 7th Earth Explorer mission. The purpose of the BIOMASS mission is to reduce the uncertainty in the worldwide spatial distribution and dynamics of forest biomass to improve current assessments and future projections of the global carbon cycle. This objective will be achieved by implementing a P-band SAR mission, providing global maps of forest biomass stocks, forest disturbance, and growth.
The BIOMASS mission will also provide 3D views of forests through the "tomographic" phase and will also support additional science needs arising from the opportunity to explore the Earth for the first time with a P-band SAR system from space offering the possibility to "see" below the vegetated areas and in beneath bare soil or icy regions.

To achieve its challenging objectives, the BIOMASS requires a specific data processing strategy that combines different technologies and techniques at different processing level to generate the final Above Ground Biomass (AGB) global map.

## 1.2. Scope of the Document

The purpose of this document is to provide the "Stack Processor Algorithms Theoretical Baseline Document (ATBD)" for the BIOMASS Processing Suite (BPS) project.
This document is organized as follows:

- Section 2: Brief introduction about BPS and Stack Processor;
- Section 3: Description of the Pre-processing algorithms;
- Section 4: Description of the Stacking algorithms;
- Section 5: Description of the Calibration algorithms;
- Section 6: Description of configurable input parameters.

## 1.3. Acronyms

| Acronym | Description |
|---|---|
| AD | Applicable Document |
| AGB | Above Ground Biomass |
| ARESYS | Advanced Remote Sensing and Systems |
| AT | Along-track (*e.g.* along-track direction) |
| ATBD | Algorithm Theoretical Baseline Document |

| Acronym | Description |
|---|---|
| AUX | Auxiliary (*e.g* AUX_PPS) |
| AWGN | Additive White Gaussian Noise |
| AZF | Azimuth Spectral Filtering |
| BIODEMPP | Biomass DEM Prototype Processor |
| BPS | BIOMASS Processing Suite |
| CFI | Customer Furnished Items |
| CoSCS | Coregistered SCS |
| DEM | Digital Elevation Model |
| DSI | DEM Synthetic Interferogram |
| DTM | Digital Terrain Model |
| ESA | European Space Agency |
| FNF | Forest/Non-forest (*e.g.* mask) |
| FR | Faraday Rotation |
| InSAR | Interferometric Synthetic Aperture Radar |
| INT | Interferometric Phase |
| IOB | Background Ionosphere Removal (also Slow Varying Ionosphere Removal) |
| IODD | Input&Output Data Definition |
| L1a/b/c | Level-1 a/b/c product |
| L1M | Level-1 Monitoring product |
| L1S | Level-1 Standard product |
| LOS | Line-of-Sight |
| LUT | Look-Up Table |
| MB | Multi-baseline |
| MPMB | Multi-polarimetric Multi-baseline |
| MS | Multi-Squint (*e.g.* coherence) |
| MSC | Multi-Squint Calibration |
| PFD | Product Format Specification Document |
| RD | Reference Document |
| RFI | Radio-Frequency Interferences |
| SAR | Synthetic Aperture Radar |
| SB | Single-baseline |
| SCS | Single-look Complex Slant-range |
| SKP | Sum of Kronecker Products |

| Acronym | Description |
|---|---|
| SNR | Signal-to-Noise Ratio |
| SVD | Single Value Decomposition |
| TEC | Total Electron Content |
| TOM | Tomographic Phase |

## 1.4. Applicable documents

[AD1] /

## 1.5. Reference documents

[RD1] BIOMASS DEM Product Processor Prototype, CoSCS Processor Algorithm Theoretical Baseline Document, BIODEMPP-CoSCS-ATBD-01, Issue 4.0, June 07th 2021.

[RD2] BIOMASS Report for Mission Selection; SP-1341/1, May 2012

[RD3] BIOMASS L2 Implementation Study, Integrated R&D Report. Report to ESA, 2018.

[RD4] BIOMASS DEM Product Processor Prototype, DEM Processor Algorithm Theoretical Baseline Document, BIODEMPP-CoSCS-DEM-01, Issue 4.0, June 07th 2021.

[RD5] BIOMASS DEM Product Prototype Processor, Critical review of CoSCS and DEM algorithms, BIODEMPP-TN-01, Issue of 07th of February 2020.

[RD6] M. Liao, H. Jiang, Y. Wang, T. Wang, L. Zhang, “Improved topographic mapping through high-resolution SAR interferometry with atmospheric effect removal”, ISPRS Journal of Photogrammetry and Remote Sensing, Volume 80, 2013, Pages 72-79

[RD7] Z. Hu, J. J. Mallorquí, G. Centolanza and J. Duro, "InSAR atmospheric delays compensation: Case study in Tenerife island," 2017 IEEE International Geoscience and Remote Sensing Symposium (IGARSS), Fort Worth, TX, 2017, pp. 3167-3170.

[RD8] M. Pinheiro, A. Reigber, R. Scheiber, P. Prats-Iraola and A. Moreira, "Generation of Highly Accurate DEMs Over Flat Areas by Means of Dual-Frequency and Dual-Baseline Airborne SAR Interferometry," in IEEE Transactions on Geoscience and Remote Sensing, vol. 56, no. 8, pp. 4361-4390, Aug. 2018.

[RD9] G. Gomba, A. Parizzi, F. D. Zan, M. Eineder, and R. Bamler, “Toward Operational Compensation of Ionospheric Effects in SAR Interferograms: The Split-Spectrum Method,” IEEE Transactions on Geoscience and Remote Sensing, vol. 54, no. 3, pp. 1446–1461, Mar. 2016.

[RD10] S. Mancon, A. M. Guarnieri, D. Giudici, and S. Tebaldini, “On the phase calibration by multisquint analysis in TOPSAR and stripmap interferometry,” IEEE Transactions on Geoscience and Remote Sensing, vol. 55, no. 1, pp. 134–147, 2016.

[RD11] S. Tebaldini, M. M. d'Alessandro, J. S. Kim, and K. Papathanassiou, "Ionosphere vertical profiling from biomass multi-squint InSAR," in 2017 IEEE International Geoscience and Remote Sensing Symposium (IGARSS), 2017, pp. 5866–5869.

[RD12] R. Scheiber and A. Moreira, "Coregistration of interferometric SAR images using spectral diversity," Geoscience and Remote Sensing, IEEE Transactions on, vol. 38, no. 5, pp. 2179–2191, 2000.

[RD13] Tebaldini, Stefano, et al. "Phase calibration of airborne tomographic SAR data via phase center double localization." IEEE Transactions on Geoscience and Remote Sensing 54.3 (2016): 1775-1792.

[RD14] Bamler, Richard und Hartl, Philip (1998) Synthetic Aperture Radar Interferometry. Inverse Problems, 14 (4).

[RD15] F. Gatelli, A. Monti Guamieri, F. Parizzi, P. Pasquali, C. Prati and F. Rocca, "The wavenumber shift in SAR interferometry," in IEEE Transactions on Geoscience and Remote Sensing, vol. 32, no. 4, pp. 855-865, July 1994.

[RD16] A. Reigber, "Range dependent spectral filtering to minimize the baseline decorrelation in airborne SAR interferometry," *IEEE 1999 International Geoscience and Remote Sensing Symposium. IGARSS'99 (Cat. No.99CH36293)*, Hamburg, Germany, 1999, pp. 1721-1723 vol.3.

[RD17] Ferretti, A., Monti-Guarnieri A., Prati, C., Rocca, F., Massonnet, D. (2007). InSAR Principles: Guidelines for SAR Interferometry Processing and Interpretation. ESA Publications, TM-19. ISBN 92-9092-233-8.

[RD18] [BPS_AUX_FMT] BPS Auxiliary Product Format, I/R 1/1

[RD19] [BPS_L1_PFD] BIOMASS L1a/b/c Products Format Specification, I/R 1/1

[RD20] BPS L1 SAR ATBD - Algorithms Theoretical Baseline Document

[RD21] Miguel Arevallilo Herraez, David R. Burton, Michael J. Lalor, and Munther A. Gdeisat, "Fast two-dimensional phase-unwrapping algorithm based on sorting by reliability following a noncontinuous path", Journal Applied Optics, Vol. 41, No. 35, pp. 7437, 2002

[RD22] Laakso, Timo I., et al. "Splitting the unit delay [FIR/all pass filters design]." IEEE Signal Processing Magazine 13.1 (1996): 30-60.

[RD23] S. Tebaldini, A. M. Guarnieri, and F. Rocca, "Recovering time and space varying phase screens through SAR multi-squint differential interferometry," in EUSAR 2012; 9th European Conference on Synthetic Aperture Radar, Apr. 2012, pp. 16–19.

[RD24] [BPS_IODD] BIOMASS Processors Input & Output Data Definition, Issue 3.0.5, February 2nd 2024.

[RD25] [BIOTOMEX_TN] BIOTOMEX TN, Technical Note on Performance Analysis, Issue 1.1, November 26th, 2024

[RD26] R. Lanari et al. "Generation of digital elevation models by using SIR-C/X-SAR multifrequency two-pass interferometry: The Etna case study." IEEE Transactions on Geoscience and Remote Sensing (1996)

[RD27] S. Tebaldini, F. Salvaterra, F. Banda, and M. Pinheiro, “Multi-layer ionosphere correction in low-frequency interferometric SAR: modeling, inversion, and application to BIOMASS”. *Authorea Preprints* (2025)

# 2. BPS and Stack Processor Overview

## 2.1. BPS Overview

The BIOMASS Processing Suite (BPS) is in charge of processing BIOMASS Level-0 data up to Level-3, generating a wide set of products. Product generation scheme is depicted in the following two figures respectively for TOM phase and for INT phase. The processing foresees the following steps:

- **L1 processing**: the BIOMASS image formation step, taking in input 1 L0 slice and generating in output $N \geq 1$ L1 frames;
- **Stack Processing**: the coregistration and stacking processing step that will define the required 7-images Tomographic stacks or the 3-images Interferometric stacks. It includes the stack calibration phase;
- **L2a Processing**: processing step for each stack that provides the inputs to the further products Tile Generation performed by the L2b processors. For one global cycle the number of stacks varies mainly with latitude, approximately from a minimum of two at the Equator (ascending/descending) to about six at higher latitudes (three ascending/descending pairs);
- **L2b Processing**: processing that aggregates all the stack-based L2a products insisting on the same location on ground (Tile) in the same time interval and generates a single BIOMASS L2b product. A different number of stacks may be available for each DGG tile, based on tile dimensions and swath coverage (which is not related to DGG tiling pattern);
- **L3 Processing**: consolidation processing removing discontinuities in L2b products.

Fig.1

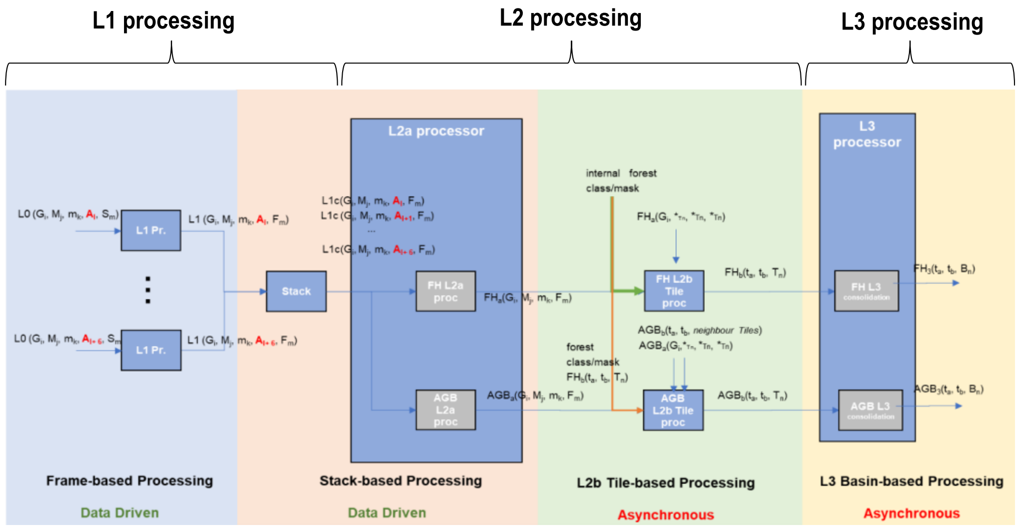


Biomass high-level processing scheme from L0 data to L3 products, TOM phase.

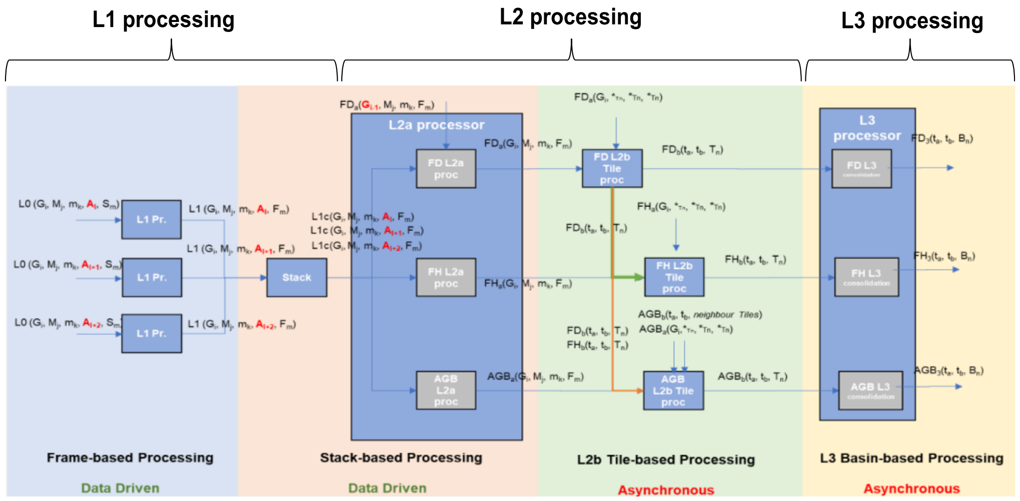


Biomass high-level processing scheme from L0 data to L3 products, INT phase.

Fig.2

## 2.2. Overview

The Stack Processor has as its main goal the generation of stacks ready to be used by the L2 Processor. It receives as input a stack of BIOMASS Level-1a images (SCS stack), including its relevant annotated data (e.g., the ionosphere screen estimated exploring Faraday Rotation). The Stack Processor performs the coregistration of the stack, as well as its calibration:

- stacking, *i.e.*, the alignment of the individual images, which will be done via a two-step approach for coregistration;
- calibration, *i.e.*, the coregistered stack and input ionospheric phase screens delivered by the L1 Processor are fed to the calibration module which will use multi-baseline techniques to compute refined ionospheric screens and baseline errors. The stack is calibrated by removing the estimated errors. The block can also perform the Sum of Kronecker Products (SKP) calibration to deliver information required for the generation of tomography-ready stacks to the L2 Processor [RD3].

Other operations, like the generation of Digital Elevation Model (DEM) and Digital Terrain Model (DTM) are outside the scope of BPS.

## 2.3. Stack Processor's Workflow and Algorithmic Overview

The main steps of the BPS Stack Processor workflow are depicted in the following figure and described in detail in the following sub-sections.

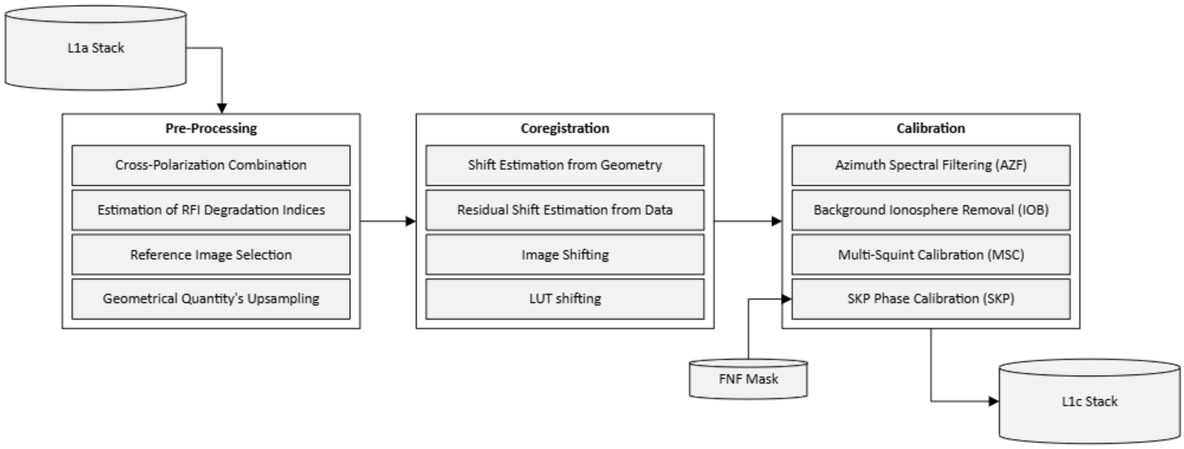


Stack Processor detailed workflow. The AUX_PPS is omitted from the figure since it is an input to each step of the Stack Processor.

**Fig.3**

### 2.3.1. Pre-processing

The *Pre-processing* block prepares and packs the data needed by the next blocks (Stacking and Calibration). The main steps of the Pre-processor are the following:

- Computation of RFI coherence degradation: Computation of the RFI masking impact on the InSAR coherence.
- Polarization combination (if enabled): The cross-polarizations of the L1a product are possibly averaged (*cross-pol merging*) or selectively dropped (*i.e.* keep only HV or VH) in a single image, the associated LUTs are respectively merged or dropped.
- Coregistration primary image selection: Selection of the most appropriate image for being utilized as reference image for coregistration . For this, the Pre-processor will employ quality indicators of the L1 stack and/or coverage information.
- Upsampling of geometric quantities stored in the L1a input products's LUTs to match the resolution of the SCS.

### 2.3.2. Stacking

The main steps of the *Stacking* block are:

- Geometry-based estimation of coregistration shifts.
- Residual offset estimation: Further estimation of residual coregistration shifts that may be due to imprecise information on the satellite's orbit, as well as ionospheric artefacts that affect the input data;
- Image and LUT interpolation: Coregistration shifts are applied to input data and LUTs to align them to the primary image grid.

### 2.3.3. Calibration

The *Calibration* block consists of the following steps:

- Azimuth spectral filtering: Apply a common band filtering in azimuth direction to crop the data spectrum to the azimuth common bandwidth.
- Slow-varying ionosphere estimation: A Multi-baseline split-spectrum-based method that estimates and removes from data low-pass ionospheric artefacts
- Baseline and residual fast-varying ionosphere correction: A Multi-Squint-based (MS) approach that estimates and corrects baseline errors and residual high-pass ionospheric artefacts from the image.
- Phase calibration by SKP: A module for estimating and possibly removing ground steering phase-screens required to generate tomography-ready stacks [RD3]. By default, the SKP phases will be estimated but not applied. The SKP phase removal can be activated by configuration.

# 3. Pre-processing

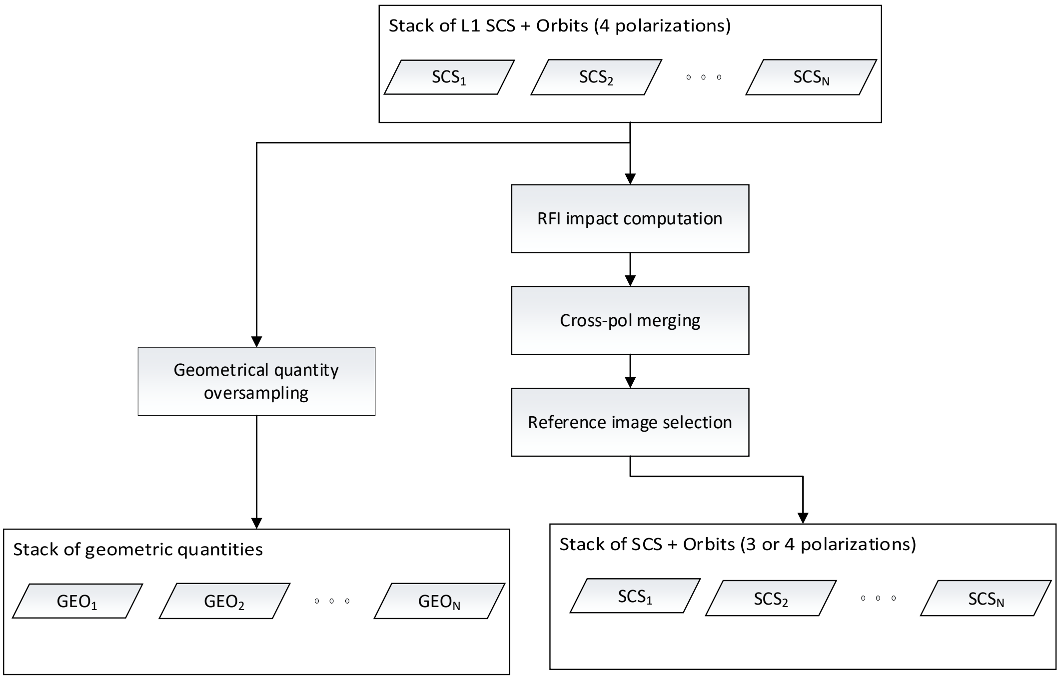


**Fig.4** Complete flow-chart of the pre-processing processor.

## 3.1. RFI-based Data Quality Measure

In this section we describe the algorithm to compute the coherence loss in case of RFI filtering done at L1. The algorithm at L1 uses two approaches for RFI removal: one in time domain and one in the frequency domain. In either cases, the amount of “lost” signal frequencies must be computed in relation to the range signal bandwidth or in relation to the azimuth Doppler bandwidth. We describe here the time-domain case, the frequency domain case is less likely due to BIOMASS operation restrictions in the areas where most of the frequency-domain RFI sources are active.

The quality measure of an interferometric pair after the RFI mitigation can be estimated as the decorrelation due to the spectral overlap reduction generated by the masking of pixels in raw data.

### 3.1.1. Overview

The purpose of this step is to deal with the interferences that may impact the images and to compute an indicator of the resulting coherence impact for each image.

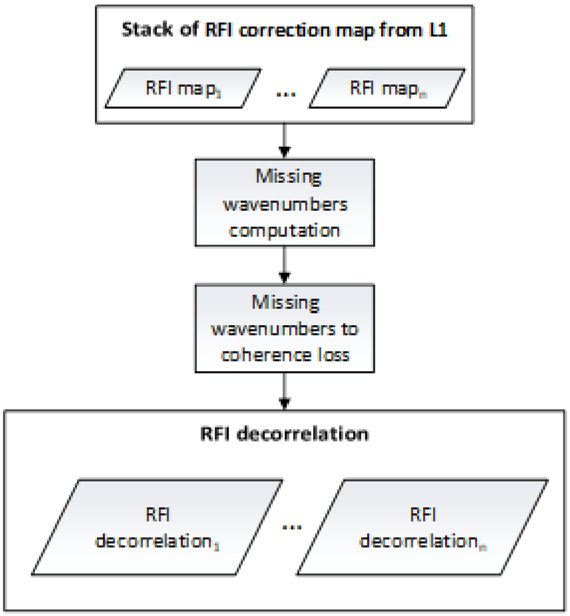


Data quality measure according to RFI pattern.

**Fig.5**

## 3.1.2. Inputs and Outputs

### Inputs

| Symbol | Name | Origin | Size | Variability | Default | Description |
|---|---|---|---|---|---|---|
| $m_{RFI}$ | | L1a | M masks of size $[N_{az} \times N_{rg}]$ | M=3 (INT) or M=7 (TOM) matrices | - | RFI masks estimated at L1 |

### Outputs

| Symbol | Name | Destination | Size | Variability | Default | Description |
|---|---|---|---|---|---|---|
| $\gamma_{RFI}$ | | Primary image selection | M Float values | M=3 (INT) or M=7 (TOM) | - | RFI degradation indices |

## 3.1.3. Mathematical Description

### 3.1.3.1. Theoretical Basis of InSAR RFI Impact

Zeroing a raw data sample is equivalent to suppressing a specific wavenumber of the targets, depending on the sample position, on the fast/slow time domain and target position in the range/azimuth plane.

Let $(t_i, \tau_i)$ be respectively the fast (range) and slow (azimuth) time coordinates of a raw data sample affected by the $i$-th RFI. For a target at $(r, a)$, zeroing the raw data sample at $(t_i, \tau_i)$ is equivalent to suppressing the spectral components

$$f_{\mathrm{r,i}}(t_i,\tau_i;r,a)=\frac{2}{c}(f_c+f_{\mathrm{RFI}})\cdot\frac{r}{R(\tau_i;r,a)}=\frac{2}{c}(f_c+f_{\mathrm{RFI}})\cdot\cos\big(\psi(\tau_i;r,a)\big)$$
$$f_{a,i}(t_i,\tau_i;r,a)=\frac{2}{c}(f_c+f_{\mathrm{RFI}})\cdot\frac{S_a(\tau_i)-a}{R(\tau_i;r,a)}=\frac{2}{c}(f_c+f_{\mathrm{RFI}})\cdot\sin\big(\psi(\tau_i;r,a)\big) \quad (3.1)$$

where:

- $f_c$ is the central (carrier) frequency (*i.e.* 435 MHz);
- $S_a(\tau_i)$ is the azimuth position of the sensor at slow time $\tau_i$;
- $R(\tau_i;r,a)$ is the distance from the target at $(r,a)$ to the sensor at $\tau_i$;
- $\psi(\tau_i;r,a)$ is the squint angle between the target at $(r,a)$ and the sensor at $\tau_i$;
- $f_{\mathrm{RFI}}$ is the temporal frequency suppressed by the RFI, which depends on $t_i$ and the chirp rate $\alpha$ as follows

$$f_{\mathrm{RFI}}(t_i,\tau_i;r,a)=\alpha\cdot\left(t_i-\frac{2}{c}R(\tau_i;r,a)\right). \quad (3.2)$$

For the sake of brevity and without loss of generality, below we will report the explicit derivation of the missing frequency in the $r$ component. The azimuth component can be obtained similarly. The missing wavenumber for each target $(r,a)$ has been defined as the union of all the RFI contributions $(n_I)$ affecting the image and belonging to the bandwidth $(B_r)$ of the images.

$$f_{r,miss}(r,a)=\left(\sum_{i=1}^{n_I}O\big(f_{r,i}(t_i,\tau_i;r,a),B_r\big)\right)-f_{r,int}(r,a), \quad (3.3)$$

where:

- $n_I$ is the list of the RFI affecting the image.
- $f_{r,int}(r,a)$ is the sum of the intersections between each RFI:

$$f_{r,int}(r,a)=\sum_{i=1}^{n_I}\sum_{j\neq i}^{n_I}O\big(f_{r,i},f_{r,j},B_r\big) \quad (3.4)$$

- $O(\bar{v}_1,\dots,\bar{v}_n)$ is defined as follows:

$$O(\bar{v}_1,\dots,\bar{v}_n)\coloneqq\max\{In(\bar{v}_1,\dots,\bar{v}_n),0\} \quad (3.5)$$

- $In(\bar{v}_1,\dots,\bar{v}_n)$ is defined as follows:

$$In(\bar{v}_1,\dots,\bar{v}_n)=\min(\max(\bar{v}_1),\dots,\max(\bar{v}_n))-\max(\min(\bar{v}_1),\dots,\min(\bar{v}_n)) \quad (3.6)$$

The RFI impact to the coherence for each image, has been defined as the product of the coherence loss due to the missing spectral components in azimuth and range:

$$\gamma_{RFI}(r,a) = \left(1 - \frac{f_{a,miss}(r,a)}{B_a}\right) \cdot \left(1 - \frac{f_{r,miss}(r,a)}{B_r}\right) \quad (3.7)$$

Where:

- $B_a$ and $B_r$ are the bandwidths in azimuth and range direction respectively.

### 3.1.3.2. Computation of Coherence Degradation Index

The algorithm to compute the coherence degradation index[1] is based on the theoretical basis described in the previous section, but some simplifications can be performed. Under the assumption that the range migration can be neglected, the impact of RFI on the spectrum can be computed separately on azimuth and range direction as the sum of the pixel values of the masks used to focus a pixel in the SLC. This can be defined as the convolution between the RFI mask and a 2D boxcar filter with the sizes of the focusing kernel, *i.e.*, the synthetic aperture $L_{sa}$ (in azimuth) and the chirp length $L_{chirp}$ (in range):

$$f_r(t,\tau) = \frac{1}{L_{sa}} \sum_{i=0}^{L_{chirp}-1} \sum_{j=0}^{L_{sa}-1} m_{RFI}(t-i, \tau-j)\,, \qquad f_a(t,\tau) = \frac{1}{L_{chirp}} \sum_{i=0}^{L_{chirp}-1} \sum_{j=0}^{L_{sa}-1} m_{RFI}(t-i, \quad \tau-j), \quad (3.8)$$

where:

- $m_{RFI}(r,a)$ is the RFI mask applied by L1 processor.
- $f_r(r,a)$ and $f_a(r,a)$ are respectively the pixel-wise estimations of the RFI impact on the range and azimuth spectra;
- $t$ and $\tau$ are the coordinates in the RFI mask (raw data domain).

Accordingly, the coherence loss can be defined as:

$$\gamma_{RFI} \coloneqq \frac{1}{L_t L_\tau} \sum_{t,\tau}^{L_t,L_\tau} \left[1 - \frac{f_r(t,\tau)}{L_{chirp}}\right] \times \frac{1}{L_t L_\tau} \sum_{t,\tau}^{L_t,L_\tau} \left[1 - \frac{f_a(t,\tau)}{L_{sa}}\right], \quad (3.9)$$

where:

- $L_t$ and $L_\tau$ are the range and azimuth sizes of RFI mask applied by L1 processor

[1] The coherence degradation index is polarization dependent. Hence, the stack Pre-processor will compute one index per polarization.

Note that the formulation of the RFI coherence degradation index can be further simplified as follows:

$$\gamma_{RFI} \approx \left(1 - \frac{1}{L_t L_\tau} \cdot \sum_{t,\tau}^{L_t,L_\tau} m_{RFI}(t,\tau)\right)^2. \tag{3.10}$$

## 3.2. Cross-pol Merging

This step is devoted to merge in a single cross-pol channel the two cross-pol channels (VH and HV) of the L1a product.

### 3.2.1. Overview

For monostatic SAR acquisition focused on natural targets (forest and ice) we can assume that the two cross-pol responses are reciprocal. Accordingly, it is worth to average them in a coherent way to obtain just one cross-pol channel with a higher SNR. Accordingly, the LUT associated to each cross-pol channel will be merged into one. Note that this merging step is optional and can be activated or not by the user via AUX_PPS.

### 3.2.2. Inputs and Outputs

**Inputs**

| Symbol | Name | Origin | Size | Variability | Default | Description |
|---|---|---|---|---|---|---|
| $m_{RFI}$ | | L1a | M Boolean masks of size $[N'_{az} \times N'_{rg}]$ (one per polarization) | M=3 (INT) or M=7 (TOM) matrices | - | RFI masks estimated by L1_P |
| $\Sigma_n$ | | L1a | M Float matrices of size $[N'_{az} \times N'_{rg}]$ (one per polarization) | M=3 (INT) or M=7 (TOM) matrices | - | Denoising maps estimated by L1_P |
| $SCS_n$ | | L1a | N images of size $[N_{az} \times N_{rg}]$ (one per polarization) | M=3 (INT) or M=7 (TOM) matrices | - | SCS images |

**Outputs**

| Symbol | Name | Destination | Size | Variability | Default | Description |
|---|---|---|---|---|---|---|
| $\gamma_{RFI}$ | | Primary image selection | M Float values | M=3 (INT) or M=7 (TOM) | - | RFI degradation indices |
| $\Sigma_n$ | | L1a | M Float matrices of size $[N'_{az} \times N'_{rg}]$ (one per polarization) | M=3 (INT) or M=7 (TOM) matrices | - | Denoising maps with (optionally) merged cross-polarizations |
| $SCS_n$ | | [BREAKPOINT] Stacking | M images of size $[N_{az} \times N_{rg}]$ | M=3 (INT) or M=7 (TOM) | - | The SCS with (optionally) merged cross-polarizations |

## 3.2.3. Mathematical description

Given the two cross-pol channels $SCS_{HV}$ and $SCS_{VH}$ affected by *i.i.d.* AWGN, we define the cross-pol merged channel, which we henceforth denote by XX, as the average of the 2 cross-pol channels HV and VH:

$$SCS_n^{XX} \coloneqq \frac{1}{2}(SCS_n^{HV} + SCS_n^{VH}). \tag{3.11}$$

Note that, owing to the above definition, it follows that

- $\mathbb{E}[SCS_n^{XX}] = \mathbb{E}[SCS_n^{HV}] = \mathbb{E}[SCS_n^{VH}]$
- $\sigma[SCS_n^{XX}] = \frac{1}{\sqrt{2}}\sigma[SCS_n^{HV}] = \frac{1}{\sqrt{2}}\sigma[SCS_n^{VH}]$

where $\mathbb{E}$ and $\sigma$ denotes the expected value and the standard deviation. Hence, it is easy to see that the noise contribution is reduced by a factor of $\sqrt{2}$, which results in the SNR being increased by a factor of 2.

**RFI masks**. Set $m_{RFI_{HV}}$ and $m_{RFI_{VH}}$ to be the RFI masks corresponding to channels HV and VH and set $m_{RFI_{XX}}$ to be the RFI mask corresponding to the cross-pol merged channel, $m_{RFI_{XX}}$ is obtained by applying a component-wise logical OR (∨):

$$m_{RFI_{XX}} \coloneqq m_{RFI_{VH}} \vee m_{RFI_{VH}}. \tag{3.12}$$

**Denoising**. From Equation 3.11, the denoising map of the cross-pol merged data can be estimated as follows: Since all noise terms are assumed to be AWGN, it holds that

$$\begin{aligned} SCS_n^{XX} &\coloneqq \frac{SCS_n^{HV} + SCS_n^{VH}}{2} \\ &= \frac{\mathbb{E}[SCS_n^{HV}] + w_{HV} + \mathbb{E}[SCS_n^{VH}] + w_{VH}}{2} \\ &= \mathbb{E}[SCS_n^{XX}] + w_{XX}. \end{aligned} \tag{3.13}$$

Thus, by evaluating the variance of both sides of Equation 3.13 and since the variance of normally distributed independent variables is a quadratic form, the denoising map $\Sigma_n^{XX}$ of the cross-pol merged channel is

$$\begin{aligned}\Sigma_n^{XX} \coloneqq Var[SCS_n^{XX}] \coloneqq Var\left[\frac{SCS_n^{HV} + SCS_n^{VH}}{2}\right] \\ = \frac{Var[\langle SCS_n^{HV}\rangle + w_{HV} + \langle SCS_n^{VH}\rangle + w_{VH}]}{4} \\ = \frac{Var[SCS_n^{HV}] + Var[SCS_n^{VH}]}{4} \\ = \frac{1}{4}(\Sigma_n^{HV} + \Sigma_n^{VH}).\end{aligned} \tag{3.14}$$

## 3.3. Coregistration Primary Image Selection

The L2 processor of BIOMASS works on an interferometric stack, for this reason the selection of the coregistration primary image is an important step of the stacking processor. This step must consider both the geometry that maximizes the valid areas and the quality of the image in order to avoid, for instance, using a reference image affected by *e.g.* strong ionosphere, which may degrade the quality of the whole stack.

### 3.3.1. Overview

The algorithm takes as input the stack of SCS images to be coregistered, the information about the ionospheric characterization from the L1 and the characterization of potential RFI signals in frequency or time domain, again from the L1 processor.
The key task of the coregistration primary image selection step is to define which image will be used as reference grid for the other images.
Besides the "classical" approach of selecting the coregistration primary as the central images with respect to acquisition geometry (baselines), here the idea is that this selection should be based also on the quality of the images as it can be inferred from the auxiliary information already available from the L1 processor.
In interferometric processing, the temporal location of the image is often used (*e.g.* avoid selection of a too "old" image). According to the BIOMASS mission, this should not be a problem thanks to the short repeat pass which will limit the time span of the whole stack to a worst case of 18 days (7 images with 3-days repeat during the TOM phase). Nevertheless, a temporal selection criterion is also available in the BPS.
In the reminder of this section we will provide general definitions of stack's *normal baselines* (Section 3.3.3.1) and *temporal baselines* (Section 3.3.3.2), and describe how these are used in combination with quality criteria for the selection of the coregistration primary image (Section 3.3.3.3).

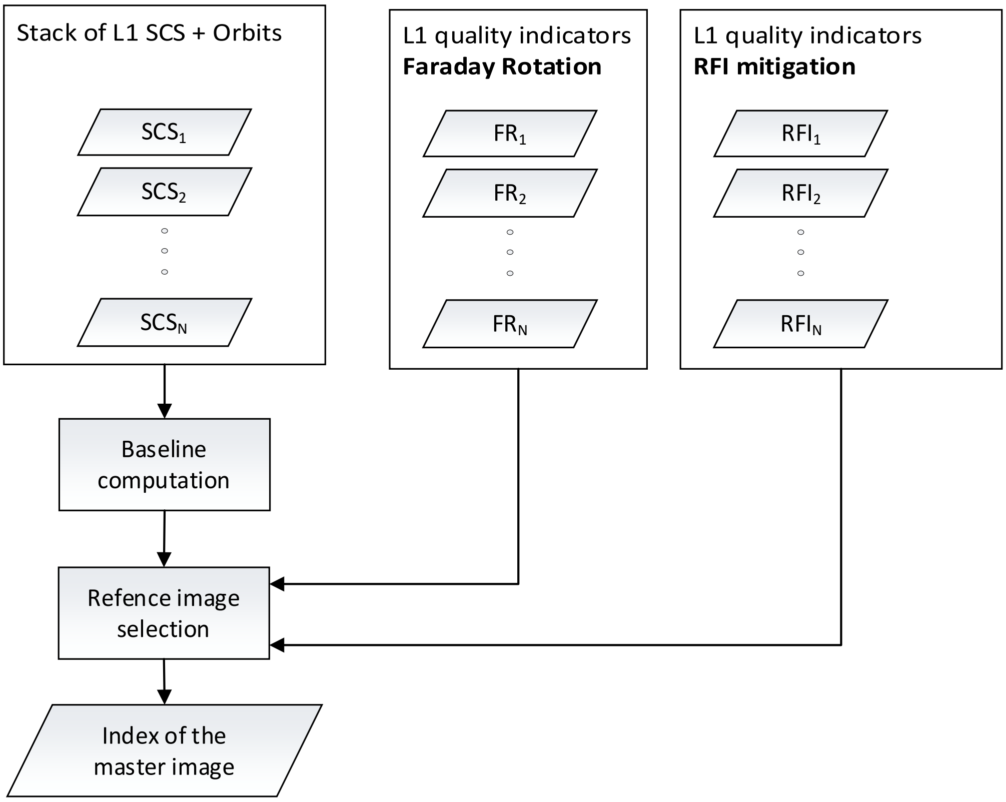


**Fig.6** Selection of the coregistration primary image.

## 3.3.2. Inputs and Outputs

### Inputs

| Symbol | Name | Origin | Size | Variability | Default | Description |
|---|---|---|---|---|---|---|
| $SCS_n$ | | L1a | M stack images of size $[N_{az} \times N_{rg}]$ | M=3 (INT) or M=7 (TOM) matrices | - | The input stack |
| $\gamma_{RFI}$ | | Pre-procesor quality measure | M Float values | M=3 (INT) or M=7 (TOM) | - | The RFI decorrelation indices |
| $\gamma_{far}$ | | L1a | M Float values | M=3 (INT) or M=7 (TOM) | - | The decorrelation from Faraday rotation coming from L1a |
| $\gamma_{RFI}^{ref}$ | | AUX_PPS | Float | 1 | 0.9 | Threshold on the RFI to discard a coregistration primary candidate |
| $\gamma_{far}^{ref}$ | | AUX_PPS | Float | 1 | 0.9 | Threshold on the FR to discard a coregistration primary candidate |

**Outputs**

| Symbol | Name | Destination | Size | Variability | Default | Description |
|---|---|---|---|---|---|---|
| $n_{ref}$ | | Stacking and calibration module | Integer value | 1 | - | The index of the coregistration primary image |

## 3.3.3. Mathematical Description

### 3.3.3.1. Spatial Baseline Computation

Given $N > 1$ SCS images and their acquisition geometry, we first direct geocode the center of an arbitrarily selected reference image $r$, say, for instance, the first image in the stack, and then perform the inverse geocoding of this point to the sensor positions of each image in the stack (with the exception of the previously selected image). This combination of direct and inverse geocoding allows for retrieving the position of the sensors of the images at the center of their scenes. We refer to Section 4.1.3.1 for more details on direct and inverse geocoding. With spatial baseline $\vec{B}_i$, we hereby refer to the sensor position of the $i$-th frame relative to the sensor position of the reference image $\vec{S}_r$ (both computed at the center of the scenes). That can be trivially calculated as follows:

$$\vec{B}_i \coloneqq \vec{S}_i - \vec{S}_r, \;\; i = 1 \dots N; \; i \neq r. \qquad (3.15)$$

Accordingly, the *normal baseline* $B_{i,\perp}$ of the $i$-th image can is defined as the signed magnitude of the projection of the $i$-th spatial baseline vector onto the vector normal to the trajectory, which is the direction normal to both the along-track (tangent) and LOS vectors, using a standard right-handed coordinate system.

### 3.3.3.2. Temporal Baseline Computation

Given $N > 1$ SCS images, the *temporal baselines* are calculated as time difference between the acquisition start times:

$$\Delta T_i = T_{0,i} - T_{0,r}\,, \;\; i = 1 \dots N, \qquad (3.16)$$

where $r$ is an arbitrarily chosen reference image, *e.g.* the first image in the stack.

### 3.3.3.3. Selection of the Coregistration Primary Image

To select the coregistration primary image, the following criteria are provided and can be chosen by the user via a configurable parameter of the AUX-PPS:

- *Temporal criterion* (AUX-PPS parameter: “Temporal Baseline”). Given the temporal baselines $\boldsymbol{\Delta T} \coloneqq (\Delta T_1, \dots, \Delta T_n)$, the primary image is selected as the image with temporal baseline closest to the median temporal baseline, that is, $n^{ref} \coloneqq \mathrm{argmin}_i |\Delta T_i - \langle \boldsymbol{\Delta T} \rangle|$, where $\langle \cdot \rangle$ represents the median operator.

- *Normal baseline criterion* (AUX-PPS parameter: "Geometry"). Similar to the temporal criterion, but with temporal baselines substituted by the normal baselines: $n^{ref} \coloneqq \mathrm{argmin}_i |B_{i,\perp} - \langle \boldsymbol{B}_\perp \rangle|$, where $\boldsymbol{B}_\perp \coloneqq (B_{1,\perp}, \dots, B_{n,\perp})$ and $\langle \cdot \rangle$ represents the median operator.

- *Normal baseline and RFI quality criterion* (AUX-PPS parameters: "Geometry and RFI correction"). This criterion combines the normal baseline criterion with quality indicators from RFI. Set $\gamma_{i,RFI} \in [0,1]$ to be the average of the expected decorrelation map due to RFI patterns in the image, *i.e.*, the average over the image polarizations of the RFI indices described in Equation 3.10 (possibly, after cross-pol merging), the coregistration primary is selected as $n^{ref} \coloneqq \mathrm{argmin}_{i \in \Gamma_{RFI}} |B_{i,\perp} - \langle \boldsymbol{B}_\perp \rangle|$ , where $\langle \boldsymbol{B}_\perp \rangle$ is defined as in the normal baseline criterion (see above) and $\Gamma_{RFI} \coloneqq \{i = 1, \dots, N \,|\, \gamma_{i,RFI} \geq \gamma_{RFI}^{ref}\}$, that is the subset of images whose RFI indices are above a user defined threshold. In other words, this criterion restricts the normal baseline criterion to the images that have low RFI disturbances.

- *Normal baseline and FR quality criterion* (AUX-PPS parameters: "Geometry and FR correction"). Similarly to the normal baseline and RFI quality criterion, the normal baseline selection is restricted to the images that have low FR disturbances, that is $n^{ref} \coloneqq \mathrm{argmin}_{i \in \Gamma_{FR}} |B_{i,\perp} - \langle \boldsymbol{B}_\perp \rangle|$ , where $\langle \boldsymbol{B}_\perp \rangle$ is defined as in the normal baseline criterion and $\Gamma_{FR} \coloneqq \{i = 1, \dots, N \,|\, \gamma_{i,FR} \geq \gamma_{FR}^{ref}\}$. The Faraday Rotation quality index $\gamma_{i,FR} \in [0,1]$ is defined as the following decorrelation index:

$$\gamma_{i,FR} \coloneqq \sqrt{\frac{1}{2\sigma_{i,FR}^2 + 1}}, \tag{3.17}$$

  with $\sigma_{i,FR}^2$ being the variance of the Faraday Rotation (phase screen) estimated by the L1 processor.

- *Normal baseline and RFI & FR quality criterion* (AUX-PPS parameters: "Geometry and RFI+FR correction"). Similarly to the normal baseline and the quality criteria above, the normal baseline selection is restricted to the images that have both low RFI disturbances and low FR disturbances, that is $n^{ref} \coloneqq \mathrm{argmin}_{i \in \Gamma_{RFI \wedge FR}} |B_{i,\perp} - \langle \boldsymbol{B}_\perp \rangle|$ , where $\langle \boldsymbol{B}_\perp \rangle$ is as in the normal baseline criterion and $\Gamma_{RFI \wedge FR} \coloneqq \Gamma_{RFI} \cap \Gamma_{FR}$, with $\Gamma_{RFI}$ and $\Gamma_{FR}$ defined in previous points.

Note that the selected criteria are also annotated in the stack for quality control, we refer to the L1_PFD for more details on how the AUX-PPS parameters map onto the L1c annotations.

### 3.3.4. Contingency Handling

Two contingency cases can be encountered by the stack processor in selecting the coregistration primary image:

- No image satisfies the quality criteria based on Faraday Rotation and/or RFI's (formally, $\Gamma_{RFI}$ and/or $\Gamma_{FR}$ may be empty sets). In such a case, the processor fallbacks to the normal baseline criterion.
- The L1 processor may have processed the input stack with no RFI estimation or no FR estimation (or both). In such cases, images with missing quality indices are treated as images with acceptable RFI or FR disturbances. More formally, if no RFI mask (FR phase screen) is computed for image $i$, $\gamma_{i,RFI}$ ($\gamma_{i,FR}$) is set to 1, hence always above threshold. Note that if the entire stack lacks RFI (FR) estimations, the normal baseline and quality RFI (FR or RFI&FR) criterion is equivalent to the normal baseline criterion.

## 3.4. Geometrical Quantity Upsampling

This step reconstructs the height of the scattering surface of the coregistration primary image from a sub-sampled version of Lat-Lon-Height LUTs. Henceforth we will generally refer to the height of the scattering surface as DEM. The DEM will be a 3-channel 2D image containing the ECEF coordinates (1 for channel) in the sampling grid the coregistration primary image.

### 3.4.1. Overview

The algorithm takes as input the sub-sampled Lat-Lon-Height LUTs related to the selected primary image, and performs an up-sampling through an interpolation method. After that, the reconstructed DEM is obtained by the conversion from Lat-Lon-Height to XYZ ECEF coordinates.

### 3.4.2. Inputs and Outputs

**Inputs**

| Symbol | Name | Origin | Size | Variability | Default | Description |
|---|---|---|---|---|---|---|
| | latitude | L1a | $[N'_{az} \times N'_{rg}]$ | 1 | - | The latitude LUT |
| | longitude | L1a | $[N'_{az} \times N'_{rg}]$ | 1 | - | The longitude LUT |
| | height | L1a | $[N'_{az} \times N'_{rg}]$ | 1 | - | The altitude LUT |
| | relativeAzimuthTimeRGC | L1a | $[1 \times N'_{az}]$ | 1 | - | The LUT's azimuth time axis |
| | slantRangeTimeRGC | L1a | $[1 \times N'_{az}]$ | 1 | - | The LUT's range time axis |
| | referenceAzimuthTime | L1a | UTC value | 1 | - | The reference time for all LUTs |

**Outputs**

| Symbol | Name | Destination | Size | Variability | Default | Description |
|---|---|---|---|---|---|---|
| | latitude | L1c | $[N_{az} \times N_{rg}]$ | 1 | - | The latitude LUT upsampled on the grid on the coregistration primary data |
| | longitude | L1c | $[N_{az} \times N_{rg}]$ | 1 | - | The longitude LUT upsampled on the grid on the coregistration primary data |
| | height | L1c | $[N_{az} \times N_{rg}]$ | 1 | - | The altitude LUT upsampled on the grid on the coregistration primary data |
| | XYZ | [BREAKPOINT] | $[N_{az} \times N_{rg}]$ | 1 | - | DEM product, *i.e.* 3 channel product containing a fill resolution upsampled DEM. |

### 3.4.3. Mathematical Description

Given an image $I_i$ which axis are $t_{X_i}$ and $t_{Y_i}$ for the columns and rows direction respectively, it is possible to perform an up-sapling though interpolation. The axis of the interpolated image $I$ will be $t_X$ and $t_Y$, which steps will be lower than the steps of $t_{X_i}$ and $t_{Y_i}$, so for each $t_X(k)$ and $t_Y(k)$ the value $I\left(t_Y(k), t_X(k)\right)$ will be evaluated using a bi-cubic kernel. In image processing, bi-cubic interpolation is often chosen over bilinear or nearest-neighbor interpolation in image resampling; in contrast to bilinear interpolation, which only takes 4 $(2 \times\ 2)$ pixels into account, bi-cubic interpolation considers 16 pixels (4x4).

**Note about the bi-cubic interpolation**. Suppose the function $f$ and the derivatives $f_x$, $f_y$ and $f_{xy}$ are knownat the four corners $(0,0), (1,0), (0,1)$ and $(1,1)$ of the unit square. The interpolated surface can be written as

$$p(x,y) = \sum_{i=0}^{3} \sum_{j=0}^{3} a_{ij} x^i y^j \qquad (3.17)$$

The interpolation problem consists of determining the 16 coefficients $a_{ij}$; matching $p(x,y)$ with the function values yields four equations:

$$f(0,0) = p(0,0) = a_{00} \qquad (3.18)$$

$$f(1,0) = p(1,0) = a_{00} + a_{10} + a_{20} + a_{30} \qquad (3.19)$$

$$f(0,1) = p(0,1) = a_{00} + a_{01} + a_{02} + a_{03} \qquad (3.20)$$

$$f(1,1) = p(1,1) = \sum_{i=0}^{3}\sum_{j=0}^{3} a_{ij} \tag{3.21}$$

Likewise, eight equations for the derivatives in the $x$ and $y$ directions:

$$f_x(0,0) = p_x(0,0) = a_{10} \tag{3.22}$$
$$f_x(1,0) = p_x(1,0) = a_{10} + 2a_{20} + 3a_{30} \tag{3.23}$$
$$f_x(0,1) = p_x(0,1) = a_{10} + a_{11} + a_{12} + a_{13} \tag{3.24}$$
$$f_x(1,1) = p_x(1,1) = \sum_{i=1}^{3}\sum_{j=0}^{3} i a_{ij} \tag{3.25}$$
$$f_y(0,0) = p_y(0,0) = a_{01} \tag{3.26}$$
$$f_y(1,0) = p_y(1,0) = a_{01} + a_{11} + a_{21} + a_{31} \tag{3.27}$$
$$f_y(0,1) = p_y(0,1) = a_{01} + 2a_{02} + 3a_{03} \tag{3.28}$$
$$f_y(1,1) = p_y(1,1) = \sum_{i=0}^{3}\sum_{j=1}^{3} j a_{ij} \tag{3.29}$$

And four equations for the $xy$ mixed partial derivative:

$$f_{xy}(0,0) = p_{xy}(0,0) = a_{11} \tag{3.30}$$
$$f_{xy}(1,0) = p_{xy}(1,0) = a_{11} + 2a_{21} + 3a_{31} \tag{3.31}$$
$$f_{xy}(0,1) = p_{xy}(0,1) = a_{11} + 2a_{12} + 3a_{13} \tag{3.32}$$
$$f_{xy}(1,1) = p_{xy}(1,1) = \sum_{i=1}^{3}\sum_{j=1}^{3} ij a_{ij} \tag{3.33}$$

This procedure yields a surface $p(x, y)$ on the unit square $[0,1] \times [0,1]$ that is continuous and has continuous derivatives; bi-cubic interpolation on an arbitrarily sized regular grid can then be accomplished by patching together such bi-cubic surfaces, ensuring that the derivatives match on the boundaries. Grouping the unknown parameters $a_{ij}$ in a vector

$$\alpha = [a_{00}, a_{10}, a_{20}, a_{30}, a_{01}, a_{11}, a_{21}, a_{31}, a_{02}, a_{12}, a_{22}, a_{32}, a_{03}, a_{13}, a_{23}, a_{33}]^T \tag{3.34}$$

and letting

$$\begin{aligned} b = [&f(0,0), f(1,0), f(0,1), f(1,1), \\ &f_x(0,0), f_x(1,0), f_x(0,1), f_x(1,1), \\ &f_y(0,0), f_y(1,0), f_y(0,1), f_y(1,1), \\ &f_{xy}(0,0), f_{xy}(1,0), f_{xy}(0,1), f_{xy}(1,1)]^T \end{aligned} \tag{3.35}$$

the above system of equations can be reformulated into a matrix for the linear equation

$$A\,\alpha = b, \tag{3.36}$$

which allows α to be calculated quickly and easily.

# 4. Stacking

In this section we will describe in detail the stacking operation, which consists in aligning both the data and the LUTs of a set of L1a input frames onto a common grid that is chosen to be the grid of the primary frame. The stacking module executes three main steps:

- *Estimation* of the pixel shifts between the L1a input frame and the coregistration primary L1a frame. This step can be executed by only using the sole information of the frames' orbits and scattering surface height (coregistration from *Geometry*), or applying a further refinement using incoherent cross-correlation applied to the actual frame data (coregistration using *Geometry and Data*)
- *Image interpolation*, which consists of warping the stack images onto the primary grid by means of the coregistration shifts computed at the previous step (see Fig. 7).
- LUT shifting and interpolation, which, similarly to the image interpolation step, warps the LUTs contained in the L1a input stack onto the common primary LUT grid.

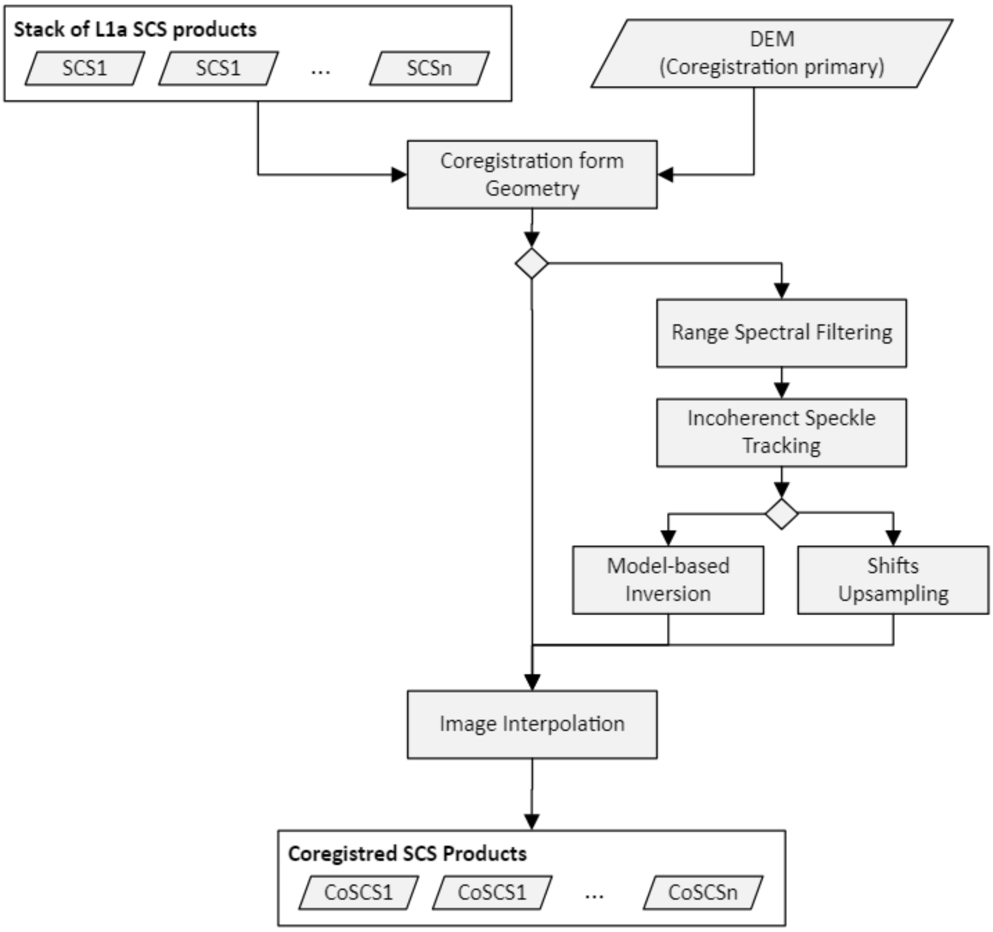


**Fig.7**

Complete flow-chart of the coregistration processor.

## 4.1. Coregistration from Geometry via Inverse Geocoding

This module is responsible for computing the shifts needed to interpolate an image in input ($SCS_n$) to the grid defined by the geometry acquisition of the coregistration primary image ($SCS_r$) using the information of the height of the scattering surface (DEM) and the orbit information contained in the input L1a products.

### 4.1.1. Overview

The algorithm for coregistration from geometric information uses the orbits and a model of the topography, *i.e.* the world model obtained by upsampling the Lat/Lon/Height LUTs from the L1a input stack (see Section 3.4.1), in order to calculate for each pixel the relative pixel distance or, equivalently, the time difference, between the primary and secondary acquisitions.

### 4.1.2. Inputs and outputs

**Inputs**

| Symbol | Name | Origin | Size | Variability | Default | Description |
|---|---|---|---|---|---|---|
| $SCS_n$ | | Cross-pol merging step | M stack images of size $[N_{az} \times N_{rg}]$ | M=3 (INT) or M=7 (TOM) matrices with 3 or 4 polarizations | - | The input stack |
| DEM | | Upsampling step | 1 image of size $[N_{az} \times N_{rg}]$ | M=3 (INT) or M=7 (TOM) single channel matrices | - | Height of scattering surfaces of the input stack |
| | flatteningPhaseBiasCompensationFlag | AUX_PPS (AIX_FMT) | Bool switch | True/False | False | Optionally, compensate phase residuals due to residuals in DEM upsampling |

**Outputs**

| Symbol | Name | Destination | Size | Variability | Default | Description |
|---|---|---|---|---|---|---|
| $CoSCS_n$ | | [BREAKPOINT] Stacking and calibration module | M images of size $[N_{az} \times N_{rg}]$ | M=3 (INT) or M=7 (TOM) matrices with 3 or 4 polarizations | - | The coregistered images. This is a breakpoint file onky if coreg mode is Geometry. |

| Symbol | Name | Destination | Size | Variability | Default | Description |
|---|---|---|---|---|---|---|
| $\tau_{rg}^{n}$ | | [BREAKPOINT] Stacking and calibration module | M images of size $[N_{az} \times N_{rg}]$ | M=3 (INT) or M=7 (TOM) matrices with 3 or 4 polarizations | - | The coregistration shifts in range component. This is a breakpoint file only if coreg mode is Geometry. |
| $\tau_{az}^{n}$ | | [BREAKPOINT] Stacking and calibration module. | M images of size $[N_{az} \times N_{rg}]$ | M=3 (INT) or M=7 (TOM) matrices with 3 or 4 polarizations | - | The coregistration shifts in azimuth component. This is a breakpoint file only if coreg mode is Geometry. |
| $\Delta\varphi_n$ | | [BREAKPOINT] Coregistration Step, L1c, and remainder of the stacking | M of size $[N_{az} \times N_{rg}]$ | M=3 (INT) or M=7 (TOM) each with a single channel | - | Synthetic phases from DEM associated to each acquisition. |
| $k_z$ | | [BREAKPOINT] Calibration and L1c product | M of size $[N_{az} \times N_{rg}]$ | M=3 (INT) or M=7 (TOM) each with a single channel | - | Vertical wavenumbers associated to each frame. |

## 4.1.3. Mathematical Description

### 4.1.3.1. Inverse Geocoding

By *inverse geocoding*, we refer to the procedure of retrieving the azimuth and range time $\tau_{az}$ and $\tau_{rg}$ at which a target point on the Earth is imaged by the sensor. Inverse geocoding is typically associated with the *direct geocoding* operation, which is the procedure of inferring the ECEF coordinates of a point onto the Earth surface with respect to an elevation model at at the time which the sensor imaged that target point. For more details we refer to [RD20]. Note that in the stack processor only inverse geocoding is executed since the results of direct geocoding for the input stack are assumed to be stored as Lat/Lon/Height LUTs in the L1a input products and mapped onto the primary grid data via oversampling as described in Section 3.4.

### 4.1.3.2. Coregistration Shift's Estimation

The purpose of this step is to compute the coregistration shifts expected from the acquisition geometry. This result is accomplished via *inverse geocoding* (see Section 4.1.3.1). More in detail, each pixel of the primary image is associated to its azimuth and range time coordinates:

$$[\tau_{az}, \tau_{rg}]^{r}(i,j) \tag{4.1}$$

that represent the (i-th, j-th) element of the primary data matrix. Since, each point $\boldsymbol{P}(i,j)$ of the DEM scattering surface (see Section 3.4), is assumed to be obtained by an approximation of the directed geocoded surface computed upstream of the stack processor, the location is inversely geocoded using orbit data of *n*-th secondary image to obtain azimuth and range times

$$[\tau_{az}, \tau_{rg}]^n(i,j). \tag{4.2}$$

Accordingly, the values of azimuth and range times are converted to pixels accordingly by setting

$$\begin{cases} s_{az}^n(i,j) = \dfrac{\left(\tau_{az}^n(i,j) - \tau_{az,0}^n\right)}{\Delta\tau_{az}^n} \\ s_{rg}^n(i,j) = \dfrac{\left(\tau_{rg}^n(i,j) - \tau_{rg,0}^n\right)}{\Delta\tau_{rg}^n} \end{cases} \tag{4.3}$$

where $[\tau_{az,0}, \tau_{rg,0}]^n$ are the acquisition start times and $[\Delta\tau_{az}, \Delta\,\tau_{rg}]^n$ are the acquisition sampling times of the n-th secondary image. The pixel shifts are then obtained as $s_{az}^n(i,j) - s_{az}^r(i,j)$ and $s_{rg}^n(i,j) - s_{rg}^r(i,j)$. Note that all the range times ($\tau_{rg}$) in this section refer to the two-way delay.

#### 4.1.3.3. Synthetic Interferogram Computation and Debiasing

By *synthetic interferogram* $\Delta\varphi_{\mathrm{syn,n,r}}$ (or henceforth *DSI*), we refer to the difference, expressed as a phase delay, of the absolute LOS distances at 0-Doppler between a ground target and the orbital positions of the RADAR in two acquisitions. The purpose of this step is to provide the geometrical quantities that are necessary to flatten the raw interferograms, that is, to remove all possible contributions of the DEM, and thus to make it easier for the calibration modules to isolate other possible sources of phase delays, such as ionosphere or baseline errors. For this, we use the results of the coregistration shifts as described in Section 4.1.3.2., that is, set $\tau_{rg}^r$ and $\tau_{rg}^n$ to be respectively the range time coordinates of primary and secondary frames, computed via inverse geocoding, it is straightforward to compute the distance between the two sensors and the ground target and accordingly convert it into phase delay by applying the following pixelwise conversion:

$$\Delta\varphi_{\mathrm{syn,n},r}(i,j) = 2\pi \cdot f_c \cdot (\tau_{rg}^n(i,j) - \tau_{rg}^r(i,j)) \tag{4.4}$$

where $f_c$ is the central (carrier) frequency. Note that, since the DEM is computed upstream of the stack processor (i.e., on L1a) on a grid that is not necessarily that of the coregistration primary frame, it follows that all inversely geocoded times $\tau_{rg}^{n}(i,j)$ (including those of the coregistration primary) may reflect the interpolation residuals[2] between the directly geocoded Earth surface and the DEM obtained via upsampling the L1a LUTs (see Section 3.4). Nonetheless, it can be observed that such an error is in fact approximately a common bias in all image frames and can be therefore estimated by inversely geocoding the coregistration primary[3]. Therefore, using as coregistration primary times $\tau_{rg}^{r}(i,j)$ in Equation 4.4 those obtained by inversely geocoding the DEM onto the orbit of the coregistration primary frame, the bias induced by the DEM upsampling can be compensated and the method described in Equation 4.6 is still sufficiently accurate and within the scope of the applications of the BPS stack processor. This bias removal can nonetheless be disabled by user via AUX_PPS.

Note that, owing to Equation 4.6, a "+" convention is required for compensating the contribution of the DEM in a coregistered image. More formally, as

$$CoSCS(i,j) \cdot \exp\{+j\,\Delta\varphi_{syn,n,r}(i,j)\}. \tag{4.4}$$

Synthetic interferograms are annotated in the L1c products as the *flatteningPhaseScreen* LUT.

#### 4.1.3.4. Vertical Wavenumber Computation

We compute the vertical wavenumbers $k_z$ for n-th frame as follows:

$$k_z(i,j) = \frac{4\pi}{\lambda} \cdot \frac{B}{d(i,j) \cdot \sin\vartheta\,(i,j)} = \frac{4\pi}{\lambda} \cdot \frac{\Delta\theta(i,j)}{\sin\vartheta(i,j)}, \tag{4.5}$$

where:

- $B$ is normal baseline between the coregistration primary and the n-th image.
- $d(i,j)$ is the 0-Doppler distance of the coregistration primary image.
- $\Delta\theta$ is the off-nadir difference[4] between the coregistration primary and the n-th image.

---

[2] Note that the residuals are only due the fact that the input L1a data has been direct geocoded by the L1_P on a grid that is not that of the data. STA_P always use the same elevation model used by L1_P, since the elevation model is stored in the L1a product as a LUT annotation.

[3] As a matter of principle, if the DEM were obtained by directly geocoding the sampling times of the coregistration primary, it would not be necessary to inverse geocode it with respect to the coregistration primary, since direct and inverse geocoding are indeed inverse operations. Hence, that would exactly return the range sampling times of the primary frame.

[4] Note that $\Delta\theta$ (relative look angle) equals $\Delta\vartheta$, that is, the relative incidence angles between primary and secondary image. Also, note that the $\Delta\theta$ is used as an approximation of the exact value $\sin(\Delta\theta)$ since $\Delta\theta \ll 1$.

- $\vartheta$ is the incidence angle of the n-th image.

## 4.2. Residual Coregistration from Data

The purpose of this step is to estimate the coregistration shifts via data cross-correlation. To obtain local shift estimations using data cross-correlation, the two images are divided into blocks. For each block, range and azimuth shifts are estimated, looking for the amplitude cross-correlation maximum.

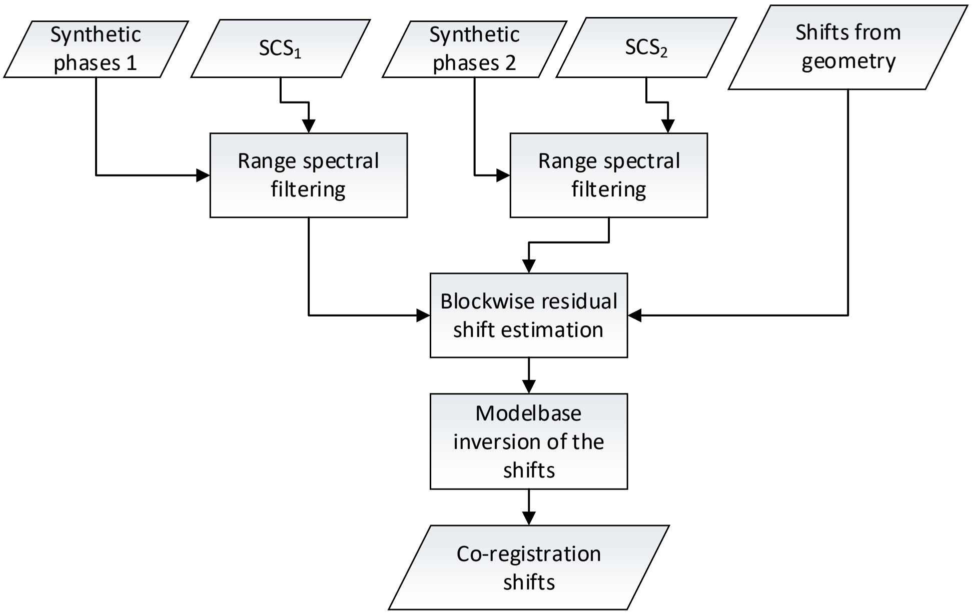


**Fig.8**

Coregistration from data.

### 4.2.1. Incoherent Speckle Tracking

The incoherent speckle tracking step exploits the cross correlation between two SAR images to estimate a refinement of the shifts computed from geometry.

#### 4.2.1.1. Inputs and Outputs

**Inputs**

| Symbol | Name | Origin | Size | Variability | Default | Description |
|---|---|---|---|---|---|---|
| $SCS_{n,m}$ | | Stacking | 2 stack images of size $[N_{az} \times N_{rg}]$ | 2 | - | A stack primary/secondary SCS interferometric pair |

| Symbol | Name | Origin | Size | Variability | Default | Description |
|---|---|---|---|---|---|---|
| $\tau_{rg}$ | | Stacking | 1 image of size $[N_{az} \times N_{rg}]$ | 1 | - | The coregistration shifts in range component |
| $\tau_{az}$ | | Stacking | 1 image of size $[N_{az} \times N_{rg}]$ | 1 | - | The coregistration shifts in azimuth component |
| | blockQualityThreshold | AUX_PPS (AUX_FMT) | Float value | 0 – 1 | 0.0 | Threshold on the block quality estimation to consider the shifts estimated on an estimation block valid. |

**Outputs**

| Symbol | Name | Destination | Size | Variability | Default | Description |
|---|---|---|---|---|---|---|
| $W_{n,m}$ | coregistrationShiftsQuality | Stacking | 1 image of size $[N'_{az} \times N'_{rg}]$ | 1 | - | Matrix of estimation accuracies (all values between [0, 1]). |
| $s_{az}$ | - | [BREAKPOINT] Stacking | 1 image of size $[N'_{az} \times N'_{rg}]$ | 1 | - | Coregistration shifts in azimuth direction (orbit + cross-correlation) |
| $s_{rg}$ | - | [BREAKPOINT] Stacking | 1 image of size $[N'_{az} \times N'_{rg}]$ | 1 | - | Coregistration shifts in range direction (orbit + cross-correlation) |

### 4.2.1.2. Mathematical Description

As well known, cross-correlation is a measure of the similarity of two signals as a function of mutual displacement. If we model the intensity of the blocks of the two images, $B^1_{n,m}$ and $B^2_{n,m}$ as continuous functions of azimuth time $\tau_{az}$ and range time $\tau_{rg}$ (translated by the shifts from geometry), the 2D cross-correlation can be defined as:

$$\begin{aligned} XC_{n,m}(a,r) &= \iint_{-\infty}^{\infty} B^1_{n,m}(a+\tau_{az}, r+\tau_{rg}) \\ &\quad \cdot \left(B^2_{n,m}(\tau_{az},\tau_{rg})\right)^* d\tau_{az} d\tau_{rg} \\ &= \left(B^2_{n,m}(-a,-r)\right)^* * B^1_{n,m}(a,r) \end{aligned} \tag{4.6}$$

where $*$ is the symbol for convolution of continuous signals. The equivalent definition in frequency domain is more convenient in terms of implementation:

$$F\left(XC_{n,m}(a,r)\right) = F(B^1_{n,m}(a,r)) \cdot F^*(B^2_{n,m}(a,r)) \tag{4.6}$$

Where $F(\cdots)$ is the Fourier Transform of the data and $(\cdots)^*$ is the complex conjugate operator.

To reduce the aliasing that is inherent in computing cross-correlation on amplitude via Fourier Transform, an oversampling that doubles the number of samples is performed prior to the actual computation of the cross-correlation matrix.

The cross-correlation estimate of the local coregistration shifts is defined as the block displacement that corresponds to the maximum of the cross-correlation matrix:

$$[s_{az}, s_{rg}](n,m) = \underset{a,r}{\operatorname{argmax}}\left(XC_{n,m}(a,r)\right) \tag{4.8}$$

The final coregistration shifts are the sum of the shifts from geometry plus the shifts estimated by the cross-correlation.
To each cross-correlation shift estimate is associated a measure $W(n,m) \in [0,1]$ of the estimation accuracy. Shift estimation accuracy is derived from two quantities: first-to-second cross-correlation peak ratio $(p2p(n,m))$ and SNR ratio between the cross-coregistration power inside the maximum search window and power inside the remaining outer rim of $XC_{n,m}$ $(snr(n,m))$

$$W(n,m) = \frac{p2p(n,m) \cdot snr(n,m)}{1 + p2p(n,m) \cdot snr(n,m)}, \tag{4.9}$$

The shifts estimated in a block are considered valid if $W(n,m)$ is above a quality threshold specified by AUX_PPS (*blockQualityThreshold*). The matrix $W(n,m)$ is written in the quality LUTs of the stack.

At this stage, the Stack Processor allow for two possible approaches for estimating the final coregistration shifts from those estimated in Equation (4.12):

- Upsample the coregistration shifts to the primary grid (see Section 4.2.3)
- Use a model-based inversion of the shifts (see Section 4.2.4)

The selection of the method is left to the user and it is configurable via the AUX_PPS parameter *modelBasedFitFlag*. By default, Stack Processor uses not model-based inversion.

## 4.2.2. Upsampling of the Coregistration Shifts

In this modality, the coregistration shifts in Equation (4.12) are filtered with a low-pass filter using either a boxcar or a Gaussian kernel, as specified by the AUX_PPS parameter *lowPassFilterType* and then upsampled to the full extent of the coregistration primary grid using a linear interpolation. Since the operation is trivial, we simply report the Inputs and Outputs table in the section below to give an overview of the parameters configurable via AUX_PPS.

### 4.2.2.1. Inputs and Outputs

**Inputs**

| Symbol | Name | Origin | Size | Variability | Default | Description |
|---|---|---|---|---|---|---|
| $s_{az}$ | - | Stacking | 1 image of size $[N'_{az} \times N'_{rg}]$ | M=3 (INT) or M=7 (TOM) each | - | Coregistration shifts in azimuth |

| Symbol | Name | Origin | Size | Variability | Default | Description |
|---|---|---|---|---|---|---|
| | | | | with a single channel | | direction (orbit + cross-correlation) |
| $s_{rg}$ | - | Stacking | 1 image of size $[N'_{az} \times N'_{rg}]$ | M=3 (INT) or M=7 (TOM) each with a single channel | - | Coregistration shifts in range direction (orbit + cross-correlation) |
| | lowPassFilterType | AUX_PPS | | Average Gaussian | Average | Kernel of the low-pass filter utilized before upsampling. |
| | lowPassFilterOrder | AUX_PPS | Integer value | $1 - \infty$ | 9 | Window size of the boxcar filter used in case “Average” is selected as low-pass filter method. |
| | lowPassFilterStdDev | AUX_PPS | Float value | $0 - \infty$ | 0.840892 | Standard deviation of the Gaussian kernel used in case the selected low-pass filter is “Gaussian” |

**Outputs**

| Symbol | Name | Destination | Size | Variability | Default | Description |
|---|---|---|---|---|---|---|
| $\tau_{az}$ | | [BREAKPOINT] Stacking | M images of size $[N_{az} \times N_{rg}]$ | M=3 (INT) or M=7 (TOM) each with a single channel | - | Coregistration shifts |
| $\tau_{rg}$ | | [BREAKPOINT] Stacking | M images of size $[N_{az} \times N_{rg}]$ | M=3 (INT) or M=7 (TOM) each with a single channel | - | Coregistration shifts |

## 4.2.3. Model-based Inversion of the Residual Shifts

With this modality, the final shifts are obtained  by a model-based inversion of the residual shifts estimated by the incoherent speckle tracking. This may mitigate the effect of artefacts in the data that may result in shifts that are not compatible with the underlying geometry of the acquisition.

### 4.2.3.1. Inputs and Outputs

**Inputs**

| Symbol | Name | Origin | Size | Variability | Default | Description |
|---|---|---|---|---|---|---|
| $W_{n,m}$ | coregistrationShiftsQuality | Stacking | M  images of size $[N'_{az} \times N'_{rg}]$ | M=3 (INT) or M=7 (TOM) each with a single channel | - | Map of mis-registration shifts |
| $M_{az}$ | azimuthMaxShift | AUX_PPS (AUX_FMT) | Float value | 1 | 5 | Maximum coregistration shift magnitude |

| Symbol | Name | Origin | Size | Variability | Default | Description |
|---|---|---|---|---|---|---|
| | | | | | | that can be estimated in azimuth direction |
| $M_{rg}$ | rangeMaxShift | AUX_PPS (AUX_FMT) | Float value | 1 | 5 | Maximum coregistration shift magnitude that can be estimated in range direction |
| $s_{az}$ | - | Stacking | 1 image of size $[N'_{az} \times N'_{rg}]$ | M=3 (INT) or M=7 (TOM) each with a single channel | - | Coregistration shifts in azimuth direction (orbit + cross-correlation) |
| $s_{rg}$ | - | Stacking | 1 image of size $[N'_{az} \times N'_{rg}]$ | M=3 (INT) or M=7 (TOM) each with a single channel | - | Coregistration shifts in range direction (orbit + cross-correlation) |

**Outputs**

| Symbol | Name | Destination | Size | Variability | Default | Description |
|---|---|---|---|---|---|---|
| $\tau_{az}$ | | [BREAKPOINT] Stacking | M images of size $[N_{az} \times N_{rg}]$ | M=3 (INT) or M=7 (TOM) each with a single channel | - | Coregistration shifts |
| $\tau_{rg}$ | | [BREAKPOINT] Stacking | M images of size $[N_{az} \times N_{rg}]$ | M=3 (INT) or M=7 (TOM) each with a single channel | - | Coregistration shifts |

### 4.2.3.2. Mathematical Description

The model of the mis-registration shifts both the error in the annotated orbits and the residual fast-time delay, which is due to the possible presence of a background ionosphere.
The model for the mis-registration in range direction reported in the following equation depends on the squint angle ($\psi$), the look angle of the image ($\theta$) and the vector of the baseline error ($[\delta B_x, \delta B_y, \delta B_z]$):

$$\begin{aligned} s_{rg}(\tau_{az}, \psi, \theta) = \ & sin(\psi) \cdot \delta B_x(\tau_{az}) + \\ & - \cos(\psi) \cdot \sin(\theta) \cdot \delta B_y(\tau_{az}) + \\ & + \cos(\psi) \cdot \cos(\theta) \cdot \delta B_z(\tau_{az}) + \\ & + s_{rg}^{iono} \end{aligned} \quad (4.10)$$

where $s_{rg}^{iono}$ is the constant residual shift due to the background ionosphere.
Assuming at the most a linear baseline error in the image the general model of the baseline error valid for each component ($x, y$ and $z$) is:

$$\delta B(\tau_{az}) = \delta B_{const} + \tau_{az} \cdot \delta B_{linear} \, . \quad (4.11)$$

As for the mis-registration in azimuth direction ($S_{az}$), the combination of a constant and a linear error (both in azimuth and in range) will be assumed:

$$S_{az}(\tau_{az}, \tau_{rg}) = m_{rg} \cdot \tau_{rg} + m_{az} \cdot \tau_{az} + s_{az} \,, \tag{4.12}$$

where $m_{rg}$ and $m_{az}$ are respectively the linear terms in range and azimuth directions, and $s_{az}$ is the constant component of the azimuth shifts.
The shifts will be inverted according to the model defined above using as weights the quality matrices $W(n, m)$, by utilizing an SVD approach with a standard cut-off value of $\epsilon \cdot \max(N, M)$, where

- $N$ and $M$ are respectively the number of blocks in azimuth and range
- $\epsilon$ is the machine precision of an IEEE-754 compliant 64-bit floating point format.

## 4.2.4. Model-based Shift Estimation Quality

The purpose of this step is to provide a quality measure of the model-based residual shifts. To flag images where the coregistration step is not accurate, the average quality of the fitting will be estimated.

### 4.2.4.1. Inputs and Outputs

**Inputs**

| Symbol | Name | Origin | Size | Variability | Default | Description |
|---|---|---|---|---|---|---|
| $r_{rg}$ | | Stacking | M images of size $[N'_{az} \times N'_{rg}]$ | M=3 (INT) or M=7 (TOM) each with a single channel | - | Difference between the fitted model and the shifts estimated from data-based coregistration in range direction (in pixels) for the reference polarization channel |
| $r_{az}$ | | Stacking | M images of size $[N'_{az} \times N'_{rg}]$ | M=3 (INT) or M=7 (TOM) each with a single channel | - | Difference between the fitted model and the shifts estimated from data-based coregistration in azimuth direction (in pixels) for the reference polarization channel |
| $M_{az}$ | azimuthMaxShift | AUX_PPS (AUX_FMT) | Float value | 1 | 5 | Maximum coregistration residual shift magnitude that can be estimated in azimuth direction |
| $M_{rg}$ | rangeMaxShift | AUX_PPS (AUX_FMT) | Float value | 1 | 5 | Maximum coregistration residual shift |

| Symbol | Name | Origin | Size | Variability | Default | Description |
|---|---|---|---|---|---|---|
| | | | | | | magnitude that can be estimated in range direction |
| | fittingQualityThreshold | AUX_PPS (AUX_FMT) | Float value | 0.0 – 1.0 | 0.0 | Threshold on the fitting quality index $Q_{shifts}$ to consider a coregistration valid |

**Outputs**

| Symbol | Name | Destination | Size | Variability | Default | Description |
|---|---|---|---|---|---|---|
| $Q_{shifts}$ | | Stacking | Float value | M=3 (INT) or M=7 (TOM) | - | Coregistration model's fitting quality |

### 4.2.4.2. Mathematical Description

The quality of the model-based shifts estimation can be measured using the following *fitting quality* metric.

$$Q_{shifts} \coloneqq \sqrt{Q_{shifts}^{az} \cdot Q_{shifts}^{rg}} \quad (4.11)$$

Where:

- $Q_{shifts}^{rg} \coloneqq \max(1 - \sigma_{r_{rg}}^2 / \sigma_{M_{rg}}^2,\ 0)$ and $Q_{shifts}^{az} \coloneqq \max(1 - \sigma_{r_{az}}^2 / \sigma_{M_{az}}^2,\ 0)$
- $\sigma_M^2$ is the variance of a uniform distribution over the interval $[-\frac{M}{2}, \frac{M}{2}]$ (*i.e.* $M^2/3$)
- $M$ is the maximum allowed coregistration residual between geometry coregistration and model-based fitting, as described in Equation 4.16 (range, or Equation 4.18 for azimuth counterpart). The quantities are expressed in pixels and defaulted to 5 but configurable via AUX_PPS___ for range and azimuth independently.
- $r_{rg}$ and $r_{az}$ are the difference between the fitted model and the shifts estimated from data-based coregistration in range and azimuth direction respectively (in pixels).

This parameter will be compared with a threshold in the AUX_PPS configuration file to identify frames which resulted in poorly estimated coregistration shifts.

### 4.2.4.3. Automatic Modality

The coregistration module exposes to the user the possibility to let the processor to automatically chose between coregistration from data and coregistration from geometry. We will henceforth call this coregistration modality *Automatic* mode.

Under Automatic mode, the coregistration model first attempts to the coregister the data using the coregistration with “geometry and data” mode and evaluates the coregistration by checking that the following conditions hold:

- The number of valid coregistration blocks is above a selected threshold. The threshold is specified by the user via AUX_PPS as the minimum number of valid blocks.

- $Q_{shifts}$ specified in Equation 4.17 is above a threshold also specified by the user via AUX_PPS (*fittingQualityThreshold*).

If one of the two conditions above failed, the coregistration results are discarded and the geometry-based estimated shifts are used as a fallback.

## 4.3. Image Interpolation

The aim of this procedure is to interpolate the complex image data onto the coregistration primary image grid, using the mapping information provided by the coregistration shifts.

### 4.3.1. Overview

Interpolation on the primary grid is performed in two steps. First, the coregistration primary image grid is divided into blocks and for each block a corresponding block is identified for the image to interpolate, using the mapping provided by coregistration shifts.

### 4.3.2. Inputs and Outputs

Inputs:

- Complex image data related to each secondary image
- Coregistration shifts related to each secondary image

Outputs:

- Complex image data of secondary image re-sampled on the same grid of the primary image

### 4.3.3. Mathematical Description

The values corresponding to each element of the primary image block are interpolated from the image block via a Global Least Square filter bank [RD22].
The filter bank is an ensemble of interpolating filters, each responsible for a specific sub-sample shift value, with customizable sub-sample precision. For each element of the block in the primary image, the interpolation algorithm chooses the filter in the bank that has the closest outcome to the desired shift.

## 4.4. Contingency Handling

In the unlikely event of an unexpected error occurring during stacking, the stack processor discards the secondary frames that resulted in a coregistration failure, and it will not pass them over to the remainder of the calibration chain. To do so, the stack processor re-packs the input stack, including a possible change of the index of the primary image. Although the stack processor attempts continuing its execution as much as possible, whenever stacking fails for all frames or a failure occurs in estimating quantities associated to the coregistration primary (*e.g.* absolute LOS absolute 0-doppler distances from satellite to ground), the execution of the stack processor terminates gracefully with an error code. Note that failures during stacking will not affect the possibility of resuming the stack processor if interrupted before the natural conclusion of the execution since all information associated with coregistration failures are cached in the stack processor's working directory.

## 4.5. LUT Shifting and Interpolation

The aim of this step is to align the input LUTs in the L1a onto the coregistration primary grid (or a sub-grid thereof) by using the coregistration shifted times output during the coregistration step. In this step, 2 possible output grids are considered:

- The *full resolution coregistration primary grid*, which is the common grid of all the L1c products output by the stack processor.
- The *subsampled primary LUT grid*, which is a subsampled version of the full resolution primary grid whose resolution is identical to that of the geometric LUTs (*i.e. latitude/longitude/height*) of the coregistration primary L1a frame. The default output resolution is approximately 90m x 90m.

Every LUT that will be exported in the L1c product will be shifted onto the subsampled primary grid with the sole exception of those associated to the IOS module (see Section 5.4), which are computed and annotated on a dedicated grid. Moreover, only some LUTs are shifted in full resolution, namely those that are required in some intermediate calibration steps (*e.g.* the L1 ionospheric phase screen for the IOB, see Section 5.2.2.1). Nonetheless, if such LUTs are also exported into the L1c products (*e.g.* the elevation angles), they are further subsampled onto the subsampled primary LUT grid before being exported in the L1c.

### 4.5.1. Algorithmic Overview

Before detailing the LUT shifting procedure we note that, for lack of a more intuitive word, with *shifting* we henceforth refer to the process of:

- Applying the coregistration shifts to a LUT in order to align it to the associated coregistrered/warped image.
- Possibly subsampling the aligned LUT to match a desired output resolution.

As it will soon be clear in the remainder of the section, shifting can be executed in a single operation.

Let us assume $L(i,j)$ be a LUT of size $N'_{az} \times N'_{rg}$, and let $T_{rg}(i,j)$ and $T_{az}(i,j)$ be respectively the $N_{az} \times N_{rg}$ matrices containing the adjusted azimuth and range times obtained via coregistration. Moreover, let $t_{az}^{L}$ and $t_{rg}^{L}$ be respectively the vectors of the azimuth and range sampling times (of size respectively $N'_{az}$ and $N'_{rg}$) associated to $L$. Let now $\Gamma[L]$ be an interpolator of $L$, that is:

$$\Gamma[L]: R \times R \rightarrow R$$
$$\Gamma[L]\left(t_{az}^{L}(i), t_{rg}^{L}(j)\right) \coloneqq L(i,j),\ \forall\, i,j, \tag{4.12}$$

and $i', j'$ a possibly regular subsampling of the indices $i$ and $j$. It is trivial to see that, owing to the definition of $T_{rg}$ and $T_{az}$, $L$ can be shifted into a new LUT $L^{|r}$ , aligned to the grid of the coregistration primary frame $r$, by evaluating $\Gamma[L]$ on the subsampled times, that is

$$L^{|r}(i',j') \coloneqq \Gamma[L]\left(T_{az}(i',j'), T_{rg}(i',j')\right). \tag{4.13}$$

Accordingly, shifting onto the *full resolution coregistration primary grid* is achieved by selecting the indices $i = i'$ and $j = j'$. Similarly, we shift onto the target *subsampled primary LUT grid* by selecting subsampling indices $i'$ and $j'$ that best approximate the target resolution (90m x 90m under default configuration of the L1a products).
In the context of coregistration with Geometry and Data, we only shift pixels that correspond to an estimation accuracy above a user selected threshold (see AUX_FMT, Table 67, *residualShiftsQualityThreshold*). For the other pixels, no shift is applied. That is achieved by setting $T_{az}(i,j) \coloneqq t_{az}^{L}(i,j)$ and $T_{rg}(i,j) \coloneqq t_{rg}^{L}(i,j)$ for each pixel $(i,j)$ so that $Q_{ij} < q_{thres}$.

Finally, note that if a LUT needs to be shifted onto the full resolution coregistration primary grid and later exported onto the subsampled primary LUT grid in the L1c product, the above operation can be performed in 2 separate steps with negligible runtime and memory overhead by first shifting onto the full resolution primary grid, obtaining the matrix $L^{|r}(i,j)$, and then by directly subsampling that matrix using indices $i'$ and $j'$.

### 4.5.2. Axes and Grids

All LUTs are defined over the same sampling grid except for the LUT that contains the fast-ionosphere phase screen and quality (see Section 5.4), henceforth called fast-ionosphere LUTs. The sampling grid for all LUTs except the fast-ionosphere-LUTs will be that of the DEM LUTs of the L1a product used as coregistration primary. Under default configuration of the L1_P processor, all stack LUTs, except for fast-ionosphere LUTs, will have a ground resolution of approximately 90m x 90m (range x azimuth), which is the resolution of the DEM used (Copernicus DEM). That is, all LUTs except the fast-ionosphere-LUTs will be defined on a grid obtained by subsampling the primary data grid using range and azimuth steps that best approximate the target resolution for each axis, irrespectively of the resolution of the LUTs in the source L1a products. For more details on LUT grids and axes, we refer to Section

6.3.4.1 of BPS_L1_PFD. All available LUTs in the stack are reported in Section 6.3.4 of BPS_L1_PFD.

# 5. Calibration

The purpose of the Calibration block is to obtain a stack of coregistered images which is self-consistent from the interferometric standpoint.
The key calibration task is to estimate possible residual ionospheric phase screens that may affect the coregistered stack images. To do so, we leverage the difference in sensitivity between Faraday Rotation, which is used by the L1 processor, and the phase component of the stack images, since the former is expected to be weaker compared to the latter.

An overview of the full stack calibration algorithms is reported in Figure 11 below. The Stack processor provides 4 calibration modules, namely:

- Common band filtering in azimuth direction, henceforth referred to as AZF. See Section 5.1
- Estimation and removal of the slowly varying residual ionospheric phase screen (see Section 5.2), henceforth referred to as the *IOB* module. See Section 5.2
- Calibrate the background phase residual via plane fitting and removal. This module is referred to as PPR and described in Section 5.3.
- Estimation and possibly compensation of ground-steering phase screen via the Sum of Kronecker Products (SKP) method. See Section 5.4.

Note that PPR and IOB are proved to be essentially equivalent, with PPR being more robust for larger baselines (*e.g.* above 35% of CB). The user is therefore recommended to avoid running the Stack Processor with both the module activated.

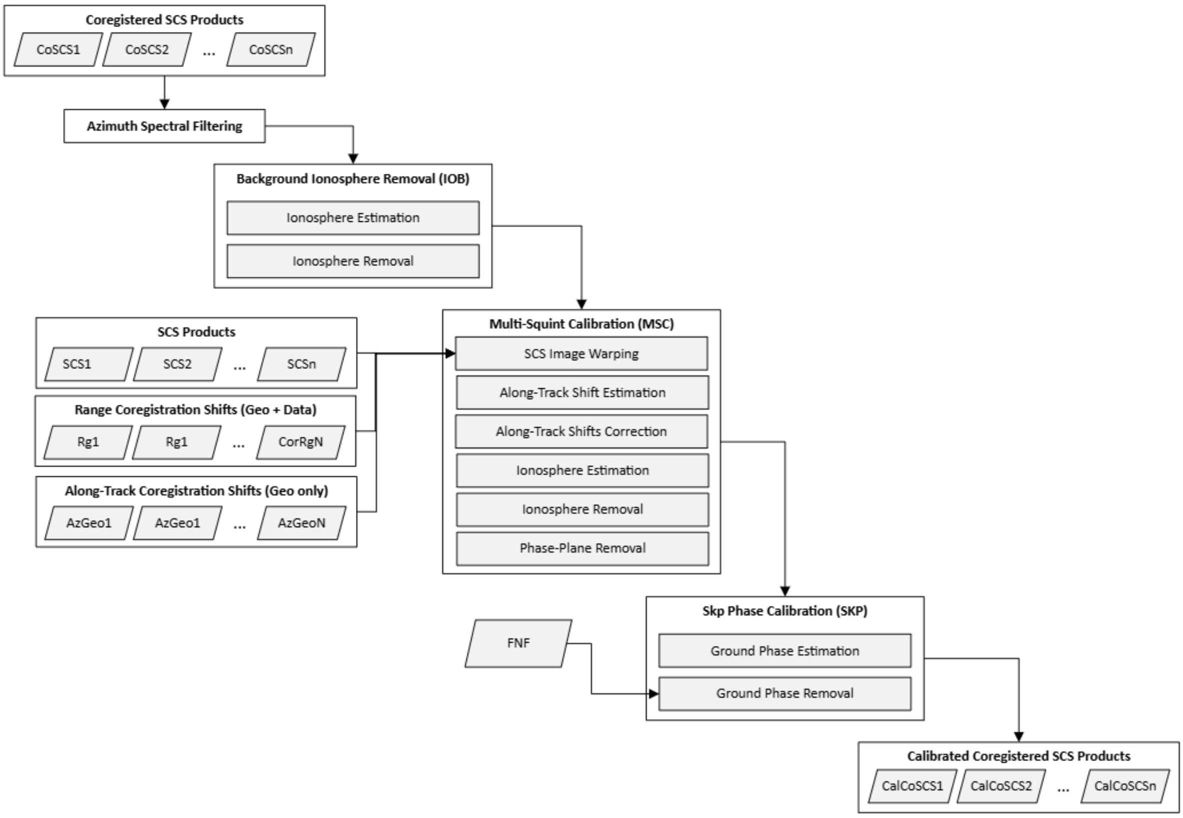


**Fig.9** Complete flow-chart of the calibration processor. Note that all steps can be optionally enabled/disabled by the user via AUX_PPS.

## 5.1. Azimuth Spectral Filtering

Due to the different Doppler centroids and viewing geometries caused by the satellite's along- and across-track baselines, two acquisitions may have non-overlapping spectral components. Therefore, a filtering operation may be required (as a matter of principle, in both directions) to ensure that the stack calibration processor uses only the common bandwidth. Such a filtering is expected to reduce the spectral decorrelation and prevents it to adversely affect the calibration procedure. Whereas range spectral filtering (see Sec. 0 for more details) is optionally applied independently in each relevant calibration module, the *Azimuth Spectral Filtering* (AZF) is provided as a standalone module that is optionally executed at the beginning of the entire calibration pipeline. By default, AZF is enabled but the user will have the option to disable it via configuration file (AUX_PPS___). The flow of the AZF is shown in the Fig. 12 below and its main steps are described in detail in the remainder of this section.

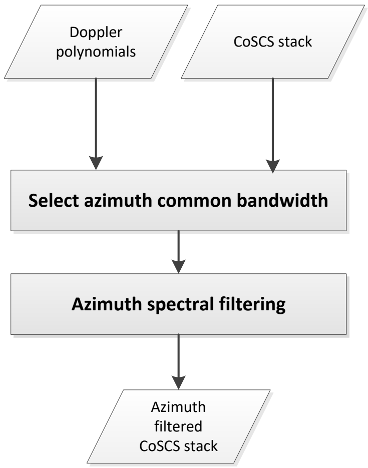


The AZF's flow diagram.

Fig.10

## 5.1.1. Inputs and Outputs

**Inputs**

| Symbol | Name | Origin | Size | Variability | Default | Description |
|---|---|---|---|---|---|---|
| $CoSCS$ | | Coregistration Step or AZF | M acquisition of size $[N_{az} \times N_{rg}]$ | M=3 (INT) or M=7 (TOM), each with 3 or 4 polarizations (2CP + 1XP or 2CP + 2XP) | - | Coregistered SCS frames |
| $\Delta\Phi$ | | Coregistration Step | M of size $[N_{az} \times N_{rg}]$ | M=3 (INT) or M=7 (TOM) each with a single channel | - | Synthetic phases from DEM associated to each acquisition |
| $f_D$ | | Coregistration Step | M of size $[1 \times N_{rg}]$ | M=3 (INT) or M=7 (TOM) vectors | - | Doppler centroids associated to each acquisition |
| | azimuthSpectralFilterFlag | AUX_PPS (AUX_FMT) | Boolean switch | True/False | True | Enable the AZF module |
| | usePrimarySpectralWeightingFlag | AUX_PPS (AUX_FMT) | Boolean switch | True/False | True | Use the azimuth spectral window of the coregistration primary as common spectral window |
| $W_\alpha$ | spectralWeightingWindow | AUX_PPS (AUX_FMT) | | Kaiser/Hamming | Hamming | A user defined common spectral window that is used for azimuth spectral windowing |
| $\alpha$ | spectralWeightingWindowParameter | AUX_PPS (AUX_FMT) | | $0 - \infty$ | | Parameter assiciated to the user provided window $W_\alpha$ |

**Outputs**

| Symbol | Name | Destination | Size | Variability | Default | Description |
|---|---|---|---|---|---|---|
| $CalCoSCS$ | | Stack Processor (next active module) or L1c output product | M acquisition of size $[N_{az} \times N_{rg}]$ | M=3 (INT) or M=7 (TOM), each with 3 or 4 polarizations (2CP + 1XP or 2CP + 2XP) | - | SCS with common bandwidth |
| $\overline{B}_{az,common}$ | azimuthCommomBandwidth | L1c output product | Float value [Hz] | 0.0 -- ∞ | - | Common bandwidth estimated by the AZF |
| $\overline{f}_{az,center}$ | azimuthCentralFrequency | L1c output product | Float value [Hz] | -∞ -- ∞ | - | Central frequency in azimuth estimated by the AZF |

## 5.1.2. Mathematical description

The AZF consists of two main components: Computing the common azimuth bandwidth and cropping the stack image spectrum to that common bandwidth. We will discuss the two in the following subsections.

### 5.1.2.1. Estimation of azimuth common bandwidth and central frequency

A range dependent common azimuth bandwidth is computed via

$$B_{\text{az,common}}[r] \coloneqq (B^{+}[r] - B^{-}[r]), \tag{5.1}$$

where

$$B^{+}[r] \coloneqq \min_{i \in \mathrm{N}} \left( f_{D,i}[r, \overline{t_{az}}] + \frac{B_{az,i}}{2} + \frac{1}{2\pi} \langle \frac{\partial \left( \Delta\Phi_i[t_{az}, r] - \Delta\Phi_p[t_{az}, r] \right)}{\partial t_{az}} \rangle \right) \tag{5.2}$$

and

$$B^{-}[r] \coloneqq \max_{i \in \mathrm{N}} \left( f_{D,i}[r, \overline{t_{az}}] - \frac{B_{az,i}}{2} + \frac{1}{2\pi} \langle \frac{\partial \left( \Delta\Phi_i[t_{az}, r] - \Delta\Phi_p[t_{az}, r] \right)}{\partial t_{az}} \rangle \right), \tag{5.3}$$

with $f_{D,i}$ and $B_{az,i}$ respectively the Doppler centroid and the processed azimuth bandwidth of the *i*-th image, $\overline{t_{az}}$ indicates the median azimuth time, $\lambda$ is the wavelength, *c* is the speed of light, $f_c$ is the RADAR's central (carrier) frequency, $p$ is the index of the coregistration primary image, $t_{az}$ is the azimuth time with respect to the image acquisition time, $\Delta\Phi_k$ are the synthetic phases of the *k*-th image, and $\langle\, . \,\rangle$ denotes the mean.

Set $\bar{r}$ to be the median range, the stack azimuth common bandwidth and the azimuth central frequency are defined as:

- $\overline{B}_{az,common} \coloneqq B_{az,common}[\bar{r}]$.

- $\bar{f}_{az,center} \coloneqq f_{az,center}[\bar{r}]$.

### 5.1.2.2. Spectral filtering

The spectral cropping component of the AZF can be summarized in the following steps, which are performed for each range bin of each image frame and for each frame polarization:

1. The azimuth lines of the image are zero-padded by rounding the number of samples to the next power of 2, that is:

$$I_i^{zp}(a,r) \coloneqq \begin{cases} CoSCS_i(a,r), & 0 \le a < N_{az} \\ 0, & N_{az} \le a < N_{zp} \end{cases} \tag{5.4}$$

   where $N_{az}$ is the number of the azimuth lines within the processed bandwidth and $N_{zp}$ is the number of zero-padded azimuth lines, defined as

$$N_{zp} \coloneqq \text{round}\left[2^{\left\lfloor \frac{\ln(N)}{\ln(2)} \right\rfloor}\right] \tag{5.5}$$

2. *Fourier transform* the azimuth line of the image ($I_i$).
3. 

$$I_i(f_a,r) \coloneqq \text{FFT}(I_i^{zp}(a,r)). \tag{5.6}$$

4. Multiply the line by the inverse of the azimuth weighting function $W_{foc}(r)$ that was used during image focusing:

$$I_i^{w}(f_a,r) \coloneqq I_i(f_a,r).\frac{1}{W_{foc}(r)} \ . \tag{5.7}$$

5. Roll the common spectral window to centre the spectrum at $f_{\text{az},center}[r] \coloneqq (B^+[r] + B^-[r])/2$, that is

$$I_i^{bb}(f_a;r) = I_i^{w}(f_a + f_{az,center}[r];r), \tag{5.8}$$

6. Multiply the line by the rolled common spectral window $W_c$, which can be either the window $W_{foc}$ used for focusing the data or a user provided window $W_\alpha$:

$$I_i^{cb}(f_a,r) \coloneqq \text{I}_i^{bb}(f_a,r) \cdot W_c(f_a + f_{az,center}[r]), \tag{5.9}$$

7. Apply the *inverse Fourier transform*:

$$I_i^{cb}(a;\, r) \coloneqq \mathrm{iFFT}\left(I_i^{cb}\left(f_a; r\right)\right), \tag{5.10}$$

8. Remove the 0-padding added at step 1:

$$CalCoSCS_i(a;r) = I_i^{cb}(a;r), \quad 0 \leq a < N_{az} \tag{5.11}$$

## 5.2. Slow-Varying Ionosphere Estimation and Removal

The *Slow-varying Ionosphere Removal* module (IOB) is an interferometric module that is responsible for detecting and correcting the low-pass phase artifacts caused by the interaction of the RADAR signal with the ionosphere, while ignoring other phase components that may derive from other sources of noise including the fast-varying ionosphere or baseline errors. The module consists of an interferometric estimator that executes a sequence of intermediate steps, which are described in detail in the remainder of the section and can be summarized as follows: Given an interferometric image pair,

1. Preprocess the two SCS images by whitening the range spectrum and removing the synthetic phases from DEM,
2. Compute range sub-looks by selecting bands at the extremities of the range spectrum (high/low range sub-looks),
3. Compute the interferometric coherences associated to the upper and lower sub-looks, and their phases,
4. Apply the *Split-Spectrum* method [RD9] on those phases to isolate the dispersive component of the ionosphere from the nondispersive one,
5. Estimate the slow-varying components of the ionosphere via *Least-Square* (LS) estimation of a phase plane on the entire swath.

It is important to note that at step 5 only a linear approximation of the ionosphere is computed. This descends from the fact that, due to the narrow bandwidth of the BIOMASS's RADAR system, only linear components of the ionospheric phase screens can be computed by the approach described in the previous steps 1 - 4.
Since the IOB core estimator is defined for an interferometric pair, to define an estimation for each stack image, we provide two (2) modalities, namely:

- *Single-baseline*: The estimated ionosphere is the ionosphere estimated for the sole interferometric image pair consisting of the image and the calibration reference (see below).
- *Multi-baseline* (default): Ionospheric phase screens are estimated for each possible image pair whose normal baseline does not exceed a user defined threshold, which is expressed as a percentage of the critical baseline and configurable via AUX_PPS. For each image a single phase-screen is defined via an optimality criterion based on least squares (LS). More details in the remainder of the section.

Note that the module is endowed with a set of configurable parameters (as reported in the Input table below or in the AUX_FMT document), most of which the reader will find self-explanatory as the method is outlined in detail. Among those, the noticeable non-trivial ones are:

- *latitudeThreshold*: As per physical (and experimental) evidence, slow-varying ionospheric effects are to be expected only at the low latitudes (tropical regions), thus it is reasonable to assume that it is better to skip any correction/estimation of the ionosphere at the high latitudes. This parameter specifies the threshold latitude (North/South) above/below which the IOB estimation is not executed.
- *calibrationPrimaryImage*: Since the module is interferometric, no absolute ionosphere can be estimated for any image. Consequently, to resolve the ambiguity, the existence of a reference ionosphere-free image must be assumed. As it will be described in the details in the next sections, no ionosphere (null phase screen) correction will be performed in any case for such reference image.
- *slowIonosphereQualityThreshold*: This parameter specifies a minimum estimation quality for the ionosphere to be corrected. Ionosphere estimations below this threshold value will be ignored.

Finally, note that since for the Single-baseline modality the slow-varying ionosphere estimator is equivalent to the results of the IOB interferometric estimator, we will identify the two and henceforth call the IOB estimator Single-baseline estimator.

## 5.2.1. Inputs and Outputs

**Input**

| Symbol | Name | Origin | Size | Variability | Default | Description |
|---|---|---|---|---|---|---|
| $CoSCS_n$ | | Coregistration Step or AZF | M acquisition of size $[N_{az} \times N_{rg}]$ | M=3 (INT) or M=7 (TOM), each with 3 or 4 polarizations (2CP + 1XP or 2CP + 2XP) | - | Coregistered SCS frames, possibly from previous calibration step (i.e. AZF) |
| $\Delta\Phi_n$ | | Coregistration Step | M of size $[N_{az} \times N_{rg}]$ | M=3 (INT) or M=7 (TOM) each with a single channel | - | Synthetic phases from DEM associated to each acquisition |
| $k_z$ | | Coregistration Step | M of size $[N_{az} \times N_{rg}]$ | M=3 (INT) or M=7 (TOM) each with a single channel | | Vertical wavenumbers |
| $\Delta\phi_{L1a}$ | | L1a and Coregistration step | M of size $[N_{az} \times N_{rg}]$ | M=3 (INT) or M=7 (TOM) | - | Ionospheric phase screen |

| Symbol | Name | Origin | Size | Variability | Default | Description |
|---|---|---|---|---|---|---|
| | | | | each with a single channel | | estimated by L1 processor and shifted onto the primary grid |
| $\delta_{\phi_{L1a}}$ | | L1a and Coregistration step | M of size $[N_{az} \times N_{rg}]$ | M=3 (INT) or M=7 (TOM) each with a single channel | | Spatial range shifts due to ionosphere estimated by the L1 processor and shifted onto the primary grid |
| $n^*$ | calibrationReferenceImage | Job_Order (*ProcParameter – calibration_primary_imge*) or AUX_PPS (*primaryImageFlag*). See Section 5.2.3.1 | Integer | 1 – M with M=3 (NT) or M=7 (TOM) | - | Index of the calibration reference image |
| | slowIonosphereRemovalFlag | AUX_PPS (AUX_FMT) | Boolean switch | True/False | True | Enable/disable the IOB module |
| $B_{sub}$ | rangeLookBandwidth | AUX_PPS (AUX_FMT) | Float value [%] | 0.0 – 1.0 | 0.3 | Percentage of bandwidth when computing the sub-looks |
| $f_{sub}$ | rangeLookFrequency | AUX_PPS (AUX_FMT) | Float value [%] | 0.0 – 0.5 | 0.3 | Percentage of frequency band when computing the sub-looks |
| | polarisationUsed[5] | AUX_PPS (AUX_FMT) | | HH / HV / VH / VV / XX | HH | Reference polarization used in the pre-processing step |
| | phaseUnwrappingFlag | AUX_PPS (AUX_FMT) | Boolean switch | True/False | True | Unwrap interferogram phase during single baseline estimation |
| | latitudeThreshold | AUX_PPS (AUX_FMT) | Float value [deg] | 0 - ∞ | 40.0 | Latitude (N/S) below (above) which IOB is skipped |
| | baselineMethod | AUX_PPS (AUX_FMT) | Literal | Multi-Basline, Single-Baseline | Mutli-Baseline | As to whether MB or SB estimation is executed |
| | unweightedMulitBaselineEstimation | AUX_PPS (AUX_FMT) | Boolean switch | True/False | False | In MB, equally weigh all estimations. If False, use weights from |

[5] Note that this parameter is configurable only at the calibration level and not module by module. In other words, the selected value is common to all calibration modules (but not necessarily the same used for coregistration).

| Symbol | Name | Origin | Size | Variability | Default | Description |
|---|---|---|---|---|---|---|
| | | | | | | the coherence map |
| | compensateL1PhaseScreenFlag | AUX_PPS (AUX_FMT) | Boolean switch | True/False | True | Pre-compensate phase screen correction from L1, if set to True |
| | sublookWindowAzimuthSize | AUX_PPS (AUX_FMT) | Float | 1 - ∞ | 201 | Number of looks in azimuth direction for computing the low/high sub-looks |
| | sublookWindowRangeSize | AUX_PPS (AUX_FMT) | Float | 1 - ∞ | 41 | Number of looks in direction range for computing the low/high sub-looks |
| | multiBaselineCriticalBaselineThreshold | AUX_PPS (AUX_FMT) | Float | 0 – 1 | 0.45 | In MB, Interferometric pairs with baseline exceeding this percentage of the critical baseline are ignored |
| $\theta_{PU}$ | maxDeltaPhaseUnwrapTest | AUX_PPS (AUX_FMT) | Float | 0 - ∞ | 0.5 rad | Threshold for the phase unwrapping test |
| $\theta_{\gamma}$ | minCoherenceThreshold | AUX_PPS (AUX_FMT) | Float | 0 – 1 | 0.0 | Threshold on the coherence that specifies which pixels should be used or not for phase-plane fitting. |
| $\theta_{PV}$ | minUsablePixelRatio | AUX_PPS (AUX_FMT) | Float | 0 – 1 | 0.05 | Minimum fraction of valid pixels according to coherence and phase unwrapping test to perform the phase-plane fitting |
| | slowIonosphereQualityThreshold | AUX_PPS (AUX_FMT) | Float value [%] | 0 – 1 | 0.0 | Estimations with quality below this threshold are ignored |

### Output

| Symbol | Name | Destination | Size | Variability | Default | Description |
|---|---|---|---|---|---|---|
| $CalCoSCS_n$ | | Stack Processor (next active module) or L1c output | M acquisition of size $[N_{az} \times N_{rg}]$ | M=3 (INT) or M=7 (TOM), each with 3 or 4 polarizations (2CP + 1XP or 2CP + 2XP) | - | SCS with no slow varying ionosphere phase |
| $\partial_{t_{az}}\phi_n$ | slowIonosphereAzimuthPhaseScreen | L1c output product | Float value [rad/s] | M real numbers | - | The azimuth slope of the slow-varying phase screen estimated by the IOB (1 per input frame) |
| $\partial_{t_{rg}}\phi_n$ | slowIonosphereRangePhaseScreen | L1c output product | Float value [rad/s] | M real numbers | - | The range slope of the slow-varying phase screen estimated by the IOB (1 per input frame) |
| $q_n$ | slowIonosphereQuality | L1c output product | Float value [%] | M values in 0.0 – 1.0 | - | The estimation qualities (1 per input frame) |

### 5.2.2. Single-Baseline Estimator

As mentioned in the previous section, the single-baseline estimation is an interferometric approach that relies on the dispersive effects of the ionospheric medium to estimate the linear components of the differential ionospheric phase. Before describing the algorithm in detail, it is worthwhile noting that the pairwise range spectral filtering is not applied as pre-processing of this module because the range sub-looks extraction in the IOB implies restricting the method on the range common band. An overview of the method is reported in Fig. 13.

The main component of the module is based on the *Split-Spectrum Method* [RD9] which exploits the separation properties of the *dispersive* ($\Delta\phi_{iono}$) and *nondispersive* ($\Delta\phi_{nd}$) interferometric phases in the range frequency domain. More precisely, the interferometric phase can be modelled as the sum of the dispersive and non-dispersive components: Setting $\Delta\phi$ to be the interferometric phase associated to an SCS image pair and $f_c$ the central (carrier) frequency, then:

$$\begin{aligned}\Delta\phi &= \frac{4\pi f_c}{c}\Delta r_{nd} - \frac{4\pi K}{c f_c}\Delta TEC \\ &= \Delta\phi_{nd} + \Delta\phi_{iono},\end{aligned} \tag{5.13}$$

where $c$ is the speed of light, and $\Delta TEC, \Delta r_{nd}$, and $K$ are physical quantities dependent upon the ionosphere scenario and whose characterization lies beyond the scope of this document.

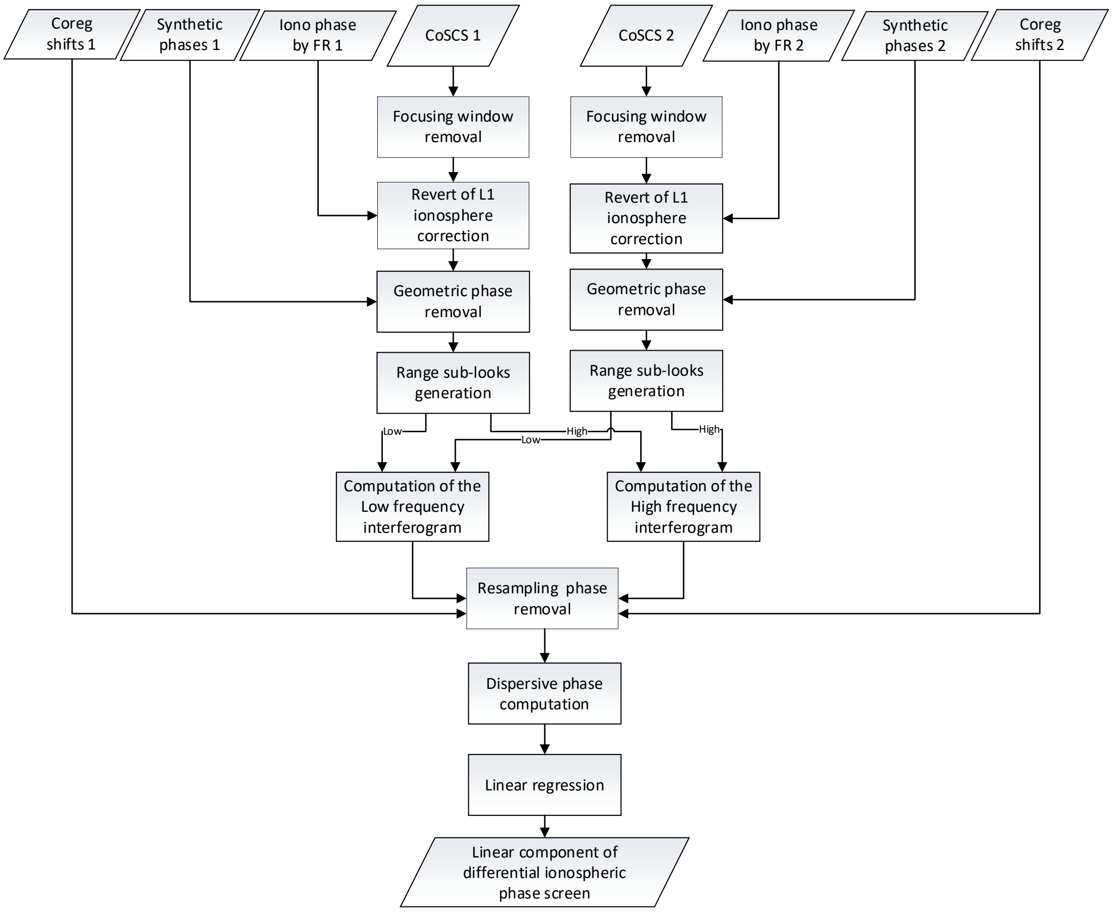


**Fig.11**

Block diagram representing the *single-baseline* IOB estimation.

The range Split-Spectrum leverages the different frequency behavior of the two ionosphere components to decouple them. In the remainder of the section, we will describe each sub-step in detail.

### 5.2.2.1. Pre-processing

The pre-processing step is applied independently to each coregistered image $CoSCS_n$ on a reference polarization, as specified in the AUX-PPS configuration, to obtain $M$ images $I_n$. The step consists of the following sub-steps:

1. Focus range spectral weighting removal: $I_n \leftarrow \mathrm{Win}_{rg}^{-1}[CoSCS_n]$
2. Removal of the geometric phase screens from DEM: $I_n \leftarrow I_n \cdot e^{j\Delta\Phi_n}$

### 5.2.2.2. Range sub-look extraction

The range sub-look generation computes two versions from each coregistered pre-processed input image. More in details, sub-looks are set to be centered within the range common bandwidth of the interferometric image pair and symmetrically with respect of the carrier frequency, that is, $f_L \coloneqq f_c - f_{sub}$ and $f_H \coloneqq f_c + f_{sub}$, where $f_{sub}$ is a user configurable parameter defaulted to one third (1/3) of the range common bandwidth. Accordingly, the two range sub-looks of the pre-processed image $I_n(a,r)$ are obtained as:

$$\begin{aligned} I_{n,L}(a,r) &\coloneqq \left\{\left(I_n(a,r) \cdot e^{-j2\pi f_L r}\right) * h(r)\right\} \cdot e^{j2\pi f_L r}, \\ I_{n,H}(a,r) &\coloneqq \left\{\left(I_n(a,r) \cdot e^{-j2\pi f_H r}\right) * h(r)\right\} \cdot e^{j2\pi f_H r}, \end{aligned} \tag{5.14}$$

where:

- $*$ denotes the linear convolution operator,
- $h(r')$ is the impulse response of a real-valued low-pass filter corresponding to range bandwidth $B_{sub}$, which is a configurable fraction of the full bandwidth and defaults to one third (1/3) of the range common bandwidth. In the implementation provided, a Gaussian low-pass filter is used.

### 5.2.2.3. Interferometric phase extraction

Given the interferometric pair of preprocessed sub-looked images $I_{k,X}$ with $k = n, m$ and $X \in \{H, L\}$, the interferometric phase for each range sub-band is computed as follows:

$$\begin{aligned} \Delta\phi_L &\coloneqq \angle \mathrm{Coh}\left(I_{n,L}, I_{m,L}\right), \\ \Delta\phi_H &\coloneqq \angle \mathrm{Coh}\left(I_{n,H}, I_{m,H}\right), \end{aligned} \tag{5.15}$$

where $\cdot^*$ denotes the complex conjugation, $\angle$ is the phase extraction operator, and $\mathrm{Coh}$ represents the interferometric coherence associated to an image pair

$$\mathrm{Coh}\left(I_p, I_s\right) \coloneqq \frac{\langle I_s \cdot I_p^* \rangle}{\sqrt{\langle |I_s|^2 \rangle \langle |I_p|^2 \rangle}}, \tag{5.16}$$

with $\langle\cdot\rangle$ being a local average operator. in the provided implementation a uniform filter with a default $201 \times 41$ boxcar kernel, which corresponds to approximately to a 200m x 200m window in azimuth and slant-range directions. The size of the filter is however configurable via AUX_PPS (see *sublookWindowAzimuthSize* and *sublookWindowRangeSize* in Section 5.2.1).

### 5.2.2.4. Split-Spectrum

Owing to Split-Spectrum method [RD9], the following equalities hold and can be exploited to estimate the dispersive and nondispersive phase screens:

$$\Delta\phi_L = \Delta\phi_{nd}\frac{f_L}{f_c} + \Delta\phi_{iono}\frac{f_c}{f_L}$$
$$\Delta\phi_H = \Delta\phi_{nd}\frac{f_H}{f_c} + \Delta\phi_{iono}\frac{f_c}{f_H} \quad (5.17)$$

where $f_c$ is the central (carrier) frequency.

Accordingly, it follows from inverting the linear system in Equation 5.16 that the slow-varying ionosphere is

$$\Delta\phi_{iono} = \frac{f_L f_H}{f_c(f_H^2 - f_L^2)}(\Delta\phi_L f_H - \Delta\phi_H f_L). \quad (5.18)$$

Although the method described above defines a general approach for discriminating the dispersive ionosphere from the non-dispersive one, it may be affected by biases caused by the different temporal shifts between the coregistration process and the synthetic phase removal. It can be proved (but the proof is not in the scope of this document) that such phase bias can be compensated into the low/high interferogram phases by setting:

$$\Delta\phi_L' \coloneqq \Delta\phi_L - f_c^{-1}(f_L - f_c)\Delta\phi_{bias},$$
$$\Delta\phi_H' \coloneqq \Delta\phi_H - f_c^{-1}(f_H - f_c)\Delta\phi_{bias}, \quad (5.19)$$

with $\Delta\phi_{bias} \coloneqq 2\pi f_c \tau_{rg} - \Delta\Phi_n + \frac{4\pi}{c} f_c\, \delta_{\phi_{L1a}} - \Delta\phi_{L1a}$, and:

- $\tau_{rg}$ are the range coregistration shifts (time) of the interferometric pair (see Section 4)
- $\Delta\Phi_n$ are the geometric phase screens from the DEM
- $\delta_{\phi_{L1a}}$ are the ionospheric spatial range shifts estimated by the L1 processor
- $\Delta\phi_{L1a}$ is the ionosphere phase screen estimated by the L1 processor.

Note that the compensation of the ionosphere phase screen and range shifts from L1 is optional and can be enabled or disabled by the user via AUX_PPS (see *compensateL1IonoPhaseScreenFlag*).

The final slow-varying ionosphere $\Delta\phi_{iono}'$ can be computed via Equation 5.16 and using the compensated high/low phase screens $\Delta\phi'_L$ and $\Delta\phi'_H$.

At this stage, phase unwrapping based on [RD21] can be optionally applied to $\Delta\phi'_L$ and $\Delta\phi'_H$ to aid the linear regression. As to whether such phase unwrapping should be performed is the responsibility of the user, which can enable or disable it using a configurable parameter. By default, the phase unwrapping is executed.

If phase unwrapping is performed, the resulting unwrapped phase screens are compared to flag pixels that are affected by possible phase unwrapping errors (see [RD25]). For this, the following simple pixelwise check is executed:

$$T_{PU} \coloneqq \left|(\Delta\phi_H - \Delta\phi_L) - \mu_{1/2}(\Delta\phi_H - \Delta\phi_L)\right| \geq \theta_{PU}, \tag{5.19}$$

where $\mu_{1/2}$ represents the median operator over the entire frame. Pixels whose $T_{PU}$ value exceeds a user defined threshold will be ignored in the phase estimation step described in Section 5.2.2.5 below.

This test is used to flag which pixels are to be considered valid for the estimation. IOB provides an accessory test based on the coherence, that is, a pixel is considered invalid if the coherence is below a threshold $\theta_\gamma$ specified via AUX-PPS. Accordingly, a pixel is considered valid if both the validity tests pass. If the ratio of valid pixel is below a user defined threshold $\theta_{PV} \in [0,1)$, the SB estimation is considered invalid and will be ignored (see Section 5.2.5 for more details on contingency cases).

### 5.2.2.5. Phase screen estimation

Due to the theoretical limitation in estimating the slow-varying ionosphere for the whole swath [RD5], we approximate via weighted Least-Square estimation the linear phase screens (plane). More formally, the estimated phase slopes $\partial_a\phi_{sb}^{p,s}$ and $\partial_r\phi_{sb}^{p,s}$ (and constant intercept $\phi_0$) for an interferometric pair $p,s$ are defined as

$$\begin{bmatrix} \partial_a\phi_{sb}^{p,s} \\ \partial_r\phi_{sb}^{p,s} \\ \phi_0 \end{bmatrix} \coloneqq (F^T \cdot W_{sb} \cdot F)^{-1} \cdot F^T \cdot W_{sb} \cdot \mathrm{vec}(\Delta\phi'_{iono}), \tag{5.20}$$

where $F$ is a $N_{az}N_{rg} \times 3$ matrix so that $F_{i0} \coloneqq \lfloor i/N_{rg} \rfloor$ , $F_{i1} \coloneqq i \pmod{N_{az}}$, and $F_{i2} \coloneqq 1$, $W_{sb}$ is the $N_{az}N_{rg} \times N_{az}N_{rg}$ diagonal matrix so that $W_{sb,i,i} \coloneqq \gamma_i \cdot T_{PU,i} \cdot (\gamma_i \geq \theta_\gamma)$ with $\gamma_i$ the $i$-th pixel's coherence of the interferometric pair $(p,s)$ computed as in Equation 5.15 but with a finer resolution (*e.g.* using a $5 \times 5$ boxcar kernel), $T_{PU,i} \in \{0,1\}$ is the $i$-th pixel's validity associated to the phase unwrapping test described in Section 5.2.2.3, if applicable, and finally, $\mathrm{vec}(\Delta\phi'_{iono})$ is the $N_{az}N_{rg} \times 1$ vector obtained by stretching the element of the ionosphere phase screen into a 1D column array.

Note that to convert $\partial_x\phi_n^{p,s}$ into $\partial_{t_x}\phi_n^{p,s}$, *i.e.* slopes expressed with respect to samples into slopes expressed with respect to time axes, it is enough to normalize the terms by the associated sampling steps.

As final step, the quality of the estimation is defined as:

$$q_{sb}^{p,s} = \frac{1}{N_{az}N_{rg}} \sum_{a,r} \sqrt{\frac{1}{2\sigma_{iono}^2 + 1}}, \tag{5.21}$$

with $\sigma_{iono}$ is the standard deviation of the ionospheric estimation computed as:

$$\sigma_{iono} \coloneqq \frac{3f_0}{4(f_H - f_L)} \sqrt{\frac{3(1-\gamma^2)}{N\,\gamma^2}}, \tag{5.22}$$

where:

- $N$ is the number of average samples,
- $\gamma$ is the absolute value of the interferometric coherence map estimated in azimuth and range directions between the interferometric pair,

If the user has selected the Single-baseline modality, the final estimated dispersive ionosphere components will be set to be

$$\partial_x \phi_{sb}^{n} \coloneqq \partial_x \phi_{sb}^{n,n^*} \cdot \boldsymbol{I}_{q_{sb}^{n,n^*} > q_{thres}}, \quad n \neq n^*, x \in \{r, a\}, \tag{5.23}$$

where $\boldsymbol{I}_{q_{sb}^{n,n^*} > q_{thres}} \in \{0,1\}$ is the quality indicator that disables the estimation if the quality does not reach the minimum estimation quality threshold, as specified by the user. Also $\partial_x \phi_{sb}^{n^*} \coloneqq 0$, *i.e.* the calibration reference image is set to have no ionosphere components.

## 5.2.3. Multi-Baseline

The Multi-baseline modality combines the single-baseline estimations associated to input $K$ interferometric pairs into $M-1$ differential ionospheric phase screens by computing the phase screens that best fit all the single-baseline estimations . Note that, with the Multi-baseline modality, interferometric pairs are selected according to their spatial baseline and only pairs whose spatial baseline does not exceed a user defined threshold are considered for estimation (see *multiBaselineCriticalBaselineThreshold* in Section 5.2 and Output Table in Section 5.2.1). By default, the threshold is set to be 45% of the critical baseline.

In the Multi-baseline modality, given the $K$ range slopes and $K$ azimuth slopes associated the selected interferometric pairs in the stack, the ionospheric phase ramps in azimuth will be estimated by solving the following linear system:

$$\left(F^T \cdot W_{sb}^l \cdot F\right) \cdot \begin{bmatrix} \partial_l \phi_{mb}^0 \\ \partial_l \phi_{mb}^1 \\ \vdots \end{bmatrix} = \left(F^T \cdot W_{sb}^l\right) \cdot \begin{bmatrix} \partial_l \phi_{sb}^{0,1} \\ \partial_l \phi_{sb}^{0,2} \\ \vdots \end{bmatrix}, \tag{5.24}$$

where:

- $F$ is the $[K \times M]$ multi-baseline matrix so that $F_{ij} \coloneqq \pm 1$ if $j$ is respectively the secondary or primary image index of the $i$-th interferometric pair, $0$ otherwise.

- $\partial_x \phi_{sb}^{p,s}$ is the single-baseline ionospheric phase ramp in azimuth or range direction $l \in \{a, r\}$ associated to the interferometric pair $p, s$.
- $W_{sb}^{l}$ is the $[K \times K]$ diagonal matrix defined as follows (see [RD25]):
$$W_{sb,i,i}^{l} \coloneqq 1/((C^T \Omega_i C)^{-1}|_l)\,,$$

  with $|_l$ representing the element of the diagonal associated to the coordinate/direction $l$ and:

$$\Omega_i \coloneqq \begin{bmatrix} \sigma_{iono,i}^2(x_1, r_1) & \dots & 0 \\ \vdots & \ddots & \vdots \\ 0 & \dots & \sigma_{iono,i}^2\left(x_{N_{az}N_{rg}}, r_{N_{az}N_{rg}}\right) \end{bmatrix}^{-1},$$

$$C \coloneqq \begin{bmatrix} x_1 & r_1 & 1 \\ \vdots & \vdots & \vdots \\ x_{N_{az}N_{rg}} & r_{N_{az}N_{rg}} & 1 \end{bmatrix},$$

  where $\sigma_{iono,i}^2$ is the variance of the ionosphere computed as in Equation 5.19 for the $i$-th interferometric pair and $x_k$ and $r_k$ are respectively the centered azimuth and centered slant-range position of the look, that is, for $k = 1, \dots, N_{az}N_{rg}$, they are defined as $x_k \coloneqq \lfloor k/N_{rg} \rfloor \cdot dx - \bar{x}$ and $r_k \coloneqq k \pmod{N_{az}} \cdot dr - \bar{r}$.

The linear system at Equation 5.21 has rank $M - 1$. To resolve the system's underdetermination, we will assume that all phase ramps will be defined with respect to a fiducial image, that it is known being the least affected by dispersive ionosphere. Accordingly, the final phase ramps will be

$$\partial_l \phi_n \coloneqq \left(\partial_l \phi_{mb}^{n} - \partial_l \phi_{mb}^{n^*}\right) \cdot \boldsymbol{I}_{q_{mb}^{n} > q_{thres}}\,, \quad l \in \{a, r\};\ n = 1, \dots, M \tag{5.25}$$

where $n^*$ denotes the index of such reference image and again $\boldsymbol{I}_{q_{mb}^{n} > q_{thres}} \in \{0,1\}$ is the quality indicator that disables the estimation if the quality does not reach a threshold specified by the user. The quality index of the multi-baseline approach $q_n^{IoB}$ can be estimated from the single-baseline quality indexes $\boldsymbol{q_{sb}}$ solving the following a linear system similarly to that of Equation 5.15:

$$F^T \cdot W_{sb} \cdot F \cdot \boldsymbol{q}_{mb} = F^T \cdot W_{sb} \cdot \boldsymbol{q_{sb}}, \tag{5.26}$$

with $W_{sb}$ defined as the $K \times K$ diagonal matrix with the $k$-th diagonal entry containing the quality terms in Equation 5.18 associated to the $k$-th interferometric pair.

Note that during Multi-baseline estimation, the weighting term $W_{sb}^{l}$ and $W_{sb}$ can be optionally substituted by a uniform weighting matrix (*i.e.* both matrices substituted with the identity matrix) using the related configuration parameter.

#### 5.2.3.1. Reference Image Selection

To select the reference image, the stack processor exposes three (3) options:

1. Manually select the reference via Job Order,
2. Use the coregistration primary image as calibration reference. This is selected via the *primaryImageFlag* tag of the AUX_PPS (see AUX_FMT for more details). Note that if both 1 and 2 are engaged, 2 is ignored.
3. If neither of the two above are specified, let the stack processor choose the best image according to the Faraday decorrelation indices and RFI indices computed by the L1 processor.

Options 1 and 2 are trivial. As for option 3, we will combine the two metrics simply by setting

$$n^* \coloneqq \underset{n}{\operatorname{argmax}}\left( \gamma_n^{FR} \cdot \gamma_n^{RFI} \right), \tag{5.27}$$

where:

- $n$ is the index of the image in the stack.
- $\gamma_n^{FR}$ denotes the decorrelation computed from the standard deviation of the residual phase provided by the L1 processor for the ionosphere correction: Setting the Faraday rotation to be $\sigma_{FR,n}$:

$$\gamma_{FR}^{n} \coloneqq \sqrt{\frac{1}{2\sigma_{FR,n}^2 + 1}}, \tag{5.28}$$

- $\gamma_n^{RFI}$ is the expected decorrelation map due to the RFI patterns in the $n$-th image corrected by the RFI mitigation of the L1 processor for the polarization used in the calibration. Details on how to compute the decorrelation from the RFI patterns is available in Section 3.1.3.2.

### 5.2.4. Slow-Varying Ionosphere Removal

The slow changing ionosphere removal takes as input the parameters estimated by the previous step and removes the corresponding phase screens from the stack.

The linear components estimated during the previous step are used to compute the phase screen on the grid of the reference image and then removed from the coregistered data $CoSCS_n$ as follows:

$$CalCoSCS_n \coloneqq CoSCS_n \cdot e^{-j\phi_{IoB,n}}, \tag{5.29}$$

where:

- $n$ is the image index,
- $\phi_{IoB,n}(a,r)$ is the slow changing ionospheric phase screen for that image defined as

$$\phi_{IoB,n}(a,r) \coloneqq \partial_a \phi_n \cdot (a - \overline{a}) + \partial_r \phi_n \cdot (r - \overline{r})\,. \tag{5.30}$$

With $a = 1, \dots, N_{az}$, $r = 1, \dots N_{rg}$, and $(\bar{a}, \bar{r})$ the central pixel of the image

### 5.2.5. Contingency Handling

Within the IOB module the only expected contingency case is the failure of the SB estimator for an interferometric pair. The module handles such a case in the following way:

- If *Single-baseline* is executed, no failures are accepted. Any failure occurring in the SB estimator will result in the stack exiting gracefully with an error.
- During *Multi-baseline*, all interferometric combinations that result in a normal baseline below the requested threshold are considered, thus failures are allowed as long as the factor graph defined by the SB (pairwise) estimations is connected. More in detail, let $G \coloneqq (v_n, \varepsilon_{ij})$ be the undirected graph with vertices $v_n$ defined as the estimation states, *i.e.* the slow-ionosphere phase screen slopes in azimuth (range) direction, and edges $\varepsilon_{ij}$ connecting vertices $v_i$ and $v_j$ if and only if the SB estimation between frames $i$ and $j$ was successful. From an information theory's standpoint, it is trivial to see that the Multi-baseline problem can be uniquely solved if and only if the graph $G$ is connected[6]. It is a well-known fact that the number of connected components equals the dimension of the null space of the Laplacian matrix $L_G$ of $G$, which can be efficiently computed. Accordingly, the Multi-baseline estimation is executed if and only if $\dim Ker\,(L_G) = 1$. The stack exits gracefully with an error otherwise.

## 5.3. Multi-Squint Calibration

The *Multi-Squint Calibration* (MSC) module ports the ionospheric calibration method described in [RD27]. MSC is responsible for estimating and correcting the along-track baseline shift and the phase artefacts due to the ionosphere. More in detail, it estimates and corrects:

1. A constant baseline shift in along-track direction
2. A high-pass single- or multi-layer phase screen associated with the ionosphere
3. A phase plane that accounts for residual low-pass phase artifacts

Note that 1- and 2- are optional and can be disabled by the user via AUX_PPS___.

[6] Note that the contingency handling of the Multi-baseline method generalizes that of the Single-baseline method.

In the reminder of this section, we will describe in detail all steps of the algorithm.

## 5.3.1. Inputs and Outputs

### Inputs

| Symbol | Name | Origin | Size | Variability | Default | Description |
|---|---|---|---|---|---|---|
| $CoSCS_n$ | | Coregistration Step or previous active calibration module | M acquisition of size $[N_{az} \times N_{rg}]$ | M=3 (INT) or M=7 (TOM), each with 3 or 4 polarizations (2CP + 1XP or 2CP + 2XP) | - | Coregistered SCS frames, possibly from previous calibration step (i.e. AZF, IOB, BAE, or IOS) |
| $\Delta\Phi_n$ | | Coregistration Step | M of size $[N_{az} \times N_{rg}]$ | M=3 (INT) or M=7 (TOM) each with a single channel | - | Synthetic phases from DEM associated to each acquisition |
| $p$ | polarisationUsed | AUX_PPS | HH,HV,VH , VV, XX | 1 | HH | Polarization used to estimate the phase screen. |
| $r_{min}$ | | AUX_PPS | Float | $0-\infty$ | 100,000 | Minimum ionospheric range candidate [m] |
| $r_{max}$ | | AUX_PPS | Float | $0-\infty$ | 700,000 | Maximum ionospheric range candidate [m] |
| $\rho_\psi$ | multiSquintCoherenceSubbandResolution | AUX_PPS | Float | $0-\infty$ | 300 | Sub-band azimuth resolution for MS coherence [m]. |
| $\rho_a$ | multiSquintCoherenceHighResAzimuthWindowSize / multiSquintCoherenceLowResAzimuthWindowSize | AUX_PPS | Float | $0-\infty$ | 0 / 250 | Filter window size in along-track direction [m] (high/low resolution) |
| $\rho_r$ | multiSquintCoherenceHighResRangeWindowSize / multiSquintCoherenceLowResRangeWindowSize | AUX_PPS | Float | $0-\infty$ | 250 / 300 | Filer window size in slant-range direction [m] (high/low resolution). |

### Outputs

| Symbol | Name | Destination | Size | Variability | Default | Description |
|---|---|---|---|---|---|---|
| $CalCoSCS_n$ | | L1c output product | M acquisition of size $[N_{az} \times N_{rg}]$ | M=3 (INT) or M=7 (TOM), each with 3 or 4 polarizations (2CP + 1XP or 2CP + 2XP) | - | Calibrated SCS with compensated dominant phase plane |

| Symbol | Name | Destination | Size | Variability | Default | Description |
|---|---|---|---|---|---|---|
| $ds$ | | L1c output product | Float [m] | M float values | - | The constant along-track baseline errors |
| $f_x$ | | L1c output product | Float [1/m] | M float values | - | The estimated azimuth frequency centroid |
| $\Delta\phi_l$ | | L1c output product | Float array [rad] | M 3D LUTs | - | The ionospheric phase screens associated to the ionosphere |
| $\partial_{t_{az}}\phi_n$ | | L1c output product | Float [rad/s] | M float values | - | The slope of the phase plane in along-track direction (1 per input frame) |
| $\partial_{t_{rg}}\phi_n$ | | L1c output product | Float [rad/s] | M float values | - | The of the phase plane in slant-range direction (1 per input frame) |

### 5.3.2. Workflow

At a high level the MSC module consists of three (3) steps: First a pre-processing step executes the following operations on all the secondary stack's frames:

- First, a pre-processing step warps the input uncalibrated stack $SCS_n$ by applying the coregistration shifts both from orbit and data in range direction, but only the coregistration shifts from orbit in along-track direction, yielding a secondary stack $CoSCS_n^\#$. Henceforth we will refer to $CoSCS_n$ and $CoSCS_n^\#$ respectively as primary and secondary stacks
- Then, compensate the flattening phases screen in both stacks, that is, update the stacks by setting $CoSCS_n \leftarrow CoSCS_n \cdot \exp(j\Delta\Phi_n)$ and $CoSCS_n^\# \leftarrow CoSCS_n^\# \cdot \exp(j\Delta\Phi_n)$, where $\Delta\Phi_n$ are the flattening phase screens computed during the coregistration steps.

Next, given a calibration pair $(CoSCS_p, CoSCS_s^\#)$ and a selected polarization:

- Compare the Multi-Squint coherence and the traditional coherence to infer whether the Multi-Squint coherence-based ionosphere calibration needs to be executed or skipped.
- In case the Multi-Squint coherence calibration is required, calibrate $CoSCS_s^\#$ by estimating and correcting a constant shift in along-track direction as well as the phase screen due to a single- or multi-layer ionosphere
- Use the calibrated image $CoSCS_s^\#$and the primary $CoSCS_p$ to estimate and correct the phase plane associated with the low-pass artifacts and correct $CoSCS_s^\#$ accordingly
- Update the primary stack's secondary image with the calibrated image: $CalCoSCS_s \leftarrow CoSCS_s^\#$

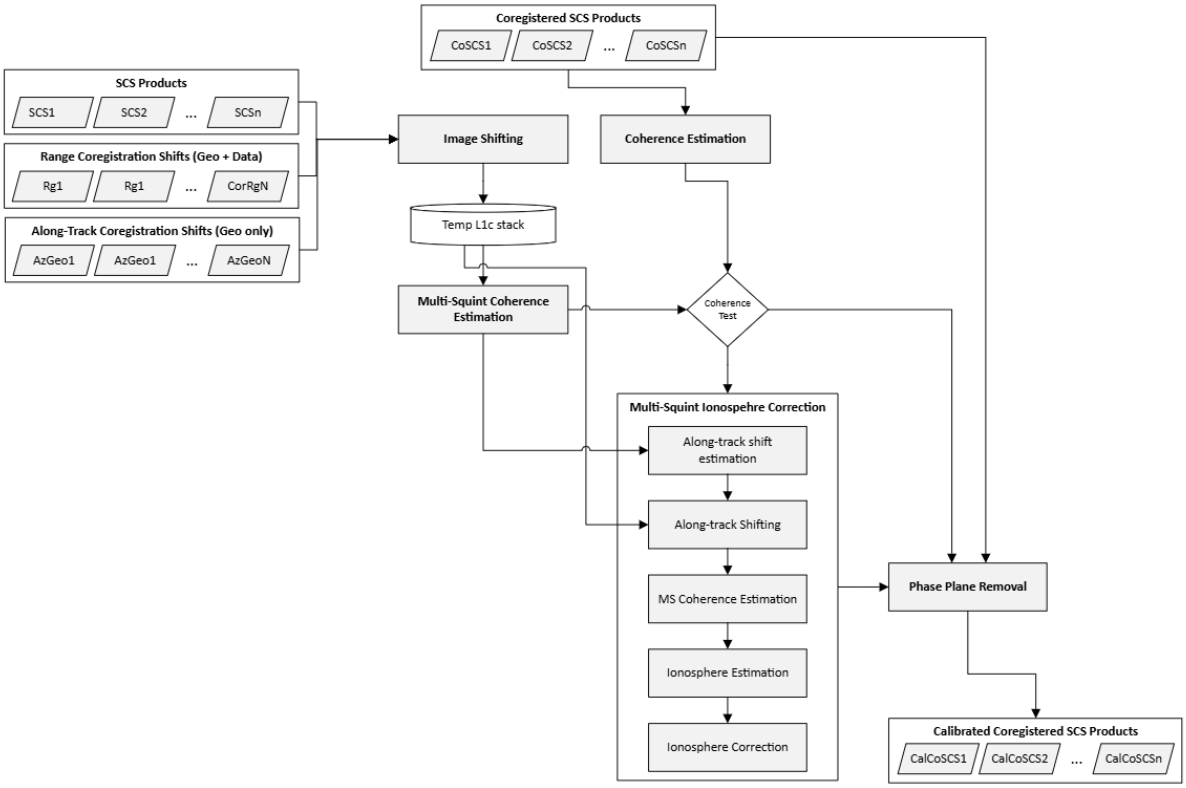


**Fig 12**. The workflow of the Multi-Squint Calibration Module

In contrast with the IOB module, which provides the Multi-Baseline and Single-Baseline modalities to leverage interferometric pairing during the computation of the ionosphere phase screens, the MSC module uses a different strategy that aims to reduce the computational cost of the algorithm. More in details, instead of computing all possible interferometric pairs and executing independent pairwise estimations that are later combined via least-square approach (Multi-Baseline) into a single one for each frame, or directly estimating the slow-varying ionosphere by pairing secondary images with the calibration reference image (Single-Baseline), MSC estimates baseline errors and ionosphere phase screens on the secondary image of an interferometric pair and then iterates on adjacent pairs assuming that the previous secondary is now calibrated. As an example, assuming a tomographic stack (*i.e.* 7 frames) and assuming that the coregistration primary image is the central one (*i.e.* $n'$=3): The MSC module will operate on the interferometric pairs as follows:

1- First, it operates independently on the pairs (3, 4) and (2, 3), since they are adjacent to the coregistration primary image ($n' = 3$). It estimates and corrects both baseline shifts and ionosphere phase screens associated to frame 4 and frame 2
2- Next, it moves on to pairs (4, 5) and (1, 2) and calibrates frames 5 and 1 independently. Frames 4 and 2 are left untouched in this step since they were corrected in the previous step
3- The procedure continues until all images are calibrated. Obviously, the coregistration primary image is not modified

Note that, despite the sequential approach, the estimated baseline shifts and ionosphere phase screens are still defined relatively to the coregistration primary image, since the corrections are applied to the secondary images before the next interferometric pair is considered.

MSC terminates by re-applying the flattening phase screens to the primary calibration stack, that is, $CalCoSCS_n \leftarrow CalCoSCS_n \cdot \exp(-j\Delta\Phi_n)$ to revert the primary stack to the base band.

### 5.3.3. Multi-Squint Coherence

At the core, the MSC utilizes the Multi-Squint (MS) coherence matrix, which is a 3D array storing the coherence of 2 image frames for a selected sets of squints $(\psi_k)_{k=1\ldots N_\psi}$ . The Multi-Squint Coherence matrix is computed as follows: Set $\rho_\psi > 0$ the sub-band (squint) resolution and $I_p$ and $I_q$ two flattened frames, we compute

$$MSI_p[a, \ldots] = I_p[a - \alpha_a : a + \alpha_{az}, \ldots]\, M_\psi, \tag{5.31}$$
$$MSI_q[a, \ldots] = I_q[a - \alpha_a : a + \alpha_{az}, \ldots]\, M_\psi, \tag{5.32}$$

where $\alpha_a \coloneqq \left\lfloor \frac{\rho_\psi}{2\,\delta_a} \right\rfloor$, $\delta_a$ is the azimuth resolution, $M_\psi \coloneqq \exp\{-2\pi j \delta_a \boldsymbol{x}_a \otimes \boldsymbol{\psi}\}$, with $\otimes$ being the outer tensor product, $\boldsymbol{x}_a \coloneqq [-\alpha_a, -\alpha_a + 1, \ldots, \alpha_a - 2, \alpha_a - 1]$ and $\boldsymbol{\psi}$ the squint axis defined by $\rho_\psi$. The Multi-Squint Coherence matrix is computed as

$$MSCoh \coloneqq \frac{\langle MSI_q \cdot MSI_p^* \rangle}{\sqrt{\langle |MSI_q|^2 \rangle \langle |MSI_p|^2 \rangle}}, \tag{5.33}$$

with $\langle\cdot\rangle$ being a local averaging and downsampling operator in slant-range direction and in azimuth direction, whose window is controlled by a user defined parameter $\rho_a$ and $\rho_r$, and $\cdot^*$ the complex conjugation. The $MSCoh$ matrix is a 3D array of size $N_{\alpha_a} \times N_{B_r} \times N_\psi$, with $N_{B_r}$ being the number of range blocks defined by the range resolution $\rho_r$.

### 5.3.4. Multi-Squint-based Ionosphere Calibration

The Multi-Squint Calibration step is responsible for estimating and correcting both the baseline shifts in along-track direction and the fast-varying phase screen due to the ionosphere. This step is conditional and executed only when the data is expected to be affected by ionosphere. Such condition is detected by the algorithm by comparing the coherence of the image pair of the primary stack with the reference coherence of the same image pair of the secondary stack. More formally given the calibration pair $(p, s)$, the following quantities are compared:

$$\mu_{Coh} \coloneqq \langle Coh(CoSCS_p, CoSCS_s) \rangle, \tag{5.34}$$

$$\mu_{MSCoh} \coloneqq \left\langle \langle MSCoh(CoSCS_p, CoSCS_s^{\#}) \rangle_{\psi} \right\rangle, \tag{5.35}$$

that is, the average over all pixels of the (traditional) coherence and the average over all pixels of the average over all squints of the Multi-Squint Coherence. The (traditional) coherence is computed as in Equation 5.15, Section 5.2.2.3 with user defined averaging window sizes. Note that $CoSCS_p$ is the pair's primary, which is calibrated at the previous MSC's calibration step.

The Multi-Squint-based ionosphere calibration step is executed if

$$\mu_{MSCoh} - \mu_{Coh} > \theta_{MS}, \tag{5.36}$$

where $\theta_{MS}$ is user-defined parameter specified in the AUX_PPS, that is, when the azimuth residual shifts are considered to have corrupted the overall coherence of the stack. The Multi-Squint-based ionosphere calibration described in the reminder of this section is hence executed only upon satisfying the above condition. Conversely, the ionosphere calibration is skipped and the MSC module executes the phase plane calibration step described later in Section 5.3.5.

### 5.3.4.1. Baseline Shifts Estimation and Correction

As first step of the Multi-Squint ionosphere calibration, we compute the along-track coregistration error introduced by the ionosphere. Set $MSCoh_{ps}$ to be the Multi-Squint Coherence defined in Equation 5.33, we compute its 2D spectrum

$$S_{MS} \coloneqq \langle \left| FFT2\left( \langle MSCoh_{ps} \rangle_r \right) \right| \rangle, \tag{5.37}$$

where $\langle\cdot\rangle$ is a local averaging operator and $\langle\cdot\rangle_r$ is the mean over the slant-range direction. The baseline shifts are computed from $S_{MS}$ by identifying the maximum of the spectrum (see [RD25]) as described below: Setting $\boldsymbol{\delta x}$ and $\boldsymbol{d\xi}$ to be search axes around the global maximum of the spectrum $S_{MS}$, we define

$$(i^*, j^*) \coloneqq \mathrm{argmax}_{ij} |W_{d\psi}^T S_{MS} W_{dx}|, \tag{5.38}$$

where $W_{d\psi} \coloneqq \exp\{-2j\pi\,(\boldsymbol{\delta\psi} \otimes \boldsymbol{\psi})\}$ and $W_{dx} \coloneqq \exp\{-2j\pi\,(\boldsymbol{x_a} \otimes \boldsymbol{dx})\}$, with $\otimes$ denoting the outer vector product, $\boldsymbol{d\psi}$ and $\boldsymbol{dx}$ are respectively the squint and spatial azimuth frequency axes, $\boldsymbol{\psi}$ is the squint axis, and $\boldsymbol{x_a}$ is the spatial azimuth axis.

The baseline shift (in pixels) and the azimuth frequency centroid are respectively defined as

$$ds := \frac{\lambda}{2}\, \boldsymbol{\delta\psi}[i^*],\ f_x := \boldsymbol{\delta x}[j^*]. \tag{5.39}$$

As a final step, the secondary image $CoSCS_s^{\#}$ is corrected as follows:

- First, the baseline shift $ds$ is applied to the image for all polarizations,
- Then, the phase screens are corrected by setting

  $$CoSCS_s^{\#} \leftarrow CoSCS_s^{\#} \cdot \exp(-2j\pi f_x \boldsymbol{x_a} \otimes \mathbf{1_r}),$$

  where $\boldsymbol{x_a}$ is the spatial axis in along-track direction defined above, $\otimes$ denotes again the outer vector product, and $\mathbf{1_r}$ is a$[1 \times N_r]$ vector of ones.

### 5.3.4.2. Ionosphere Layers Estimation

To estimate the ionospheric layers, MSC uses a set of ionospheric layer heights and identifies those that most effectively explain the phase distortions observed in the Multi-Squint Coherence. The algorithm evaluates a predefined set of range candidates and iteratively selects the most informative ones using a greedy, score-driven procedure. More in details, given a set of range candidates $R_{iono} := (r_{min}, r_{min} + \delta r, r_{min} + 2\delta r, \ldots, r_{max})$, with $r_{min}, r_{max}$ and step $\delta r$ tunable by user via AUX_PPS, the ionospheric layers $L_{iono}$ are obtained with an iterative procedure as follows: Given a set of test set $R_{test}$ of slant-range samples, loop until there are no more candidate left in $R_{iono}$:

- For each $r_{iter}$ in $R_{iono}$
  - Define the test layers $L_{iter} := L_{iono} \cup \{r_{iter}\}$
  - Compute the residuals $\rho_{iono} := \Re\langle \sum_{r \in R_{test}} MSCoh_{test} \cdot e^{-j\Delta\phi_r} \rangle$, where $\Re$ denotes the real part, $\langle\cdot\rangle$ the average over all entries, $MSCoh_{test}$ is the Multi-Squint Coherence matrix $MSCoh_{ps}$ restricted over the slant-range samples $R_{test}$, and $\Delta\phi_r$ are the phase residual associated to $R_{test}$ and $L_{iter}$ obtained via *composite iterative inversion* (see Section 5.3.3.4)
  - Define the scores $\alpha(r_{iono}) := \rho_{iono}/|R_{test}|$
- Select the $r_{iter}^* := argmax\ \alpha(r_{iter})$
- Move $r_{iter}^*$ from $R_{iono}$ to $L_{iter}$, *i.e.*, $R_{iono} := R_{iono} \setminus \{r_{iter}^*\}$ and $L_{iono} := L_{iono} \cup \{r_{iter}^*\}$.

The procedure above is prematurely interrupted if one of the following conditions are met:

- A maximum gain is reached, that is, $\alpha(r_{iter}^*) < \alpha(r_{iter-1}^*) + \theta_{ranges}$, for a user selected threshold $\theta_{ranges}$.
- A maximum number of ionospheric layers is reached, *i.e.*, $|L_{iono}| \geq N_{layers}$, where $N_{layers}$ is a user selected threshold.

The test set $R_{test}$ is selected as follows: Set $\mu_{MSCoh}$ as in Equation 5.34, then

- Select the *seed* slant-range sample $r_{seed}$ so that $|\mu_{MSCoh}[\ldots, r_0]|$ contains the largest number of elements above a user selected threshold $\theta_{test}$

- Set $N_{MS,az}$ and $N_{MS,rg}$ to be respectively the number of lines and samples of the Mult-Squint Coherence matrix $MSCoh_{ps}$ and $\theta_{test,min}$ being a user selected threshold: If the number of elements of $\mu_{MSCoh}[\dots, r_0]$ whose absolute values exceed $\theta_{test}$ is below $\theta_{test,min} N_{MS,az}$, the previously selected seed is discarded and $r_{seed}$ is set to be the central slant-range sample, *i.e.*, $r_{seed} \coloneqq \lfloor N_{MS,rg} / 2 \rfloor$
- Finally, the test set is defined as

$$R_{test} \coloneqq \left\{ \left( r_{seed} + i \cdot \left\lfloor \frac{N_{MS,rg}}{N_{slices}} \right\rfloor \right) mod\ N_{MS,rg} \mid i = 1 \dots N_{slices} \right\} \tag{5.40}$$

where $N_{slices}$ is a user selected parameter.

### 5.3.4.3. Sequential Ionospheric Estimation

Once the ionospheric layers $L_{iono}$ and the seed slant-range sample $r_{seed}$ are estimated as described in Section 5.3.4.2, the MSC module computes the ionosphere phase screens $\boldsymbol{\Delta\phi_l}$ at the ionospheric height and its projection $\boldsymbol{\gamma_{MS}}$ on the grid of the Multi-Squint coherence matrix. To do so, the MSC module first computes the value of $\boldsymbol{\Delta\phi_l}$ and $\boldsymbol{\gamma_{MS}}$ at the slant-range seed sample and then propagates the estimation over the whole extent of the image. Below we describe the approach only for $\boldsymbol{\Delta\phi_l}$, $\boldsymbol{\gamma_{MS}}$ is estimated similarly:

- Compute the ionosphere phase screens $\Delta\boldsymbol{\phi}_{l,seed}$ at the seed slant-range sample via *composite iterative inversion* (see Section 5.3.4.4)
- Increasingly iterate over the slant-range pixels $r_{curr} = r_{seed} + 1, \dots, N_{MS,rg}$ and $r_{curr} = r_{seed} - 1, \dots, 0$ and compute the current ionospheric phase screens by setting $\Delta\boldsymbol{\phi}_{\boldsymbol{l,curr}} \coloneqq \Delta\boldsymbol{\phi}_{\boldsymbol{l,curr-1}} + \Delta\boldsymbol{\phi}_{\boldsymbol{l,inv}}(MSCoh_{pq}[\dots, r_{curr}, \dots])$ , with $\Delta\boldsymbol{\phi}_{\boldsymbol{l,inv}}$ being the integration term obtained via *iterative ionospheric inversion* (see Section 5.3.4.4).

### 5.3.4.4. Iterative Model Inversion

In this section we describe the core steps of the Multi-Squint ionosphere calibration steps, namely the *iterative model inversion* and the *composite iterative inversion.*

The *iterative model inversion* consists of iteratively estimating phase screens associated to each layer by conditioning on the other ionospheric layer, which are assumed to be known at each iteration. More formally, given a maximum number of iterations $N_{iter}$ specified by the user, the following iterative approach is executed: Set the iteration counter $n_{iter} = 0$, $\Delta\boldsymbol{\phi} = \boldsymbol{0}$, $\widehat{\boldsymbol{\phi}} = \boldsymbol{0}$, and $\boldsymbol{\gamma}_{MS} = MSCoh_{pq}[\dots, r, \dots]$

while $n_{iter} < N_{iter}$

for each estimated layer $l$

- Compute $\widehat{\boldsymbol{\phi}}(x, \psi) \coloneqq \Sigma_{r_{iono}} \widehat{\boldsymbol{\phi}}_{r_l}(x - r_l, \psi)$
- $\boldsymbol{\gamma}_{MS} \coloneqq MSCoh_{ps}[\dots, r, \dots] \cdot \exp\{-j\widehat{\boldsymbol{\phi}}\}$

- $\delta\widehat{\boldsymbol{\Phi}}_{r_l} \coloneqq O_{method}(\boldsymbol{\gamma}_{MS})$
- $\widehat{\boldsymbol{\Phi}}_{r_l} \coloneqq \widehat{\boldsymbol{\Phi}}_{r_l} + \delta\widehat{\boldsymbol{\Phi}}_{r_l}$

where $O_{method}$ is one of the following two estimation operators:

- The *azimuth projection operator*

$$O_{proj}(\boldsymbol{\gamma}_{MS}) \coloneqq \angle\langle\boldsymbol{\gamma}_{MS}(x + r_l\psi, \psi)\rangle_{\psi}, \quad (5.41)$$

  with $\langle\cdot\rangle_{\psi}$ the averaging over the squint angles

- The *ionospheric derivative operator*

$$O_{der}(\boldsymbol{\gamma}_{MS}) \coloneqq \int_x \langle\gamma_{MS}^{tr}(x, x' + \Delta x')\gamma_{MS}^{tr}(x, x')^*\rangle_x dx' \quad (5.42)$$

  where $x'$ represents the along-track spatial coordinate at the ionospheric range, $\boldsymbol{\gamma}_{MS}^{tr}(x, x') \coloneqq \boldsymbol{\gamma}_{MS}(x, (x - x')/r_l)$, $\Delta x'$ is the spacing of the $x'$-coordinate, and $\langle\cdot\rangle_x$ is the averaging operator over the spatial along-track direction.

The user can select which operator to use using the switch parameters provided in the AUX_PPS. Also, the user can select threshold gains $\theta_{proj}$ and $\theta_{der}$ to control the convergence of the above methods by checking $\left\langle\delta\widehat{\boldsymbol{\Phi}}^{iter}{}_{r_l}\right\rangle < \left\langle\delta\widehat{\boldsymbol{\Phi}}^{iter+1}{}_{r_l}\right\rangle + \theta_{method}$.

The *composite iterative inversion* sequentially uses the *azimuth projection* as a first estimation step and the *ionosphere derivative* as a final refinement step.

### 5.3.4.5. Ionosphere Removal

As final step of the Multi-Squint-based ionospheric calibration, the ionosphere is removed from the input stack. The approach used for removing the ionosphere depends on whether the estimated ionosphere is single-layer or multi-layer.

In case of a single-layer ionosphere, the ionosphere is corrected as follows:

1. First the image is focused at the estimated layer $r_l$ by convolving $CoSCS_s^{\#}$, That is, $DefocCoSCS_s^{\#} \coloneqq iFFT_a(FFT_a(CoSCS_s^{\#}) \cdot k(r_l)))$, with $k$ the focusing kernel
2. Second, the ionosphere is compensated as usual by applying the inverse ionosphere phase screen mask:

$$DefocCoSCS_s^{\#} \leftarrow DefocCoSCS_s^{\#} \cdot e^{-j\Delta\phi_l}, \quad (5.43)$$

3. Finally, focus the image back at the ground level by inverting the focusing a t step 1, that is $CoSCS_s^{\#} \leftarrow iFFT_a(FFT_a(DefocCoSCS_s^{\#}) \cdot k(r_l)^*)$.

In case of a multi-layer ionosphere, MSC utilizes the following approach: The secondary image $CoSCS_s^{\#}$ is first decomposed into sub-band components $CoSCS_s^{\#,\prime}[\dots,\psi]$, such that

$$CoSCS_s^{\#} \approx \sum_{\psi} CoSCS_s^{\#,\prime}[\dots,\psi]. \tag{5.44}$$

Each sub-band image is then individually corrected using the ionospheric phase estimates obtained from the inversion algorithm. Denoting the corrected sub-bands by $CalCoSCS[\dots,\psi_n]$ the corrected sub-band, the final high-resolution ionosphere-corrected image is reconstructed by summing the corrected components:

$$CalCoSCS_s^{\#} \leftarrow \sum_{\psi} CalCoSCS[\dots,\psi]. \tag{5.45}$$

Each calibrated sub-band $CalCoSCS^{\#}$ is compensated in frequency domain using a standard FFT2-based approach and projected phase screens $\angle\boldsymbol{\gamma}_{MS}$ as described above.

### 5.3.5. Phase Plane Removal

The final step of the calibration algorithm executes the phase plane removal, that is, as first step we compute the interferogram

$$\Delta\phi_s \coloneqq \angle Coh(CoSCS_p, CalCoCSC_s^{\#}), \tag{5.46}$$

where Coh is defined as in Equation (5.14). To compute the phase slopes, we need to estimate the peak of the 2D spectrum of $\Delta\phi_n$. For that, we first zero-pad $CoCSC_s^{\#}$ to match the shape $\lceil N_{az}\ \alpha \rceil \times \lceil N_{rg}\ \alpha \rceil$[7], where $N_{az}$ and $N_{rg}$ are respectively the stack size in along-track and slant-range direction. Then, we set

$$F_s \coloneqq FFT2(\zeta_\alpha(\Delta\phi_s)), \tag{5.47}$$

where $\zeta_\alpha$ is the zero-padding operation described above. After shifting the zero-frequency component of $F_s$ at the center of the spectrum, we set

$$i', j' \coloneqq \mathrm{argmax}_{ij} |F_s(i,j)|. \tag{5.48}$$

To refine the peak estimation, we employ a local parabolic approximation around $(i', j')$, of size $w \geq 3$. More in detail, we fit a paraboloid of the form

[7] Note that the shape is rounded to the next size that results in the most efficient execution of FFT.

$$P_2(i,j) \coloneqq ai^2 + bj^2 + cij + di + ej + f, \tag{5.49}$$

via least-square estimation and compute the maximum $(\delta i, \delta j)$ in sub-pixel resolution via analytically solving for the stationary point of $P_2(i,j)$. It is trivial to see that such maximum is

$$\begin{bmatrix} \delta i \\ \delta j \end{bmatrix} \coloneqq \begin{bmatrix} 2a & c \\ c & 2b \end{bmatrix}^{-1} \begin{bmatrix} d \\ e \end{bmatrix}. \tag{5.50}$$

Thus, the peak of the 2D spectrum is estimated to be attained at

$$(i^*, j^*) \coloneqq (i' + \delta i, j' + \delta j), \tag{5.51}$$

which can be trivially converted into phase slopes component as follows:

$$\partial_{t_{az}} \phi_n \coloneqq 2\pi(\lceil N_{az}\,\alpha \rceil\, \Delta t_{az})^{-1} \left( i^* - \frac{\lceil N_{az}\,\alpha \rceil}{2} \right), \tag{5.52}$$

$$\partial_{t_{rg}} \phi_n \coloneqq 2\pi(\lceil N_{rg}\,\alpha \rceil\, \Delta t_{rg})^{-1} \left( i^* - \frac{\lceil N_{rg}\,\alpha \rceil}{2} \right), \tag{5.53}$$

where $\Delta t_{az}$ and $\Delta t_{rg}$ are respectively the sampling steps in along-track and slant-range direction. Finally, to compensate for the estimated phase screen, we set

$$CalCoSCS_s[t_{az}, t_{rg}] \coloneqq CalCoSCS_s^{\#}[t_{az}, t_{rg}] \cdot e^{-j(\partial_{t_{az}} \phi_n \cdot t_{az} + \partial_{rg} \phi_n \cdot t_{rg})}. \tag{5.54}$$

## 5.4. Phase Calibration via SKP

This section deals with the calibration strategy to estimate the ground steering phases. The aim of this procedure is to estimate the phase contributions due to both the ground and the disturbance. This approach cannot separate the contribution of external DEM error $(DTM - DEM_{EXT})$ from the residual phase disturbance. Accordingly, the output is a calibration screen containing both the phase disturbance and the phase contributions of the terrain height at P-band for each pixel.

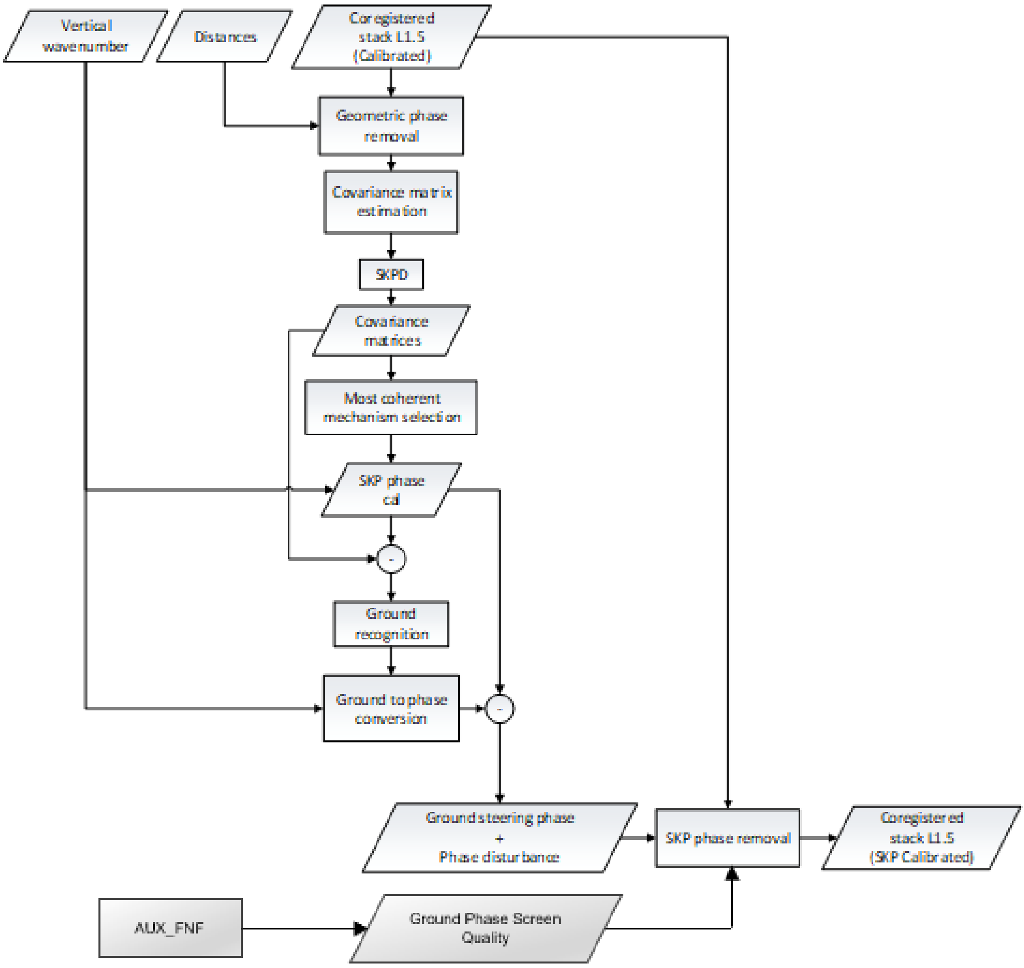


**Fig 13** Phase calibration by SKP.

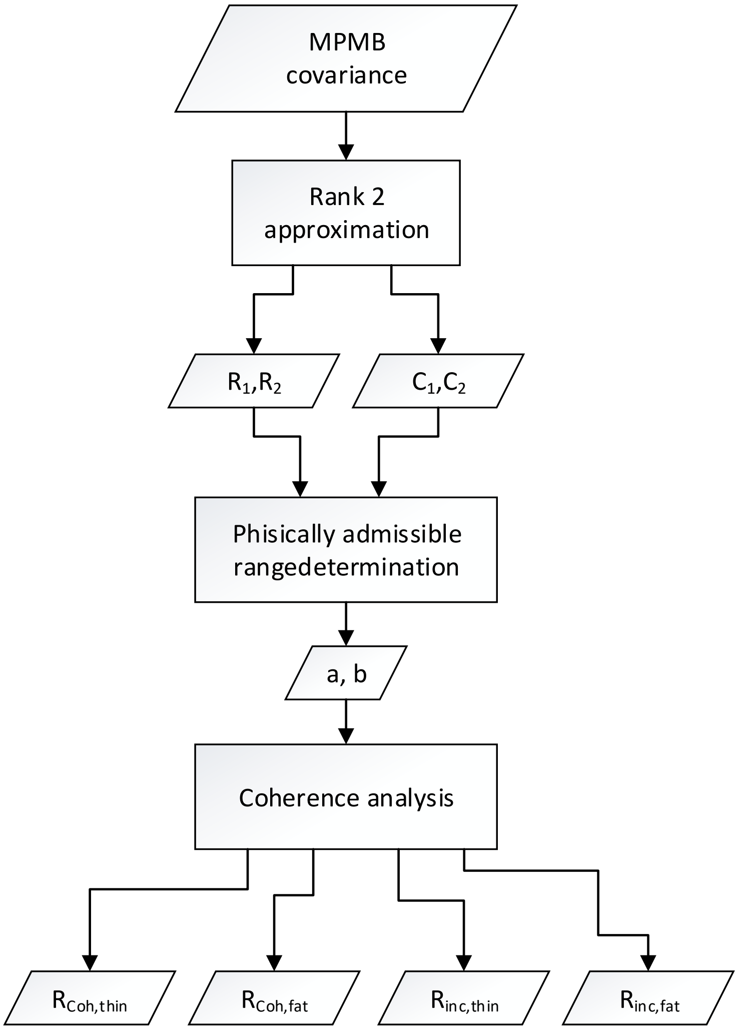


**Fig. 14** SKP decomposition.

## 5.4.1. Inputs and Outputs

**Input**

| Symbol | Name | Origin | Size | Variability | Default | Description |
|---|---|---|---|---|---|---|
| $CoSCS_n$ | | Coregistration Step or previous active calibration module | M acquisition of size $[N_{az} \times N_{rg}]$ | M=3 (INT) or M=7 (TOM), each with 3 or 4 polarizations (2CP + 1XP or 2CP + 2XP) | - | Coregistered SCS frames, possibly from previous calibration step (i.e. AZF, IOB, BAE, or IOS) |
| $\Delta\Phi_n$ | | Coregistration Step | M of size $[N_{az} \times N_{rg}]$ | M=3 (INT) or M=7 (TOM) each with a single channel | - | Synthetic phases from DEM associated to each acquisition |

| Symbol | Name | Origin | Size | Variability | Default | Description |
|---|---|---|---|---|---|---|
| $k_z$ | | Coregistration Step | M of size $[N_{az} \times N_{rg}]$ | M=3 (INT) or M=7 (TOM) each with a single channel | | Vertical wavenumbers |
| | skpPhaseEstimationFlag | AUX_PPS (AUX_FMT) | Boolean switch | True/False | True | Enable/disable the SKP module |
| | phaseCorrection | AUX_PPS (AUX_FMT) | Boolean switch | True/False | False | Type of phase correction that needs to be applied by the SKP ("None", "FlatteningPhaseScreen" or "Ground Phase Screen") |
| $w_{est}$ | estimationWindowSize | AUX_PPS (AUX_FMT) | Float | 1 -- ∞ | 500 | Size of the estimation window [m]. |
| | calibrationPhasePostprocessing | AUX_PPS (AUX_FMT) | Enumeration | Goldstein Boxcar Median None | None | Whether to post-process the SKP calibration phase screen via Goldstein filter ("Goldstein"), boxcar filter ("Boxcar"), or pivotal median filter ("Median", see Stack ATBD Section 5.4.2.6), or no filtering ("None"). It defaults to "None". |
| $w_f$ | postprocessingFilterWindowSize | AUX_PPS (AUX_FMT) | Float | 1 -- ∞ | 1000 | Size of the filtering window to be used for post-processing the SKP phase screen [m] (Only "Boxcar" and "Median"). Recommended value is 1,000 meters. |
| $w_G$ | goldsteinFilterWindowSize | AUX_PPS (AUX_FMT) | Int | $1 - \infty$ | 5 | Size of the filtering frequency window applied to the Golstein filter weights to be used for post-processing the SKP phase screen [px] (only "Goldstein"). Recommended value is 5 pixels (5 frequency bins). |
| $\alpha_G$ | goldsteinFilterAlpha | AUX_PPS (AUX_FMT) | Float | 0-1 | 0.5 | Parameter that controls the filtering level of the Goldstein filter. 0 is no filterimg, 1 is maximum filtering. Recommended values are between 0.2 and 1. |
| | excludeMPMBPolarizationCrossCovarianceFlag | AUX_PPS (AUX_FMT) | Boolean Switch | True/False | False | If MPMB coherence matrix should only contain autocovariances. |
| | crossPolMergingFlag | AUX_PPS (AUX_FMT) | Boolean Switch | True/False | False | If true, merge the cross-polarizations |

| Symbol | Name | Origin | Size | Variability | Default | Description |
|---|---|---|---|---|---|---|
| | | | | | | before estimating the SKP calibration phase screen. |
| $q_{thresh}$ | skpCalibrationPhaseScreenQualityThreshold | AUX_PPS (AUX_FMT) | Float value [%] | 0.0 – 1.0 | 0.5 | Apply the phase correction only if the estimated qualities are above this threshold |
| $Q_{thresh}$ | overallProductQualityThreshold | AUX_PPS (AUX_FMT) | Float value [%] | 0.0 – 1.0 | | If the fraction of valid ionosphere estimation is below this threshold, the fast-ionosphere estimation is flagged as failed |

**Output**

| Symbol | Name | Destination | Size | Variability | Default | Description |
|---|---|---|---|---|---|---|
| $CalCoSCS_n$ | | L1c output product | M acquisition of size $[N_{az} \times N_{rg}]$ | M=3 (INT) or M=7 (TOM), each with 3 or 4 polarizations (2CP + 1XP or 2CP + 2XP) | - | SCS with *optionally* no ground phase screen (depending on whether phase removal is enabled by AUX_PPS__) |
| $\varphi_{skp}$ | skpCalibrationPhaseScreen | L1c output product - | M images of size $[N_{az} \times N_{rg}]$ [rad] | M=3 (INT) or M=7 (TOM), with estimated phase | - | The phase screen that is estimated by the SKP |
| $q_n$ | skpCalibrationPhaseScreenQuality | L1c output product | M images of size $[N_{az} \times N_{rg}]$ | M=3 (INT) or M=7 (TOM), with the estimation quality | - | The phase quality associated with the FNF map |

## 5.4.2. Mathematical Description

### 5.4.2.1. Geometric Phase Removal

As first step the ground phase contribution will be removed from each image of the stack.

$$I_n^{flat}(a,r) = CoSCS_n(a,r) \cdot e^{j\Delta\Phi_n(a,r)} \tag{5.55}$$

where $d_i$ is the distance between the orbit of the image $i$ and the DEM interpolated on the SAR coordinates of the reference image.

### 5.4.2.2. Multi-polarimetric Multi-baseline Coherence Matrix Estimation

The Covariance estimation block aims to estimate the second order statistics of the data. The size of the spatial averaging window used to estimate the second order statistics must be provided as an input; this depends on the final resolution of the products to be provided. The output of the Covariance estimation block is a 4D array with dimensions: $\left[N \cdot N_{pol} \times N \cdot N_{pol} \times N_{a,subs} \times N_{r,subs}\right]$ where $N$ is the number of images, $N_{pol}$ the number of polarizations, and $N_{r,subs}$ and $N_{a,subs}$ are the numbers of range and azimuth samples after subsampling. For each (subsampled) range azimuth position a multi-baseline multi-polarimetric covariance matrix is returned. This is a block matrix made of $N_{pol} \times N_{pol}$ matrices of size $N \times N$. Each $N \times N$ block gathers the covariances estimated by considering each image pair for a fixed polarimetric channel couple. Mathematically, the $pq$-th block (from row $(p-1)N+1$ to row $pN$ and from column $(q-1)N+1$ to column $qN$) can be expressed as:

$$MPMBCov[(p-1)N+n,(q-1)N+m] = \frac{1}{N_{\Omega_r} N_{\Omega_x}} \sum_{r\in\Omega_r} \sum_{x\in\Omega_x} y_{p,n}(x,r) \cdot y_{q,m}^*(x,r)\,, \tag{5.56}$$

where $p$ and $q$ denote the $p$-th and $q$-th polarimetric channels respectively; $n$ and $m$ denote the $n$-th and $m$-th images in the stack; $r$ and $a$ denote the range (sample) and azimuth (line) indices; $\Omega_r$ and $\Omega_a$ denote the neighborhood in the range and azimuth directions of the desired position; $y_{p,n}(x,r)$ denotes the pixel value of the $n$-th image in polarimetric channel $p$; $*$ denotes conjugation. A normalized version of the multi-baseline multi-polarization covariance matrix is needed for the subsequent processing steps: the phases are the same, but the absolute value of its element's ranges from 0 to 1. It is referred to as the multi-baseline multi-polarimetric coherence matrix, $MPMBCoh$, and its elements are defined as follows:

$$MPMBCoh[(p-1)N+n,(q-1)N+m] = \frac{\sum_{r\in\Omega_r}\sum_{x\in\Omega_x} y_{p,n}(x,r)\cdot y_{q,m}^*(x,r)}{\sqrt{\sum_{r\in\Omega_r}\sum_{x\in\Omega_x}\left|y_{p,n}(x,r)\right|^2}\cdot\sqrt{\sum_{r\in\Omega_r}\sum_{x\in\Omega_x}\left|y_{q,m}(x,r)\right|^2}}\,. \tag{5.57}$$

Note that the user can use the parameter *excludeMPMBPolarizationCrossCovarianceFlag* in the AUX_PPS to only consider the auto-correlation terms, *i.e.* setting to 0 the entries of the $MPMBCoh$ matrix that are associated with cross-polarizations. Depending on which combination polarization method was executed by the Stack pre-processor, the SKP can optionally merge the cross-polarizations before computing the MPMB coherence matrix via AUX_PPS. Note that the Stack's polarizations are not affected. The cross-pol merging executed by SKP does not affect the structure of the stack.

#### 5.4.2.3. SKP Decomposition

The SKPD block implements the Sum of Kronecker Product Decomposition. The main purpose of this processing step is to separate the ground and volume scattering mechanisms

so that their vertical structures can be processed separately. The outputs of SKP decomposition are 4 coherence matrices of the structure ($[N \times N \times N_{a,sub} \times N_{r,sub}]$) classified according to their average interferometric coherence.
The Rank 2 approximation block of Figure 19 aims to find a set of matrices $\tilde{R}_1, \tilde{R}_2, \dots$ and $\tilde{C}_1, \tilde{C}_2, \dots$ and a set of real-valued positive scalars $\{\lambda_1, \lambda_2, \dots\}$ such that the matrix $MPMBCoh$ (hereafter referred to as $W$ for ease of notation) can be expressed as:

$$W = \sum_k \lambda_k \cdot \tilde{C}_k \otimes \tilde{R}_k \,, \tag{5.57}$$

$$\widetilde{W} = \lambda_1 \cdot \tilde{C}_1 \otimes \tilde{R}_1 + \lambda_2 \cdot \tilde{C}_2 \otimes \tilde{R}_2 \approx W. \tag{5.58}$$

where $\otimes$ denotes the Kronecker product. Among the different possible solutions to this problem the desired solution has the following property: by truncating the summation in Equation 5.61 the resulting matrix $\widetilde{W}$ is the best approximation of $W$ given the limited number of Kronecker products being summed together. These constraints are analogous to those defining the SVD decomposition; the only difference is that in the SVD context, the Kronecker products are outer products between vectors. It follows that by rearranging the $W$ matrix so that its blocks become vectors, the standard SVD routine can be used to determine the desired matrix sets. This is how the Rank 2 approximation block implements the search for the sets of matrices $\tilde{R}_1, \tilde{R}_2, \dots$ and $\tilde{C}_1, \tilde{C}_2, \dots$ . By analogy with SVD we can define the subspace spanned by the first two subspaces as the signal subspace. Matrices $\tilde{R}_1$ and $\tilde{R}_2$ identify the subspace in which the interferometric covariance of the scattering mechanisms associated with the ground ($R_g$) and canopy ($R_v$) lies. The $N \times N$ interferometric covariance matrix gathers all the second order statistics obtained by considering all possible pairs of images. It also gathers the information associated with the vertical structure of the scattering mechanism, which can be extracted by means of spectral estimation techniques. The same is the case for matrices $C_g$ and $C_v$ that represent the polarimetric signatures of the ground and volume backscattering. Once the signal subspace is identified the polarimetry and structure associated with the two scattering mechanisms can be obtained by a linear combination of the basis matrices; the linear combinations are reported below[8]:

$$R_g(a) = a \cdot R_1 + (1-a) \cdot R_2 \,, \tag{5.59}$$

$$R_v(b) = b \cdot R_1 + (1-b) \cdot R_2 \,, \tag{5.60}$$

$$C_g(b) = \frac{1}{a-b}\big((1-b) \cdot R_1 - b \cdot R_2\big), \tag{5.61}$$

$$C_v(a) = \frac{1}{a-b}\big(-(1-a) \cdot R_1 + a \cdot R_2\big). \tag{5.62}$$

[8] Note that, for the sake of clarity, it is here assumed that parameter $a$ rules the ground structure and the volume polarimetry, but this could be assumed for parameter $b$ instead.

The linear combination is ruled by just two real valued parameters, $a$ and $b$. *Any* value of the two parameters leads to the same matrix $\widetilde{W}$ given by Equation 5.59. However, only a limited subset of values of $a$ and $b$ leads to semi-positive definite matrices, in other words physical consistency of the matrices returned by the decomposition is ensured only within a limited range of values of $a$ and $b$.

The Physically admissible range determination block returns two vectors, associated with $a$ and $b$ respectively, which sample the range of admissibility for the two parameters. At the edges of the admissibility range of the $a$ parameter either $R_1(a)$ or $C_2(a, b)$ is singular, and similarly for the $b$ parameter, as shown in the figure below.

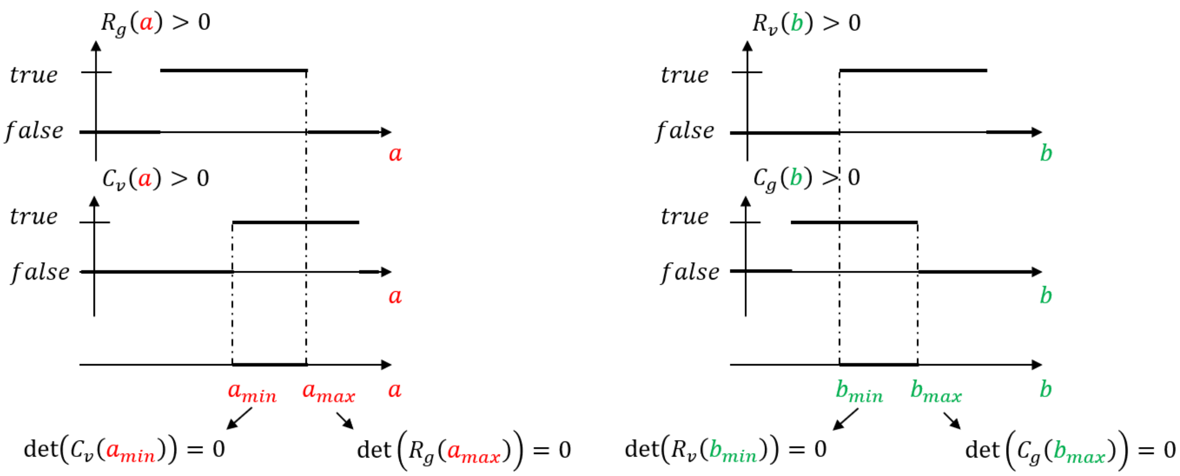


**Fig.12** Schematic representation of the range of admissible values for parameters a and b, i.e., the range of values that ensures that the matrices returned by the decomposition are semi-definite positive matrices.

The Coherence analysis block analyzes the structure matrices returned by the decomposition and classifies them according to their average interferometric coherence. The scattering mechanism that provides the highest coherence is labeled as "coh" and the other as "inc". The matrices resulting from the extreme values of the parameters giving the highest coherence are labeled as "thin", the other extreme values lead to the "fat" matrices. These four matrices are the main output of the SKPD block of Figure 19 and are gathered by the MBas covariances block in the same figure.

### 5.4.2.4. Selection of Most Coherent Mechanism

The aim of this block is to identify the coherence matrix providing the maximum coherence.

The quality of each mechanism for calibration purposes is evaluated by computing the ratio between the largest singular values and their overall sum, and the vector containing the phases associated with the highest quality singular vectors gives the desired calibration phases. The SKP calibration phase is the output of the SKP decomposition exploiting the most coherent mechanism:

$$\varphi_{cal} = k_z \cdot (z_{unkn} - z_{DEM}) + \alpha, \tag{5.63}$$

where $k_z$ is the vector the vertical wavenumbers; $z_{unkn} - z_{DEM}$ is the height of the most coherent mechanism referred to the external DEM; $\alpha$ is the residual noise.

#### 5.4.2.5. Ground Recognition

This step aims to identify which of the 4 coherence matrices calibrated by $\varphi_{cal}$ contains the lowest peak. The ground recognition process is described as follows:

1. Estimation of the vertical power profile (beamforming)
2. Peak selection
3. Lowest peak selection

The elevation of the peaks here refers to $z_{unkn}$:

$$z_{g,rel} = z_{unkn} - z_g \,. \tag{5.64}$$

#### 5.4.2.6. SKP Ground Phase

The output of the Phase calibration by SKP is thus the $\varphi_{cal}$ minus the $z_{g,rel}$ converted to phase plus the synthetic phase computed by the external DEM:

$$\varphi_{skp} \coloneqq k_z \cdot (z_{unkn} - z_{DEM}) - k_z \cdot \left(-z_g + z_{unkn}\right) + \alpha + \Delta\Phi_n \tag{5.65}$$

$$= \Delta\Phi_n + k_z \cdot \left(z_g - z_{DEM}\right) + \alpha \tag{5.66}$$

Linearizing the synthetic phases around the linearization value $z_{DEM}$ and setting $\Delta\Phi_n^g$ to be the synthetic phases on the ground, we get $\varphi_{skp} \approx \Delta\Phi_n^g$.

Optionally, the user can enable via AUX_PPS a post-processing of the estimated SKP phase screen $\varphi_{skp}$ via pivotal median filter, *i.e.* a median filter with local unwrapping (see [RD26]), a standard boxcar filter, or a Goldstein filter[9]. Similarly, the relevant filter parameters can be specified by the user via AUX_PPS.

#### 5.4.2.7. SKP Phase Removal

---

[9] The implemented Goldstein filter performs the following filtering on the estimated phase screen: Set $H \coloneqq FFT2\left(\exp(j\varphi_{skp})\right)$, the filtered $\varphi_{skp}$ is defined as $\angle iFFT2(|\langle H\rangle_{w_G}|^{\alpha_G} H)$, where $\langle\cdot\rangle_{w_G}$ is a boxcar smoothing operator, $0 \leq \alpha_G \leq 1$ is the filtering parameter, and $\angle$ is the phase operator.

If enabled in the AUX_PPS configuration, that is if *phaseCorrection* is set to any of *"Flattening Phase Screen" or "Ground Phase Screen"*, the SKP phase contribution will be removed from each image of the stack as reported in Equation 5.67 below. Setting $\varphi_{cal}$ to be $k_z(z_g - z_{DEM})$ as in the Equation of Section 5.5.2.6 above, we correct the ground phase as follows:

$$CalCoSCS_n(a,r) \coloneqq CoSCS_n(a,r) \cdot e^{j(\Delta\Phi_n + s\boldsymbol{I}_{a,r}(q_n)\cdot\varphi_{cal})}, \qquad (5.67)$$

where, as for the IOS, $\boldsymbol{I}(q_n)$ is the indicator matrix so that $\boldsymbol{I}_{\boldsymbol{a},\boldsymbol{r}}(q_n) = 1$ iff $q_{n,a,r} > q_{thresh}$, $0$ otherwise. The switch $s \in \{0,1\}$ is $0$ if *phaseCorrection* is set to *"Flattening Phase Screen"*, and it is $1$ if *phaseCorrection* is set to *"Ground Phase Screen"*. In other words, the correction will always compensate for the synthetic phases from DEM, while the ground phases will be corrected if and only if the user has enabled it via AUX-PPS and the estimation quality is above threshold. Details on how the quality is computed are reported in the next section.

#### 5.4.2.8. SKP Ground Phase Quality

SKP uses the forest/non-forest (FNF) mask provided as auxiliary input via FNF product as a pixel-wise quality indicator (see Section 5.5.2.7). This relies on the fact that the SKP calibration algorithm assumes and requires the presence of both ground and forest in each pixel and thus the SKP is expected to work correctly on forested areas and incorrectly on non-forested ones. Accordingly, the SKP estimation quality map will be defined to contain 1.0 (valid) on pixels covering forested areas and 0.0 (invalid) on those associated to non-forested areas. Moreover, since the forest/non-forest map allows for representing invalid data as well, the pixel associated to invalid FNF data will be treated as invalid (*i.e.* they will not be used for calibration) and populated using the no-data value specified by the user via AUX_PPS (i.*e.* defaulted to -9999.0).

Finally, note that the FNF mask contained in the FNF product is defined on the WGS84 coordinate system with a latitude-longitude grid spacing of 0.002778°, corresponding to approximately 300m at the Equator and 200m in the mid-latitude (for more details see the BIO_IODD [RD24]). Hence, it requires to be mapped onto the target grid of the SKP estimated phase screen. For this, we first query the Lat/Lon LUTs of the coregistration primary at the azimuth and slant range times of the target grid, then we query the FNF mask at those Lat/Lon values using a standard nearest neighbor interpolation.

Finally, similarly to Section 5.4.5.1, the estimation is considered successful and accordingly reported in the output product validity index only if the percentage of valid estimation exceeds the overall quality threshold $Q_{thresh}$.

### 5.4.3. Contingency Handling

The SKP module separates contingency cases into two categories: *blocking* and *nonblocking.* Blocking cases are cases in which the execution of the SKP is prematurely stopped or completely skipped. Conversely, nonblocking contingency cases may or may not stop the execution. If the SKP hit the former case (*i.e.* the SKP is executed), the situation of hitting a contingency case will be reported in the L1c annotation using the *skpDecompositionIndex* field. The contingency cases handled by the SKP module are the following:

- Small estimation window: SKP requires the estimation window $w_{est}$ to be sufficiently large compared to the DEM resolution of the L1a products. Accordingly, we require the DEM resolution from L1a to be at most 90% of $w_{est}$. Failing such a check is considered a *blocking* case.
- Missing polarizations: SKP requires at least 2 polarizations. Failing to provide an input stack with at least 2 usable polarizations will result in *blocking* the SKP execution.
- SKP decomposition failure (Section 5.5.2.3): This is considered a *nonblocking* contingency case. As a fallback procedure, a white volumetric noise is used as scattering coherence. Note that, in the provided implementation, the volumetric noise is seeded and pre-computed upfront to ensure repeatability across different (multithreaded) executions.
- Most coherence mechanism selection (Section 5.5.2.4): Errors may solely incur during SVD decomposition. Such a case is considered a *nonblocking* one and $\varphi_{cal}$ is set to 0 (no ground phase).

# 6. Configurable Input Parameters

A comprehensive list of configurable input parameters for the different Stack Processor modules can be found in the BPS Auxiliary Products Format document [RD18] and in the Auxiliary Stack Processing Parameters product (AUX_PPS____).